# DEVELOPMENT OF A THREE DIMENSIONAL DYNAMIC LOAD DISTRIBUTION PROGRAM

A Thesis

Presented in Partial Fulfillment of the Requirements for

the Degree Master of Science in the

Graduate School of The Ohio State University

By

Tugan Eritenel, B.S.

*****

The Ohio State University
2003

Master's Examination Committee:

Professor Donald R. Houser, Adviser

Professor Robert G. Parker

Approved by

_____

Adviser
Department of Mechanical Engineering

# ABSTRACT

Gearbox manufacturers put some of their effort to reduce noise and vibration radiated from gearboxes. Previous research has shown that noise radiated can be related to many parameters, but transmission error and dynamic bearing forces are considered to be the exciters of the system and the source of noise. In the OSU GearLab a number of finite element and lumped models have been created ranging from nonlinear time variant (NTV) to linear time invariant (LTI). In three dimensions, finite element models require intense computational effort if contact mechanics are considered. The objective of this thesis is to solve numerically the nonlinear differential equations of motion of a geared shaft system in time domain, and combine this solution with the contact solver of LDP in three dimensions. In the case of optimized gear sets, this analysis is expected to become important, and may lead to self-excited vibrations. The friction force, runout and backside contact are included in the thesis and consequently in the computer program. The results of this numerical analysis are compared with Calyx and DYTEM, time domain solvers, which reportedly agree with experiments

# ACKNOWLEDGMENTS

I am very grateful to my adviser Dr. Donald Houser for his support and motivation in every aspect of this research. His invaluable guidance and experience as well as his incredible collection of academic material in GearLab have provided a continuous inspiration for this thesis. I am very thankful to Dr. Robert Parker who has served on my Masters Examination Committee and also guided me through his courses on vibrations and dynamics. I am indebted to Dr. Sandeep Vijayakar for allowing me to use his finite element program Calyx, and his support regarding the program. This study is made possible by the continuous financial support from the sponsors of the GearLab.

I would like to express my appreciation to Jonny Harianto for sharing his experience in computer programming and management. I also acknowledge the students of the GearLab for their assistance in numerous problems.

Finally I am very indebted to my family for their constant support and encouragement.

# VITA

| | |
|---|---|
| August 5, 1979 | Born – Izmir, Turkey. |
| June 2001 | B.S. Mechanical Engineering, Middle East Technical University, Ankara, Turkey. |
| January 2002 – Present | Graduate Research Associate, The Ohio State University, Columbus, Ohio. |

## FIELDS OF STUDY

Major Field: Mechanical Engineering

TABLE OF CONTENTS

LIST OF FIGURES

LIST OF TABLES

# NOMENCLATURE

| | |
|---|---|
| $c_D$ | Drive shaft torsional damping |
| $c_L$ | Load shaft torsional damping |
| $c_{PB}$ | Pinion bearing damping |
| $c_{GB}$ | Gear bearing damping |
| $c_m$ | Viscous mesh damping |
| e | Cam excitation at gear mesh |
| $e_i$ | Tensor basis for rotated reference frame |
| $E_i$ | Tensor basis for fixed reference frame |
| EI | Bending constant for beam |
| $F_{rightBearing}$ | Right bearing force |
| $F_{leftBearing}$ | Left bearing force |
| $F_{mesh}$ | Mesh force |
| $F_{Gear}$ | Gear force |
| h | Discretized beam length |
| H | Angular momentum |
| $I_P$ | Mass moment of inertia of pinion |
| $I_G$ | Mass moment of inertia of gear |
| $I_D$ | Mass moment of inertia of driver |
| $I_L$ | Mass moment of inertia of load |
| $I_{ii}$ | Elements of inertia tensor |
| J | Inertia tensor |
| $k_D$ | Drive shaft torsional stiffness |

| | |
|---|---|
| $k_L$ | Load shaft torsional stiffness |
| $k_m$ | Mesh stiffness of gear pair |
| $k_{PB}$ | Pinion bearing stiffness |
| $k_{GB}$ | Gear bearing stiffness |
| $k$ | Stiffness tensor |
| $k_{ii}$ | Elements of stiffness tensor |
| $m_P$ | Pinion mass |
| $m_G$ | Gear mass |
| $M_{Gear}$ | Gear moment |
| $M_{Shaft}$ | Shaft moment |
| $r_P$ | Base circle radius of pinion |
| $r_G$ | Base circle radius of pinion |
| $R_r$ | Radius of curvature |
| STE | Static transmission error in translation |
| TE | Transmission error in translation |
| $T_L$ | Load torque |
| $T_D$ | Driving torque |
| V | Shear force in beam |
| $V_e$ | Entraining velocity |
| $V_s$ | Sliding velocity |
| $x_P$ | Pinion bearing displacement |
| $x_G$ | Gear bearing displacement |
| $\beta$ | Angular displacement in free rotation direction |
| $\phi$ | Angular displacement in helix angle direction |
| $\varphi_n$ | Normal pressure angle |
| $\mu$ | Friction coefficient |
| $\nu$ | Oil viscosity |
| $\theta$ | Angular displacement perpendicular to helix angle direction |
| $\theta_P$ | Angular displacement of pinion |

| | |
|---|---|
| $\theta_G$ | Angular displacement of gear |
| $\theta_D$ | Angular displacement of drive inertia |
| $\theta_L$ | Angular displacement of load inertia |
| $\omega$ | Frequency |
| $\psi$ | Helix angle |

Superscripts

| | |
|---|---|
| $\cdot$ | Time derivatives of first order |
| $'$ | Rotated basis |
| $\rightarrow$ | Vector quantity with elements $(x_1, x_2, x_3)$ |

Abbreviations

| | |
|---|---|
| DOF | Degree of freedom |
| LOA | Line of action |
| O-LOA | Off-line of action |
| TE | Transmission error |
| STE | Static transmission error |

# CHAPTER 1

# INTRODUCTION

## 1.1 Introduction

The field of dynamics of gears is at a high level of maturity in terms of two dimensions that are most appropriate for spur gears. Accurate dynamic factor and load distribution studies have been conducted with various numerical computer programs specialized in gear contact analysis. The problem, however, becomes computationally intense when three-dimensional finite element dynamic analysis is required, although static analysis can be performed with reasonable computational effort. Analytical tools have been developed for the two and three-dimensional problem that helps the understanding of the problem. In this chapter the tools for dynamic analysis are reviewed to lead to a way for the intended analysis, and motivation behind the research is given.

## 1.2 Literature Review

### 1.2.1 *Dynamic Factor*

The actual tooth load on gear teeth can be considered in two basic components, namely the static and dynamic component. The main concern is the dynamic factor,

which is the ratio of static load and dynamic load, depending on the gear accuracy and speed of the system. This factor can also be formulated as the ratio of stresses to give a better design guideline as shown by Harianto [7]. Consequently, the maximum allowable stresses can be modified for the dynamic factor. Expressions for dynamic factor do not involve loading, inertias, or other specifically system dependent parameters. They are usually functions of pitch line velocity, and the quality of the gears. An early expression for the dynamic factor is:

$$DF = \sqrt{\frac{78}{78 + \sqrt{V}}} \tag{1.1}$$

Where $V$ is the pitch line velocity in fpm. A detailed study of dynamic factor can be found in the study by Houser and Seireg [3]. Even though derivation of dynamic factors can be from simple vibratory models, they are generally empirical or semi-empirical. The most recent formulation suggested by AGMA incorporates the gear accuracy in the dynamic factor.

### 1.2.2 *Tooth Compliance Models*

The second approach to determine a dynamic factor is to use a vibratory mathematical model that employs Newton's Laws of Motion. Many kinds of models are possible such as lumped parameter, finite element, and continuous system having different levels of complexity. There has been research and a large number of publications in vibratory modeling of mating gears. A comprehensive review of models that have been used by researchers are presented in the work by Ozguven and Houser [1] Simplest models start treating the compliance of the teeth, as a spring element, and

inertia of the gears. This simple model can be either translational or rotational, depending on how the compliance element is chosen. Dynamic response of gears is due to external excitation and internal excitation. The internal excitation exists because the tooth compliance varies with number of teeth in contact; this excitation frequency is at “mesh excitation frequency”. Usually this parametric excitation is not at a single frequency, but can be expressed as a combination of frequencies from Fourier expansion. Therefore, higher harmonics also excite the system. On the other hand, the resonant frequency is a result of the compliance of the mesh. Again the compliance is not a pure sinusoidal wave. This results in superharmonics and subharmonics in resonance. Aida et al [13] studied the one DOF model with the varying mesh stiffness to get unstable operating regions. They investigated effects of gear parameters on noise, and pointed out that the noise generating mechanism is complex, requiring a more complex model than a single DOF, possibly a three dimensional model. The reduced model is also studied by Ozguven and Houser [2] to obtain predictions for mesh force and dynamic transmission error. Computational results were compared to experiments for dynamic factor and found to be in reasonable agreement. The program is named DYTEM and later incorporated in LDP by Harianto [7], so that the dynamic root stresses can be predicted.

### 1.2.3 *Gear Dynamics Models*

The simplified model does not take into account the bearing compliance, shafts, and other system parameters. The reliability of the results provided by the simple model depends on the level of coupling between other components. The need for modeling

bearings and shafts arises if the dynamic coupling is considerable, because the parametric mesh excitation may also excite bearing and shaft modes in that case. Therefore, a more general vibratory model should include translational bearing and torsional shaft compliances and inertias. There is another effect introduced if the bearings are considered in the model. Bearing displacements, or in general, any displacement that changes the meshing parameters, changes the expected load distribution, mesh stiffness, and transmission error. This is the second motivation for modeling more components of the system. Also it should be pointed out that this effect is independent of dynamic coupling, so that it can be treated as a static problem. Several researchers have modeled bearings and shafts. Kasuba [10] developed a computation method for solving dynamic loading and compared the results with the AGMA dynamic factor. The instability of the equations has been studied and was concluded that although the undamped system is not stable for some speeds, damping makes it stable. The AGMA factor was found to be conservative for high-speed, high accuracy gearing. Kasuba [9] and Evans [11] have modeled a gear pair with the torsional shaft deflections. They also developed a scheme for evaluating mesh stiffness and incorporated the profile modifications. An iterative procedure was used to solve for contact and load sharing of spur gear teeth, similar to LDP, whereas equations of motion are solved by Runge-Kutta method. This program also involves variable mesh stiffness. Procedure-wise, their implementing of the equations of motion is similar to the work that is carried out in this thesis. Their results show that the vibrations can be coupled, and also torsional compliance can be used as a means of

reducing vibrations. In addition, they point out that contact ratio is another important parameter, and higher it is lower the dynamic loads.

### 1.2.4 *Geared Rotor Dynamics and Flexible Shafts*

Furthermore, a three-dimensional shaft model allows locating bearings at a distance from the gear. This is suitable for a more generalized system because shaft displacements do not necessarily result in a transverse displacement at the gears. It should be pointed out that bearings are not the only elements that deform. But shaft deformations cannot be neglected if they are long and thin enough. This results in a center distance error and misalignment in addition to the same errors caused by bearing deflections. It is conceivable that some shaft modes can couple with gear mesh vibrations. For further generalization of the system being modeled, considering shaft flexibility in the transverse direction may also be helpful. This way, a three-dimensional model also allows rocking motion due to uneven bearing deflections, even if whirling is not critical. Iida and Tamura [15] showed this case, that transverse and torsional vibrations are coupled although gyroscopic effects are not taken into account. Furthermore, at high speeds of rotation, it is necessary to consider whirling of shafts because it introduces instabilities that may be important in some cases. Experimental work of translational-torsional coupling at high speed of a geared rotor system is studied by Seireg [14] and an approximate expression for whirl frequency for the gear pair was given. Three-dimensional motion of gears is of particular interest because LDP handles load distribution in 3-D. If bearings are at a distance from the gear, or their stiffnesses are not equal, for an accurate 3-D load distribution output it is

possible only if the positions of gears are known. In other words, the capability of LDP would be wasted and the 3-D load distribution results will be useless in this case. Blankenship and Singh [6] developed a three dimensional gear mesh model. The model is six DOF, and the load distribution can be evaluated to account for moments developed in the gear mesh. Velex and Cahouet [12] developed a load distribution program and modeled shafts as Timoshenko beams in three dimensions. They used the model to predict friction force excitation and compared the results with an experimental setup.

Vibrations of gears can be reduced with compliant supporting shafts. Either numerical techniques such as finite element or analytical expressions from continuous system dynamics are applicable to the problem. The complexity of models can be increased depending on the system being modeled. Kahraman et al [16] developed a finite element model including torsion and flexibility of shafts, translation of bearings and used a constant mesh stiffness. Effect of shaft and mesh parameters on mesh force were studied.

### 1.3 Motivation

The gear contact problem can be approximated with simplified elements when the accuracy of the contact is far more less than the dynamic response. However, the precise load distribution is required if modifications are applied so that the dynamic response is predicted to be relatively low. In addition, the three-dimensional problem also depends on the load distribution since moments are introduced apart from mesh forces. The existing LDP is a fast numerical computer code that allows accurate load

distribution analysis in three dimensions, hence making it a valuable tool for evaluating the mesh properties. The aim of this thesis is to convert LDP into a dynamic load distribution program by utilizing equations of motion for geared shafts. This tool can allow the characterization of exciters to gear dynamics problem other than the well-known transmission error excitation.

## 1.4 Outline of Thesis

First, several models for the gear dynamics problem without explicit discussion of the mesh forces are formulated in chapter 2. Chapter 3 collects the forces and moments arising from the contact problem and incorporates them in the models developed. In chapter 4 the solution method is discussed. Chapter 5 presents some comparisons and results from the program. Comparisons with other models and excitation from parameters other than transmission error are discussed. In chapter 6 conclusions and recommendations for future research is presented.

# CHAPTER 2

# DYNAMIC MODELS

## 2.1 Introduction

In this chapter the problem of modeling of a gear pair is explained and some methods to solve the problem are reviewed. The details of the gear mesh are ignored and a solution for the rest of the system is sought. After a suitable approach is decided upon, mathematical relations are derived for four different models that have different levels of complexity and assumptions.

## 2.2 Model for Tooth Compliance

A simple dynamic model for a gear pair consists of two rotational inertias, representing the gears, and a spring, representing the compliance due to meshing of the gear teeth. This model assumes that the torsional vibrations of the mesh are uncoupled from any other transverse or torsional mode of the remaining system. This assumption holds for physical systems that have distinct natural frequencies, to some extent. In this model, the aim is to study the parametric excitation that arises from varying numbers of teeth in contact and profile errors. Figure 2.1 shows the model that is used to derive the equations of motion. The equations of motion are:

$$I_P\ddot{\theta}_P = T_D - F_{mesh}.r_P$$
$$I_G\ddot{\theta}_G = F_{mesh}.r_G - T_L \tag{2.1}$$

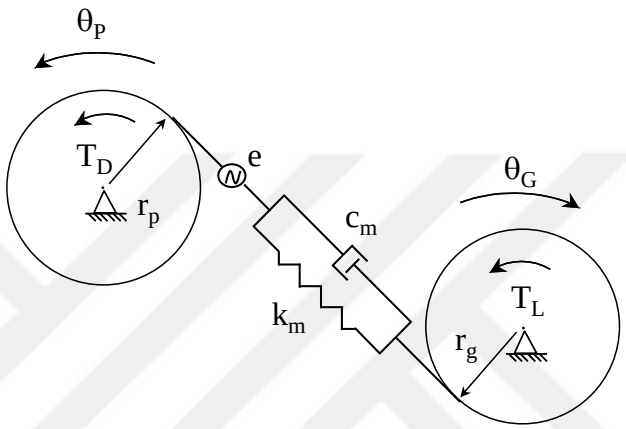


Figure 2.1. Simple dynamic model of a gear pair.

This 2 DOF system can be reduced to a single DOF system, eliminating the rigid body motion which results in a model that excitation can be visualized very easily. However, it is desirable to keep track of the rigid body motion also, to consider position dependent meshing parameters. In order to continue developing equations, mesh force is expanded as the spring force, although, the mesh force generation depends on load distribution and other factors. For the purpose of determining the mesh natural frequency, taking $c_m = 0$, $e = 0$, and constant mesh stiffness, mesh force, ignoring the damping, can be written as:

$$F_{mesh} = k_m \cdot TE \tag{2.2}$$

Where transmission error is defined as translational displacement,

$$TE = \theta_G \cdot r_G - \theta_P \cdot r_P \tag{2.3}$$

Substituting these into (2.1), the equations of motion in matrix form are:

$$\begin{pmatrix} I_P & 0 \\ 0 & I_G \end{pmatrix} \cdot \begin{pmatrix} \ddot{\theta}_P \\ \ddot{\theta}_G \end{pmatrix} + \begin{pmatrix} k_m \cdot r_P{}^2 & -k_m \cdot r_P \cdot r_G \\ -k_m \cdot r_P \cdot r_G & k_m \cdot r_G{}^2 \end{pmatrix} \cdot \begin{pmatrix} \theta_P \\ \theta_G \end{pmatrix} = \begin{pmatrix} T_D \\ -T_L \end{pmatrix} \tag{2.4}$$

Assuming the solution to be harmonic: $\Theta = \theta \cdot e^{i \cdot \omega \cdot t}$ , and substituting for $\theta$, *we* get the algebraic equation for the natural frequency:

$$\omega^4 \cdot I_P \cdot I_G - \omega^2 \cdot \left( I_G \cdot k_m \cdot r_p{}^2 + I_P \cdot k_m \cdot r_G{}^2 \right) = 0 \tag{2.5}$$

Solutions are $\omega = 0$, and

$$\omega = \sqrt{k_m \cdot \frac{I_G \cdot r_P{}^2 + I_P \cdot r_G{}^2}{I_P \cdot I_G}} \tag{2.6}$$

Therefore an equivalent mass for the single degree of freedom model is:

$$m_{eq} = \frac{I_P \cdot I_G}{I_G \cdot r_P{}^2 + I_P \cdot r_G{}^2} \tag{2.7}$$

It is possible to include the displacement excitation and damping at the mesh with a single DOF model of the form shown in Figure 2.2.

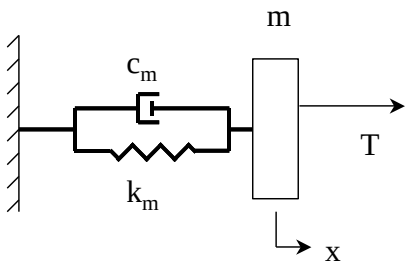


Figure 2.2. Equivalent SDOF translational model of gear mesh.

To keep track of position dependence of mesh properties, equations of motion for the 2 DOF system (2.1) is used in the solution of this gear pair model. But this single DOF model can yield information regarding the time varying properties of the mesh, such as dependence of mesh stiffness on number of teeth in contact, separation due to backlash and backside contact. As long as angular position of the gears is known, it is possible to consider effects of profile and lead modifications, runout, and spacing errors. The friction force can also be obtained depending on individual tooth loads, and the resulting moment from friction force can be added to the mesh force. Generation and application of some of these forces to dynamic models are discussed in the next chapter.

## 2.3 Model for Gear Dynamics

For the purpose of more general modeling of a gear pair, researchers have included bearings on which gears are resting, and torsional flexibility of pinion and gear shafts. In case the natural frequencies of the system are close to the mesh natural frequency, that particular element should also be modeled for accurate results. Most of the time

bearing modes couple with the mesh mode, and torsional stiffness of the gear carrying shaft may couple with the mesh if the shaft is short and thick enough. The two dimensional model of a gear pair in the previous section can be extended to include lateral bearing housing, shaft, and torsional shaft compliance.

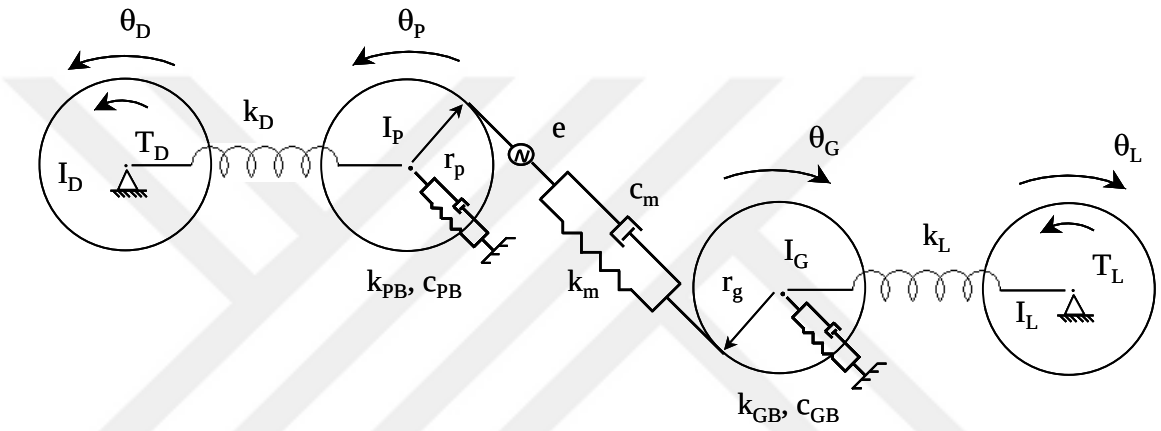


Figure 2.3. Geared shaft model with torsional stiffness and bearing.

Figure 2.3 shows a schematic of the extended model. Here, a single bearing stiffness is considered, the bearings are assumed to be just under the gears. In practice it can be assumed that this stiffness value is the combination of stiffness of bearings if more than one bearing exists. In the same way, the compliance of multiple shafts of various geometries can be added, and the inertia of these shafts can be shared between gears and drivers. This model, should predict the coupling effect between gear mesh,

bearings, and load and drive shafts. In addition to that, there are issues even if there is no considerable dynamic coupling to mesh with any of those:

The center distance variation due to bearing deformation can be important in load distribution analysis and the mesh stiffness itself. That is; the bearing vibrations may be uncoupled but gears may operate at a greater center distance because of bearing deflections, consequently, decreasing the mesh stiffness, total contact ratio, and parametric mesh excitation.

Similar to this, when taking into account the friction forces, the deceleration of the complete system will be determined by the drive and load inertias. It is also true when a speed runup or rundown analysis is desired.

Bearings and drive & load shafts can end up in transient vibration when there is repeating separation and contact of gear teeth. This rattle condition may happen near mesh natural frequency if there is enough backlash and the driving loads are light.

Equations of motion for this model can be derived as:

$$
\begin{aligned}
I_D\ddot{\theta}_D &= T_D - k_D\cdot(\theta_D-\theta_P) - c_D\cdot(\dot{\theta}_D-\dot{\theta}_P)\\
I_P\ddot{\theta}_P &= k_D\cdot(\theta_D-\theta_P) + c_D\cdot(\dot{\theta}_D-\dot{\theta}_P) - F_{mesh}\cdot r_P\\
I_G\ddot{\theta}_G &= F_{mesh}\cdot r_G - k_L\cdot(\theta_G-\theta_L) - c_L\cdot(\dot{\theta}_G-\dot{\theta}_L)\\
I_L\ddot{\theta}_L &= k_L\cdot(\theta_G-\theta_L) + c_L\cdot(\dot{\theta}_G-\dot{\theta}_L) - T_L\\
m_P\cdot\ddot{x}_P &= F_{mesh} - k_{PB}\cdot x_P - c_{PB}\cdot x_P\\
m_G\cdot\ddot{x}_G &= F_{mesh} - k_{GB}\cdot x_G - c_{GB}\cdot x_G
\end{aligned}
\tag{2.8}
$$

These equations are used in the computations, but for modal analysis using (2.2), and (2.3), equations can be written in matrix form.

$$\begin{pmatrix} I_D & 0 & 0 & 0 & 0 & 0 \\ 0 & I_P & 0 & 0 & 0 & 0 \\ 0 & 0 & I_G & 0 & 0 & 0 \\ 0 & 0 & 0 & I_L & 0 & 0 \\ 0 & 0 & 0 & 0 & m_P & 0 \\ 0 & 0 & 0 & 0 & 0 & m_G \end{pmatrix} \cdot \begin{pmatrix} \ddot{\theta}_D \\ \ddot{\theta}_P \\ \ddot{\theta}_G \\ \ddot{\theta}_L \\ \ddot{x}_P \\ \ddot{x}_G \end{pmatrix} + \begin{pmatrix} k_D & -k_D & 0 & 0 & 0 & 0 \\ -k_D & k_D + k_m \cdot r_P^{\,2} & -k_m \cdot r_P \cdot r_G & 0 & 0 & 0 \\ 0 & -k_m \cdot r_P \cdot r_G & k_L + k_m \cdot r_G^{\,2} & -k_L & 0 & 0 \\ 0 & 0 & 0 & k_L & 0 & 0 \\ 0 & k_m \cdot r_P & -k_m \cdot r_G & 0 & k_{PB} & 0 \\ 0 & -k_m \cdot r_P & -k_m \cdot r_G & 0 & 0 & k_{GB} \end{pmatrix} \cdot \begin{pmatrix} \theta_D \\ \theta_P \\ \theta_G \\ \theta_L \\ x_P \\ x_G \end{pmatrix} = \begin{pmatrix} T_D \\ 0 \\ 0 \\ T_L \\ 0 \\ 0 \end{pmatrix}$$

Since this is a 2 dimensional model, rotor dynamics are ignored. So that the rocking motion of the gears, effects of misalignment on load distribution due to shafts are not considered. A three dimensional model is needed for these effects to be handled.

## 2.4 Model for geared rotor dynamics

At high speeds of rotation, proper models should include rotation and translation of shafts in three dimensions. Whirling of shafts becomes a significant problem at high speeds independent of the application. Even if gyroscopic effects are neglected in a certain problem, there exists research [15] that shows transverse vibrations are coupled with torsional vibrations. Here, it is assumed that shafts are rigid, but they are supported on two flexible bearings at each shaft. The formulation of forces and displacements are in vector form, therefore, it is possible to place bearings and gears either centered or overhung. This 3-D rigid shaft model replaces the gear pair and bearings in the previous model, but the drive and load modeling remains the same. So that, gyroscopic effects are taken into account between gears and where bearings are mounted. The rest of the system is treated as only torsional.

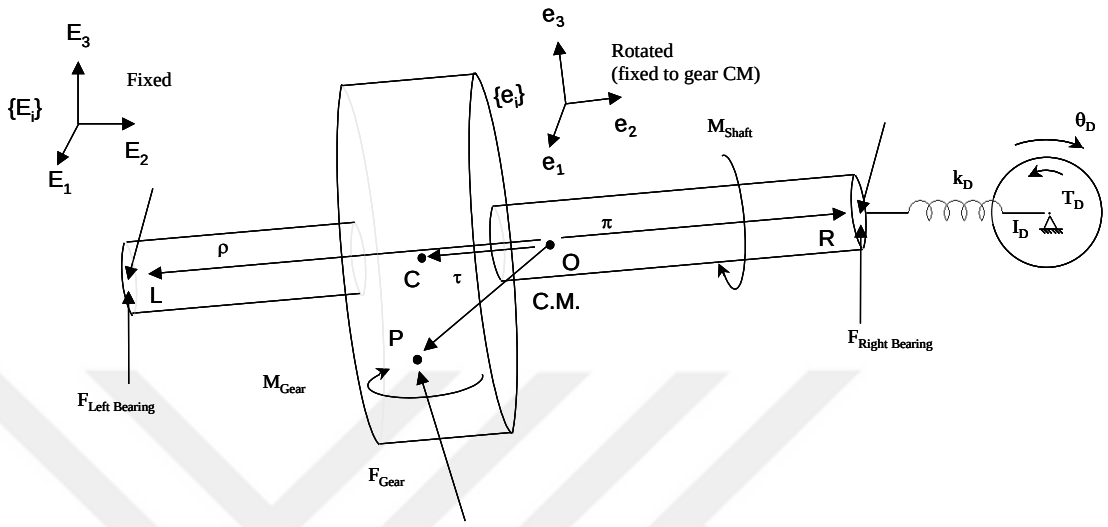


Figure 2.4. Schematic of rigid shaft model. Only pinion shaft is shown.

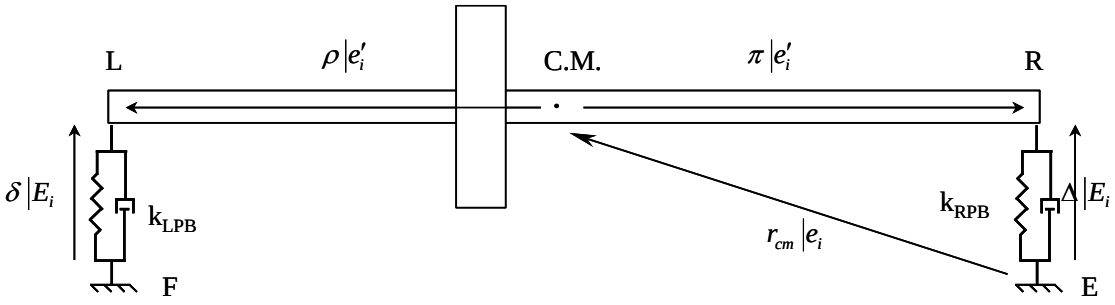


Figure 2.5. Bearing and damper positions for the rigid shaft model. Bearings are fixed to the housing.

Figure 2.4 shows the free body diagram of a geared shaft. The other gear is modeled in exactly the same way.

Figure 2.5 shows the bearings and how they are attached to the housing. Equations of motion are derived for only one shaft, and it is applied to the other gear. Some definitions are:

E: A fixed point on the fixed reference frame. Selected to be the bearing position where it is attached to the housing for simplicity.

O: Center of mass of the geared shaft.

EO: $\vec{r}_{cm}$ Location of mass center of the geared shaft.

EF: $\vec{\gamma}$ Relative distance between two bearings. This distance is fixed.

ER: $\vec{\Delta}$ Right bearing displacement vector.

FL: $\vec{\delta}$ Left bearing displacement vector.

OR: $\vec{\pi}$ Distance to the right bearing location with respect to center of mass.

OL: $\vec{\rho}$ Distance to the left bearing location with respect to center of mass.

OC: Distance to the center of the gear with respect to center of mass.

OP: $\vec{\tau}$ Relative distance between point of contact of gears and the center of mass.

Let $\{E_i\}$ be the fixed frame of reference.

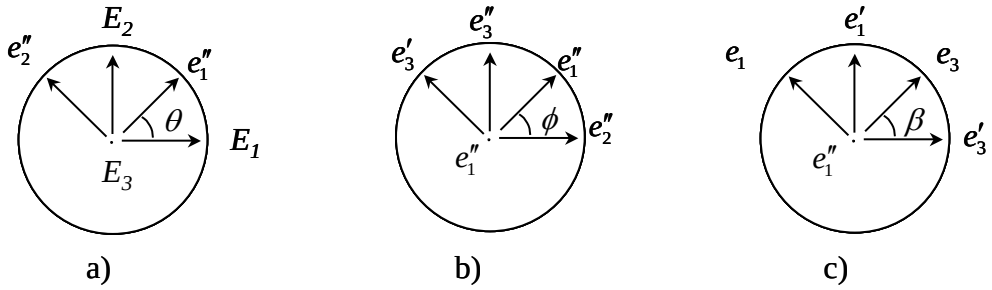


Figure 2.6. Coordinate rotation.

a) Rotate $\{E_i\}$ an angle $\theta$ about $E_3$.

b) Rotate $\{e_i''\}$ an angle $\phi$ about $e_1''$

c) Rotate $\{e_i'\}$ an angle $\beta$ about $e_2'$

Generalized coordinates for rotation are chosen as $\theta$, $\phi$, $\beta$. And for translation, right bearing displacements are used $\Delta_1$, $\Delta_2$, $\Delta_3$ being in the fixed reference frame *{Ei}*.

Here $\theta$, $\phi$, and $\beta$ are variables that are to be solved. Misalignment of shafts can be added to these angles as constants as $\theta_m$, and $\phi_m$Angular velocity can be written as:

$$\omega = \dot{\theta}\, E_i + \dot{\phi}\, e_1'' + \dot{\beta}\, e_2' \tag{2.9}$$

The inertia tensor is:

$$J = \begin{pmatrix} I_{11} & I_{12} & I_{13} \\ I_{21} & I_{22} & I_{23} \\ I_{31} & I_{32} & I_{33} \end{pmatrix} e_i \tag{2.10}$$

And the general form of a stiffness tensor for a bearing is:

$$k = \begin{pmatrix} k_{11} & k_{12} & k_{13} \\ k_{21} & k_{22} & k_{23} \\ k_{31} & k_{32} & k_{33} \end{pmatrix} E_i \tag{2.11}$$

Balance of angular momentum is:

$$\dot{H} = J \cdot \dot{\omega}_{rel}\Big|_{e_i} + \omega \times J \cdot \omega \ , \ \dot{H} = M \tag{2.12}$$

Where $\dot{\omega}_{rel}$ is the relative angular acceleration of the rotating basis $\{e_i\}$, and it is obtained by taking the time derivative of the angular velocity, and converting to $\{e_i\}$ basis.

The total moment acting on the pinion shaft is:

$$\vec{M} = \vec{M}_{Gear} + \vec{M}_{Shaft} + \vec{\tau} \times \vec{F}_{Gear} + \vec{\pi} \times \vec{F}_{RB} + \vec{\rho} \times \vec{F}_{LB} \tag{2.13}$$

Bearing forces $\vec{F}_{RB}, \vec{F}_{LB}$ can also be expanded as:

$$\begin{aligned} \vec{F}_{RB} &= k_{RB} \cdot \vec{\Delta} \\ \vec{F}_{LB} &= k_{LB} \cdot \vec{\delta} \end{aligned} \tag{2.14}$$

Combining (2.12) and (2.13), the balance of angular momentum is written in terms of unknown angles and displacements is:

$$J \cdot \dot{\omega}_{rel}\Big|_{e_i} + \omega \times J \cdot \omega = \vec{M}_{Gear} + \vec{M}_{Shaft} + \vec{\tau} \times \vec{F}_{Gear} + \vec{\pi} \times \left(k_{RB} \cdot \vec{\Delta}\right) + \vec{\rho} \times \left(k_{LB} \cdot \vec{\delta}\right) \tag{2.15}$$

In the same way the sum of forces is written as:

$$\vec{F} = \vec{F}_{Gear} + k_{RB} \cdot \vec{\Delta} + k_{LB} \cdot \vec{\delta} \tag{2.16}$$

Balance of linear momentum is:

$$m \cdot \ddot{\vec{r}}_{cm} = \vec{F} \tag{2.17}$$

However, both $\vec{r}_{cm}$, $\vec{\delta}$ are unknowns and they should be written in terms of the generalized coordinates. From Figure 2.5

$$\vec{r}_{cm} = \vec{\Delta} - \vec{\pi} \tag{2.18}$$

And,

$$\vec{\delta} = \vec{\Delta} - \vec{\pi} + \vec{\rho} - \vec{\gamma} \tag{2.19}$$

Using these, the 6 equations of motion can be finalized as:

$$J \cdot \dot{\omega}_{rel} \big| e_i + \omega \times J \cdot \omega = \vec{M}_{Gear} + \vec{M}_{Shaft} + \vec{\tau} \times \vec{F}_{Gear} + \vec{\pi} \times \left( k_{RB} \cdot \vec{\Delta} \right) + \vec{\rho} \times \left[ k_{LB} \cdot \left( \vec{\Delta} - \vec{\pi} + \vec{\rho} - \vec{\gamma} \right) \right] \tag{2.20}$$

Hence;

$$m \cdot \left( \ddot{\vec{\Delta}} - \ddot{\vec{\pi}} \right) = \vec{F}_{Gear} + k_{RB} \cdot \vec{\Delta} + k_{LB} \cdot \left( \vec{\Delta} - \vec{\pi} + \vec{\rho} - \vec{\gamma} \right) \tag{2.21}$$

These equations need to be written in open form and solved for the generalized coordinates. The open form and the solution is given in Appendix A.

Taking the shaft as rigid is the main assumption of this model. It is possible to have more compliance in the system due to the translational flexibility of the shaft. Moreover, gyroscopic effects can be coupled with translation of the shaft. Another assumption of this model is in the calculation of reaction forces of the bearings. All bearing deformations are assumed to be on the fixed reference frame, which is the housing. So that if the shaft has an angle to the housing, the stiffness matrix decomposes the corresponding displacements in the fixed reference frame and react accordingly. This assumption may hold for small angular displacement of the shaft.

## 2.5 Model for Flexible Geared Shaft

The aim of using a flexible shaft model is to consider the possible coupling between shaft modes and the gear mesh mode. A rigid shaft assumption in the previous model may not be valid in some cases. Furthermore, a flexible shaft model can predict misalignment due to shaft deflection even though there is no dynamic coupling. If this is the case, this model acts as a static deflection model of the shafts.

A flexible shaft can be modeled by finite element methods, or as a continuous system. Previously, the gears and bearings were modeled as a lumped parameter system. Because of this, computational procedure is chosen to be the numerical integration of equations of motion using Runge-Kutta method, as discussed in chapter 4. This choice limits the solution techniques for the flexible shaft, because a simultaneous numerical solution of the complete system is desired. Therefore, equations of motion involving partial derivatives of time and displacement are used. In fact this problem is a boundary value problem with numerical boundary conditions and forcing from gears. Having a predetermined time step from Runge-Kutta method, a semi-discrete solution is necessary. This needs discretizing the PDE in space, but leaving the time variable as continuous. This approach results in a system of ODEs, which can be included in the lumped parameter equations of motion from the gears and bearings. Although this method divides the shaft in discrete points, the result is not a series of corresponding masses and springs, because resulting equations are coupled through the PDE from mechanics of materials.

The Euler equation for a beam with mass of the beam can be written as:

$$EI\frac{\partial^4 y}{\partial^4 x}+m\cdot\frac{\partial^2 y}{\partial^2 t}=f(x,t) \tag{2.22}$$

With boundary conditions:

$$M=\frac{d^2 y}{d\,x^2}=k_t\cdot\theta\,,\ V=\frac{d^3 y}{d\,y^3}=0 \tag{2.23}$$

where $E$ is the modulus of elasticity of the shaft material, $I$ is the moment of inertia of the shaft, $m$ is the mass per unit length of the shaft, $M$ is the moment, $V$ is the shear at the boundary condition, $k_t$ is the torsional stiffness at the boundary condition, and f is the transverse force applied on the shaft at a specified position $x$ and time $t$.

The fourth order central difference equation approximates the fourth derivative as:

$$\frac{\partial^4 y}{\partial^4 x}\approx y_i^4=\frac{1}{h^4}\cdot\left(y_{i+2}-4\cdot y_{i+1}+6\cdot y_i-4\cdot y_{i-1}+y_{i-2}\right)+O\left(h^2\right) \tag{2.24}$$

Third order central difference equation approximates the third derivative, after successive use of Taylor Series expansion as:

$$\frac{\partial^3 y}{\partial^3 x}\approx y_i^3=\frac{1}{h^3}\cdot\frac{3}{8}\cdot\left(y_{i+2}-2\cdot y_{i+1}+2\cdot y_{i-1}-y_{i-2}\right)+O\left(h^2\right) \tag{2.25}$$

Similarly the second order central difference equation is:

$$\frac{\partial^2 y}{\partial^2 x}\approx y_i^2=\frac{1}{h^2}\cdot\left(y_{i+1}-2\cdot y_i+y_{i-1}\right)+O\left(h^2\right) \tag{2.26}$$

At $i=1$:

$$EI\cdot\frac{1}{h^4}\cdot\left(y_3-4\cdot y_2+6\cdot y_1-4\cdot y_0+y_{-1}\right)+m_1\cdot\frac{d^2 y_1}{d\,t^2}=f_1(x,t) \tag{2.27}$$

$$EI\cdot\frac{1}{h^4}\cdot\left(y_4-4\cdot y_3+6\cdot y_2-4\cdot y_1+y_0\right)+m_2\cdot\frac{d^2 y_2}{d\,t^2}=f_2(x,t) \tag{2.28}$$

This is the equation of motion at i=1 and i=2, but there are two unknown points $y_0$, and $y_{-1}$ which does not have a physical meaning. They are eliminated using the boundary conditions.

## 2.6 Summary

Four different mathematical models for dynamic analysis of a gear pair are developed. The model for tooth compliance consists of two rotary disks. The model for gear dynamics includes the torsion of shafts. The model for geared rotor dynamics includes the three dimensional motion of the shafts, and the flexible shaft model considers the bending of the shaft. The assumptions and physical cases where each model might be appropriate are stated for these models. The equations of motion resulting from basic Newtonian mechanics are developed for these models. All four models are used in the LDP. However the model for the forces developed in the gear mesh is not investigated. This is the topic of the next chapter.

# CHAPTER 3

# GEAR MESH MODEL

## 3.1 Introduction

A gear pair encounters resonance close to the torsional mesh natural frequency. Because the main purpose of this thesis is to obtain a three-dimensional dynamic load distribution of gear teeth, properties of the mesh become indispensable. In the previous chapter the properties of the mesh are not investigated, but stiffness is assumed to simplify the models. This chapter is intended to study the forces developed in the gear mesh and to put the model into a form so that it can be combined with the models developed in chapter 2.

## 3.2 Review of mesh force

Many dynamical models are developed to analyze gear pairs and most of them employ a precalculated stiffness for the gear mesh such as the DYTE code [2], and the research by Harianto [7]. Parker et al [5] and Ozguven and Houser [2] has shown that the precalculated stiffness approach agrees well with experiments and finite element analysis.

However, it has been shown that a model with a simple stiffness value for the mesh neglects a number of excitations because; most of the time, number of teeth in contact changes, which is one of the major reasons for the total deflection to change. Therefore, if an equivalent mesh stiffness is obtained, one finds it varying with angular position of the gears. Position varying stiffness in a system usually has more than one resonant frequency because it is possible to represent the excitation as multiple harmonics. Thus, at integer multiples of natural frequency, there is resonance

Deflection due to meshing is also because of profile and lead modifications and other geometrical features such as spacing errors and runout. These errors act as an excitation to the system causing forced vibration response analysis necessary for these inputs. The aim here is to find out the generating mechanisms of forces arising from meshing that affect dynamic analysis. Statically meshing force is constant, but deflections and *TE* (Transmission Error) are functions of:

- $T_{Load}$ (Load Torque): Load torque applied to the gear pair,
- $\beta$ (Roll Angle): The angular position for the contacting teeth in a mesh cycle, which is also referred as POSCON number.
- $CD_{error}$: Center distance error,
- $\phi_1$, $\phi_3$ (Angular Misalignment): The misalignment in two possible rotational degrees of freedom excluding rolling, which may be due to mounting or shaft and/or bearing deflections.

There are many other gear and material parameters, but the above ones vary in time if a dynamical analysis is done. In addition to a mesh force, there is also a reaction

moment if a misalignment exists. Therefore, the output from a mesh can be listed as a force and a moment;

- $M_1$ ,$M_3$: Moments in three dimensions, other than driving moment,
- $F_{mesh}$: Meshing force acting in the line of action.
- $k_{mesh}$: Mesh stiffness that relates the meshing force with transmission error.

It is realized that the transmission error is not a pure function of mesh stiffness because deflection of gear teeth is nonlinear.

### 3.3 Model for Mesh Force

For the purpose of modeling, it is necessary to express the mesh as a spring and a displacement excitation. Some previous models used the displacement excitation as a representation of gear errors. That approach assumes, in case there are no modifications, the transmission error is given by the spring deflection. This is an approximation because of the nonlinearity of mesh stiffness. In other words, not all deflection is because of mesh stiffness change, but because of nonlinearity in base rotation, shear, translation, and Hertzian deflection. To clarify the use of stiffness and displacement excitation consider the simple dynamic model of a gear pair.

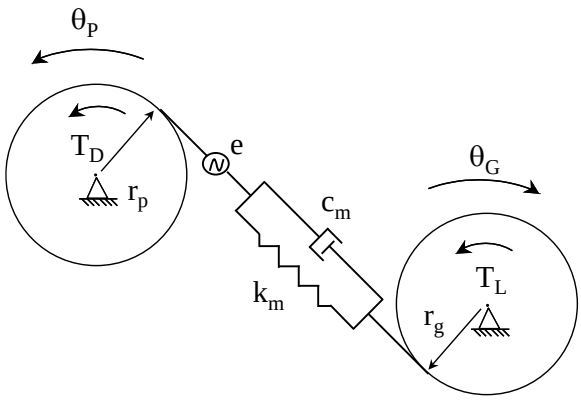


Figure 3.1. Model of tooth stiffness for dynamic analysis.

Equations of motion for the above system are:

$$\begin{aligned} \ddot{\theta}_P \cdot I_P &= T_D - \left(\theta_P \cdot r_p - \theta_G \cdot r_G - e\right) \cdot k_m \cdot r_P \\ \ddot{\theta}_G \cdot I_G &= -T_L + \left(\theta_P \cdot r_p - \theta_G \cdot r_G - e\right) \cdot k_m \cdot r_G \end{aligned} \tag{3.1}$$

where transmission error is defined by:

$$TE = \theta_P \cdot r_P - \theta_G \cdot r_G \tag{3.2}$$

At static equilibrium:

$$TE = STE \text{ , and } \ddot{\theta}_P = 0 \text{ , } \ddot{\theta}_G = 0 \tag{3.3}$$

Then:

$$\frac{T_D}{k_m \cdot r_G} = \theta_P \cdot r_P - \theta_G \cdot r_G - e \tag{3.4}$$

Using (3.3):

$$e = STE - \frac{T_D}{k_m \cdot r_P} \tag{3.5}$$

Here the displacement excitation *e* represents both profile errors, and gear errors in general, and nonlinearity in displacement. By this way, the equilibrium point of the gear pair in terms of transmission error is the static transmission error. This would be an expected result because if suddenly rotary motion of gears were stopped, the vibrations will die out and come to equilibrium at static transmission error. Substituting (3.5) into (3.1) where $\ddot{\theta}_P \neq 0$ gives:

$$\begin{aligned} \ddot{\theta}_P \cdot I_P &= T_D - F_{mesh} \cdot r_P \\ \ddot{\theta}_G \cdot I_G &= -T_L + F_{mesh} \cdot r_G \end{aligned} \tag{3.6}$$

Where meshing force is given by:

$$F_{mesh} = \left( \theta_P \cdot r_p - \theta_G \cdot r_G - STE + \frac{T_D}{k_m \cdot r_P} \right) \cdot k_m \tag{3.7}$$

Equations of motion can be simplified further as (3.8). This kind of approach is employed in [2] and the computer code DYTEM developed with the paper.

$$\begin{aligned} \ddot{\theta}_P \cdot I_P &= \left(STE - TE\right) \cdot k_m \cdot r_P \\ \ddot{\theta}_G \cdot I_G &= -\left(STE - TE\right) \cdot k_m \cdot r_G \end{aligned} \tag{3.8}$$

However, this reduction is possible if load varying stiffness and static transmission error change is neglected. That is: $k_m = k_m\left(F_{mesh}\right)$, and $STE = STE\left(F_{mesh}\right)$. Here $F_{mesh}$ is the dynamic loading. Mesh stiffness and force are dependent on dynamic loading because the deflection of gear teeth itself is nonlinear. Predominantly Hertzian contact tends to get more compliant with increasing loads. In addition, a decreased loading in perfect involute gears can cause a decrease in contact ratio, which changes the general shape of both mesh stiffness and static transmission error. These dependencies are not

very amplified in perfect involute gears excluding the possibility of corner contact, and therefore can be ignored. But when optimized profiles are of concern, the peak-to-peak value of the dynamic transmission error might vary considerably from the static transmission error. Figure 3.2 and Figure 3.3 show the transmission error and mesh stiffness dependence on torque and roll angle. This gear pair is optimized for 1660 in-lb, so that at that torque value, there is a very small peak-to-peak transmission error. Also, due to corner contact, the increase in contact ratio with higher loads can be seen from mesh stiffness values. Although at static analysis peak-to-peak transmission error is almost zero, dynamically this may not be the case. Because an increase of loading due to dynamical effects can change the mesh stiffness values, and the POSCON at which the number of teeth are in contact. Also dynamic loading can affect the transmission error, because the gear pair may not be running at the optimized torque always and this instantaneous torque can change deflection of the shaft. If the torque dependence is taken into account, then (3.7) needs to be modified so that the deflection is not double counted.

$$F_{mesh} = \left( 2 \cdot \theta_P \cdot r_p - 2 \cdot \theta_G \cdot r_G - STE + \frac{T_D}{k_m \cdot r_P} \right) \cdot k_m$$

$$TE = 2 \cdot \theta_P \cdot r_p - 2 \cdot \theta_G \cdot r_G \tag{3.9}$$

Mesh deflection is from STE and Kmesh both. Hence resulting TE is double the actual value, which is compensated in (3.9).

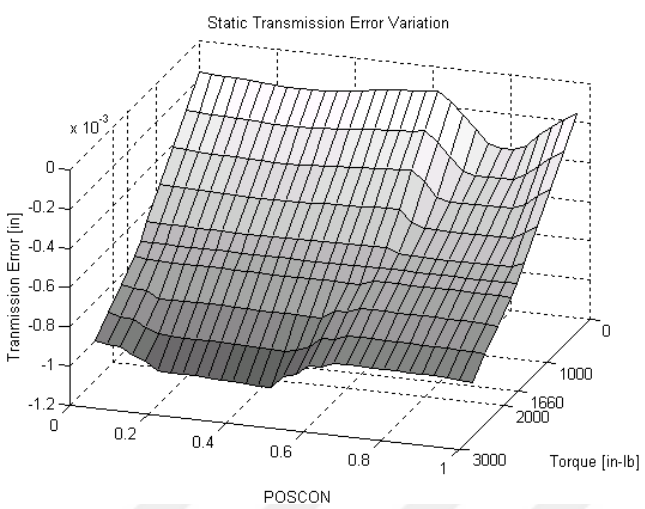


Figure 3.2. Transmission error variation with mesh position and torque for an optimized gear set for transmission error at 1660 in-lb.

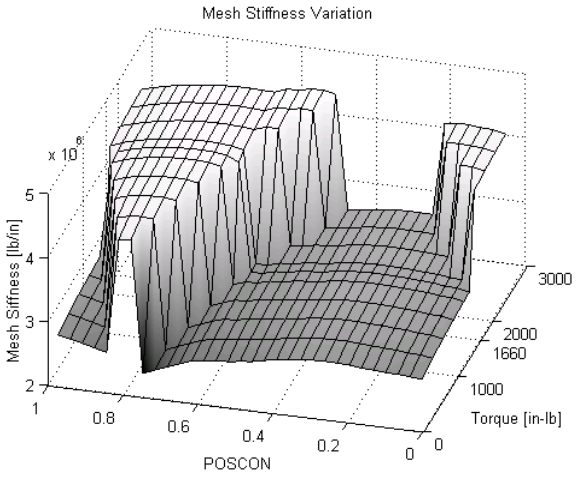


Figure 3.3. Mesh stiffness variation with mesh position and torque for an optimized gear set for transmission error at 1660 in-lb.

Figure 3.5 and Figure 3.4 show mesh stiffness variation and transmission error for a perfect involute gear set, which is the unmodified version of the previously discussed set. It can be observed that the mesh stiffness variation is almost negligible with load torque. So that dynamic loading is unlikely to change mesh stiffness. Also transmission error varies less than that of the optimized set. Therefore, unmodified gear sets are not expected to show different results whether *STE* and $K_{mesh}$ dependence are evaluated or not. But, *STE* and $K_{mesh}$ dependence are expected to change the response of the optimized sets.

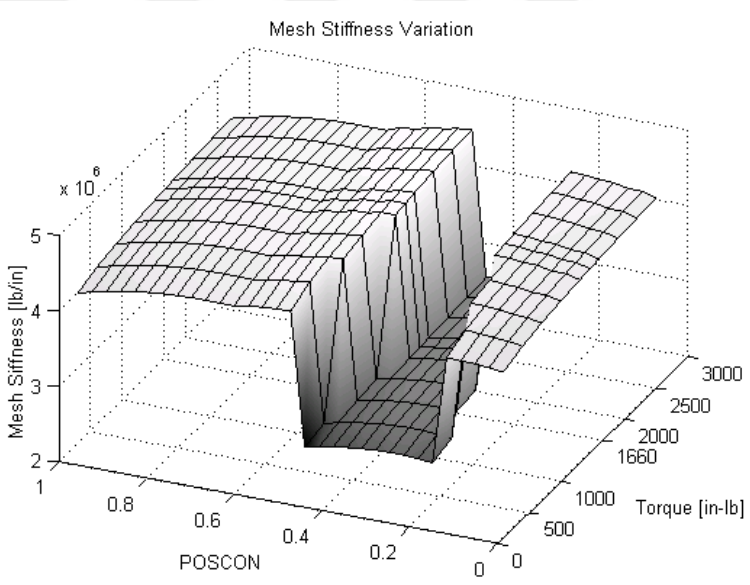


Figure 3.4. Mesh stiffness variation with mesh position and torque for a perfect involute gear set.

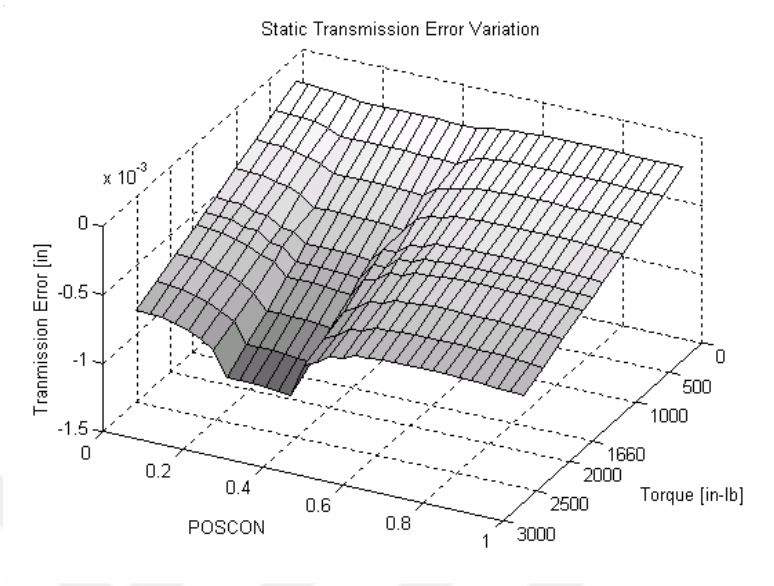


Figure 3.5. Transmission error variation with mesh position and torque for a perfect involute gear set.

For the program developed (3.7) is used with the instantaneous values mesh stiffness $k_m$ and static transmission error *STE*, which are obtained from LDP subroutine. It can also be viewed as the linear spring damper model with the cam excitation defined as in (3.5).

## 3.4 Summary

A qualitative discussion of mesh force in gears is given. An equivalent vibratory model is used to approximate the mesh force using given results from experiments or LDP. This model is suited in the previous models developed in chapter 2 for the gear pair and combined to form a complete model. The procedure in combining the mesh model along with the vibratory model and solution is given in the next chapter.

# CHAPTER 4

# IMPLEMENTATION IN LDP

## 4.1 Introduction

In this chapter a short review of the approach of the Load Distribution Program (LDP) is given and a method for implementing the previously developed dynamic models in LDP is discussed. A solution method for the equations of motion in the time domain is sought in connection with LDP. In addition, friction, shuttling force and moment are studied.

## 4.2 Review of LDP Analysis

The load distribution calculation of a gear pair in LDP is based on the analysis of general elastic bodies in contact by Conry and Seireg [4]. The first step is the calculation of possible contact zones using the geometry of the gears. Possible contact zone is divided into discrete points. Depending on the driving torque, a constant total meshing force is required. The mesh deflection is required to obtain the load distribution. The deflection in the contact zone satisfying the load is iterated until the deflection from influence coefficient matrix satisfies the separation constraint. The influence coefficient matrix is also referred to as compliance matrix and it specifies

the deflection for each contact point due to a force at any point. Therefore, forces at discrete contact points are calculated, and they constitute the load distribution on gear teeth. A study involving the base rotation and deflection of gears has been conducted by Yau [8] and this approach was incorporated in LDP analysis. Another output is the transmission error, which is the total rigid body motion of the gear set due to deflections of gear teeth and gear body. Any profile and lead modifications are treated as initial separation in contact analysis. The rigid body deflection comprises three parts:

1) Hertzian Deflection
2) a) Tooth Deflection due to Shear force
   b) Tooth deflection due to bending moment
3) a) Base Rotation due to Bending Moment
   b) Base Rotation due to Shear Force
4) a) Base Translation due to Bending Moment
   b) Base Translation due to Shear Force

Hertzian deflection and base translation and rotation are determined by analytical expressions. Detailed analysis of base flexibility and its application to LDP can be found in the thesis by Stegemiller [18]. The tooth deflection calculation however, requires a numerical solution technique, where a theoretical background of it can be found in the thesis by Yakubek [19]. In LDP tooth deflections are calculated using Rayleigh-Ritz method for gear tooth modeled as flat or tapered beams.

There are three conditions that need to be satisfied for the above calculated deflections and forces to exist. These are condition of compatibility, condition of equilibrium and condition for contact.

Condition of contact can be summarized as:

$$w_i^1 + w_i^2 + \delta_i - r_b \cdot \theta \geq 0 \tag{4.1}$$

Where $w_i^1$, and $w_i^2$ are total deflection of a point *i*. 1, and 2 represent the pinion and gear respectively. $\delta$ is the initial separation from gear errors, and $r_{b,}$. $\theta$ is the rigid body motion. This condition ensures that rigid body motion is at least equal to the deflection and separation of gear teeth for contact to occur. For all possible contact points:

$$[C]\cdot[F]+[\delta]-I\cdot r_b\cdot\theta \geq 0 \tag{4.2}$$

Here *[F]* is the force vector with forces of discrete points of contact, and *[C]* is the corresponding compliance matrix. It is the result from the deformation calculations mentioned above.

Condition of equilibrium states that the total contact force should be equal to the driving torque on the pinion. This condition holds for the static case, and it is not valid for a dynamic case, because there are additional dynamic loads involved.

Condition of equilibrium for static case:

$$[F]^T \cdot I \cdot r_b = T_D \tag{4.3}$$

This is modified for a dynamic case by replacing the driving torque by an instantaneous dynamic torque on pinion.

$$[F]^T \cdot I \cdot r_b = M_{P2} \tag{4.4}$$

The subscript 2 stands for the direction of the instantaneous torque in the three dimensional model developed in chapter 2.

Condition for contact is the modified form of condition of compatibility with the inequality replaced by an equality to make it possible to solve the equations. It can be stated as:

$$[C]\cdot[F]+[\delta]-I\cdot r_b\cdot\theta+[Y]=0 \tag{4.5}$$

This equation is solved in LDP using several iterations in a modified simplex algorithm.

## 4.3 Determination of Forces and Moments in Gear Mesh

### 4.3.1 *Mesh stiffness*

From the analysis embedded in LDP the mesh stiffness is nonlinear. It is not possible to obtain the mesh stiffness with directly dividing the mesh force to transmission error. This is because gear mesh tends to get stiffer with higher loads. Also suppose there are profile errors on a hypothetical gear pair in which there are always same number of teeth in contact. This gear pair has almost same stiffness for all roll angles but, variable transmission error because of profile errors. A ratio of mesh force to transmission error will be highly erroneous for mesh stiffness in this case. For each position LDP can linearize the deflection force curve and provide mesh stiffness.

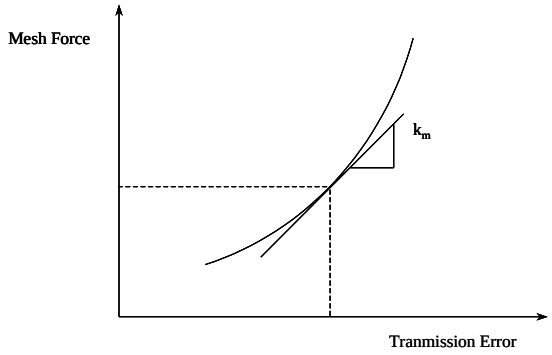


Figure 4.1. Calculation of mesh stiffness in LDP for a given mesh force.

This is done in LDP up to some accuracy with finite differences instead of derivatives, because there are no analytical expressions to differentiate, but numerical values. Once a stiffness value is obtained, expressions in the chapter 3 are used to get the mesh force.

### 4.3.2 *Mesh Forces and Moments*

There are two other reactions from the possible unequal load distribution and friction forces. In the three dimensional model, these inequalities in load distribution and friction force result in moments. Since the load distribution is known, moments can be calculated:

$$[M_1] = [h_1] \cdot [F] \tag{4.6}$$

$$[M_3] = [L] \cdot [F_{Fric}] \tag{4.7}$$

Where, $M_1$ and $M_3$ are the resulting moments, $h_1$ is the distance of the discrete tooth force to the center of the face width, and $L$ is the distance of the friction force from the

gear reference frame. This calculation reduces the vector of load distribution and vector of friction force to an equivalent forces and moments without loss of generality.

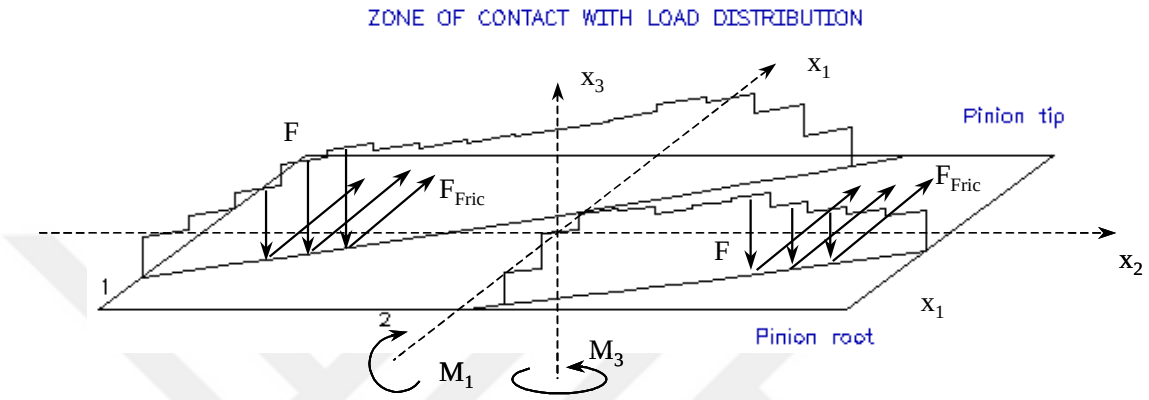


Figure 4.2. Superimposed load distribution and friction forces of two teeth of a helical gear.

Figure 4.2 shows the load distribution and some of the discrete forces from load distribution and friction force vector. All forces are assumed to be in the line of action except friction forces. Friction forces are perpendicular to lead direction and line of action. All contacting surfaces of the gear pair are projected on the involute plane, which is composed of the face width direction and the profile direction. Although the profile direction is a curve rather than a straight line, given by the conjugate action, there is no assumption when all forces are considered in this plane. This is because mesh forces are always parallel to the line of action direction, which does not change direction. It must be noted here that $x_1$, $x_2$, and $x_3$ are the coordinates of the fixed reference frame of the corresponding gear, but they are carried to gear teeth for easy

intuition of direction of forces and moments. In fact the origin is in the center of the corresponding gear, not in the teeth as the figure may imply.

### 4.3.3 *Friction Force*

Friction between gear teeth has been investigated, but efforts have been mostly towards the determination of the coefficient of friction. Iida et al [20] investigated the vibrations of gear pairs excited by friction force. Ishida [21] investigated the noise due to friction force and concluded that noise due to friction is highest at the pitch point, where sliding velocity is zero and changes direction. Hochmann [22] performed a detailed study on friction force excited vibration of gears and energy loss due to friction. Velex and Cahouet [12] developed a three-dimensional model for a gear set and computed load distribution. They evaluated the friction force with various models and reported that friction force excites the system at low operating speeds.

The simplest friction model is the Coulomb friction, which suggests constant friction force, and its sign depending on the relative motion between mating surfaces. Any more complicated model than coulomb friction requires also the relative sliding velocity of gear teeth. From [23] the sliding velocity of a contact line is equivalent to

(4.10)

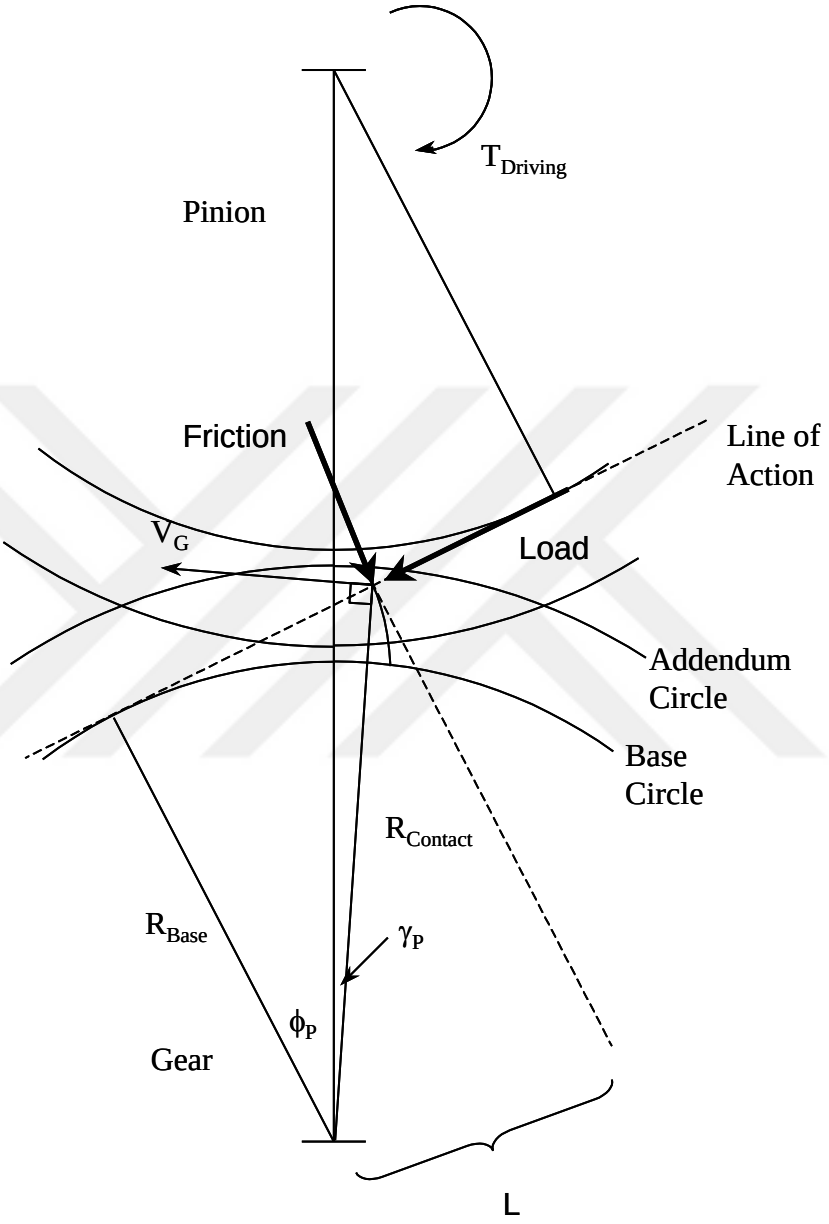


Figure 4.3. Translational velocity of gear at the contact point and the moment arm for friction force.

A way to calculate sliding velocity is to calculate the velocity of each contact point in LDP. The vectoral difference of the speed of each contact point in pinion and gear gives the sliding velocity for each point. The radius of a contact point is calculated in LDP as $R_{Contact}$. Figure 4.3 shows a schematic of a gear pair and a contact point. From the reference frame of the pinion and gear, the absolute velocity is:

$$\vec{v}_G = \vec{R}_{Contact} \times \vec{\omega}_G \tag{4.8}$$

From geometry vector components are:

$$v_{Gx} = |\vec{v}_G| \cdot \cos(\gamma),\ v_{Gy} = |\vec{v}_G| \cdot \sin(\gamma) \tag{4.9}$$

For each contact point, sliding velocity is:

$$v_{Sliding} = \sqrt{(v_{Px} - v_{Gx})^2 + (v_{Py} - v_{Gy})^2} \tag{4.10}$$

In the Coulomb friction model the product of the constant friction coefficient with friction force in the line of action per face width division gives the friction force per face width division. For helical gears, load at each point is different so that the summation is necessary. In spur gears force can be extended to the active face width without summing.

$$F_{fric} = \sum_i \mu_i \cdot F_{ni} \tag{4.11}$$

According to Merritt [17] coefficient of friction is affected by the lubrication properties, surface roughness, and hence lube film thickness. An equivalent friction coefficient takes into account the radius of curvature, viscosity of the lubricant and sliding velocity. The work of Benedict and Kelley is referred for the expression of a friction coefficient:

$$\mu = \frac{1.6}{\upsilon^{0.15} \cdot \left(\frac{V_e}{V_s}\right)^{0.15} \cdot V_s^{0.5} \cdot R_r^{0.5}} \tag{4.12}$$

Where ν is the viscosity of the oil in centistokes, $R_r$ is the radius of curvature of the contact, $V_s$ is the sliding velocity, and $V_e$ is the entraining velocity, all in feet, and minutes. Entraining velocity is defined as:

$$V_e = \frac{\omega_p \cdot r_p + \omega_g \cdot r_g}{\cos(\psi)} \cdot \sin(\varphi_n) \tag{4.13}$$

Radius of curvature can be calculated at the contact point:

$$R_r = \frac{r_p \cdot r_g}{r_p + r_g} \cdot \frac{\sin(\varphi_n)}{\cos^2(\psi)} \tag{4.14}$$

This allows the calculation of μ for each division in the face width. (4.11) is then used to evaluate the total friction force acting on the gear teeth. Merritt [17] limits the use of (4.12) up to $\mu=0.2$ since this equation is empirical.

### 4.4 Runout Model

Gears cannot be manufactured as perfect disks. A deviation in the centerline of gears exists and categorized with AGMA runout quality. Runout in gears adds a sinusoidal component on the static transmission error because the center distance is not constant but periodic for each shaft rotation. For runout caused by mounting error the frequency is one revolution. Whereas, for runout due to injection molding process of plastic gears, the frequency depends on gating and material. Runout can be modeled equivalently by successive spacing errors also. Wijaya [24] has studied the effect of runout of various AGMA quality gears using the equivalent spacing error approach.

Here, the spacing error is assumed to be harmonic and a corresponding center distance variation is given to pinion and gear as follows:

$$CD_{err} = (x_{P3} - x_{G3} + x_{PR3} - x_{GR3}) \cdot \sin(\varphi) + (x_{P1} - x_{G1} + x_{PR1} - x_{GR1}) \cdot \cos(\varphi) \tag{4.15}$$

Where the runout is simply defined by cyclic variation as:

$$\begin{aligned} x_{PR3} &= \frac{R_P}{2} \cdot \sin(\beta \cdot \omega_{PR}) \quad , \quad x_{PR1} = \frac{R_P}{2} \cdot \cos(\beta \cdot \omega_{PR}) \\ x_{GR3} &= \frac{R_G}{2} \cdot \sin(\beta \cdot \omega_{GR} + \theta) \quad , \quad x_{GR1} = \frac{R_G}{2} \cdot \cos(\beta \cdot \omega_{GR} + \theta) \end{aligned} \tag{4.16}$$

(4.15) represents the center distance variation from shaft displacements and runout in LOA and O-LOA directions. $\omega_{PR}$ and $\omega_{GR}$ represent the frequency of runout and $R_P$, $R_G$ represent the magnitude of the runout in displacement units and $\theta$ is the phase difference. This magnitude is defined as the peak-to-peak variation in the position of the pitch point per runout frequency. In this model, runout does not cause unbalances so although in real life it can. For unbalances the inertia matrix needs to be modified separately.

### 4.5 Numerical Solution of the Problem

Depending on the vibratory model used for the gear pair there is a maximum of 97-second order nonlinear ordinary differential equations that needs to be solved. A numerical solution becomes necessary because of the time varying properties of the static transmission error, mesh stiffness, and reaction moments. Secondly, the three-dimensional rigid shaft model includes trigonometric nonlinearities due to coordinate transformations. For general solution of these equations of motion, Runge-Kutta method of order four is used with a fixed step size. Since Runge-Kutta methods are for

solution of first order systems, second order equations are expanded to 194 first order differential equations. The gear mesh forces and moments are evaluated using the existing LDP subroutines. Therefore, it is necessary to combine outputs of LDP with the equations of motion. Although a quantitative analysis was not conducted, it is observed that a calculation for a position in LDP takes longer CPU time than one step of the Runge-Kutta method. The time difference for obtaining solution between the two components is high and the number of equally spaced positions in LDP governs the total CPU time for an analysis. Because of this reason, the number of equally spaced positions (POSCON) is limited, and the Runge-Kutta solution is allowed to take steps in between two positions. Figure 4.4 helps to clarify the explanations below.

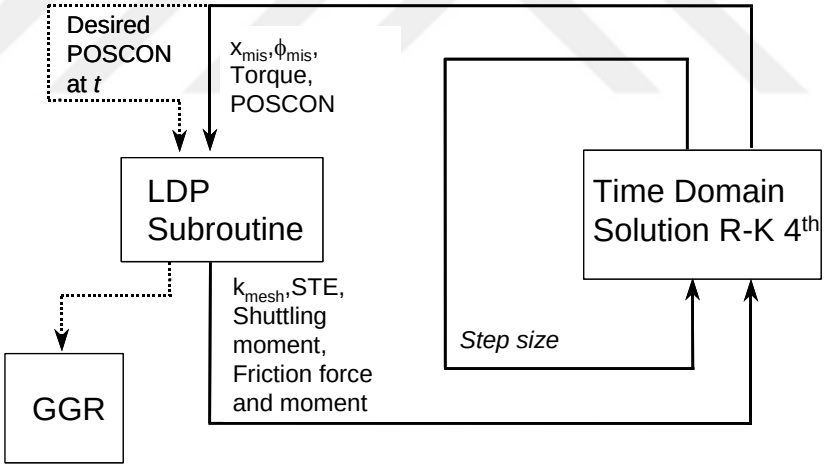


Figure 4.4. Diagram of the time domain solution method in LDP.

During the time passed between the calculations of two POSCONs the Runge-Kutta method needs more than one step in order to converge. To avoid excessive simulation time, the mesh stiffness is assumed to be constant between two POSCONs and

equations of motion continue to evaluate the solution. It is possible not to use mesh stiffness, but to keep the forces constant between two POSCONs. This can result in inaccuracies if not enough POSCONs are used. However other reactions such as friction force and moments are kept constant, because stiffness values for these reactions are not available. Few POSCON number should be used when the rotational speed of the gears are high. If the period of the POSCON is defined as the time it takes for each POSCON to pass, then;

$$\omega_p = \frac{2 \cdot \pi}{T_P}, \qquad \omega_n : \text{Natural Frequency.} \tag{4.17}$$

$$\omega_p >> \omega_n \tag{4.18}$$

This is the approximate condition to eliminate the effect of step response. Otherwise the frequency content from the step changes in mesh stiffness and transmission error is low enough to appear in the range of gear mesh frequency, and orders.

### 4.6 Summary

Since the equations of motion for the gear pair are in time domain and forcing terms are only numerically available, a Runge-Kutta solution method is used to implement the models into LDP. The flow in LDP is modified so that, time dependent variables change during the simulation. This allows LDP to perform dynamic analysis in time. A discussion of friction force between gear teeth is given. A model for friction force is implemented in LDP analysis. An expression to calculate shuttling forces and moments is given and these forces along with friction are connected to the dynamic model in LDP.

# CHAPTER 5

# COMPARISONS AND STUDY OF EXCITATION IN GEARED SHAFTS

## 5.1 Introduction

In the previous chapters four models for vibration of geared shafts have been developed and the models are implemented in LDP. This chapter first compares this code and other models for gear pairs. Next the effect of dynamic loading on the response is studied and results from an optimized gear set with the dependence and without the dependence are compared. Last, the effect of transmission error force, shuttling force and friction force on the response of dynamic bearing forces are investigated.

## 5.2 Comparisons with Calyx

### 5.2.1 *High Contact Ratio Spur Gear Set 1*

Before studying the more complicated problem, it is desirable to start from a simple case and compare the dynamics of simple gear pairs. The model for meshing between gears that has been developed in chapter 3 is slightly different from the traditional lumped parameter models because it considers the transmission error as a function of

not only position, but also mesh force, center distance, and misalignment. Since the equivalent cam excitation involves the static transmission error itself, and the static transmission error is a function of the variables mentioned above, it is not very straightforward to estimate the actual stiffness. In other words, it may be possible that, the stiffness is double counted. Experiments were carried out on very stiff bearings and shafts so that the torsional meshing mode is isolated from bearing and shaft modes. Research by Parker et al. [5] shows that these experiments match the results obtained using Calyx, which is a finite element contact mechanics computer program specialized in gears of any kind. To evaluate the meshing model in this chapter, Calyx is taken as a reference. However, for a dynamic comparison, the two models for contact, namely LDP and Calyx should be matching. For instance, the mesh stiffness and transmission error predictions in static case should match. Usually gears have rims that are large diameters when compared to tooth length. LDP analysis has been extended to cover rims, but the program has not been fully functional to be used by end users. For this reason the current LDP model that assumes the rim has no compliance is used in the analysis, although inertias due to rim are calculated. The gear pair used in the following analysis, from a deformation point of view has no rim, but has the inertia of the rim. Although this case may be physically difficult to reproduce, it is suited well for comparisons, because added inertia decreases the resonant frequency, hence reducing computational effort. The parameters of the gear pair are listed in Table 5.1. The finite element model created by Calyx is shown in Figure 5.1. The stiffness and inertia values for shafts and bearings are used depending

on the model chosen. The spur gear set used in analysis has no profile modifications. LDP and Calyx seem to agree on mesh stiffness and transmission error for this case. The comparison of transmission error and mesh stiffness from both models is shown in Figure 5.2 and Figure 5.3 respectively.

| | Pinion | Common | Gear |
|---|---|---|---|
| Number of teeth | 28 | | 28 |
| Center Distance [in] | | 3.5 | |
| Diametral Pitch [in] | | 8 | |
| Pressure Angle | | 20 | |
| Outside Diameter [in] | 3.75 | | 3.75 |
| Root Diameter [in] | 3.1875 | | 3.1875 |
| Inner Diameter for Calyx [in] | 2.625 | | 2.625 |
| Face Width [in] | | 0.25 | |
| Theoretical Contact Ratio | | 1.64 | |
| Pinion Torque [in-lb] | | 1128 | |
| Pinion Speed | | 2.143 rpm | |

Table 5.1. Gear set parameters

| | Pinion | Gear |
|---|---|---|
| Inertia [in-lb-s$^2$] | $0.27.10^{-2}$ | $0.27.10^{-2}$ |
| Mass [lb-s$^2$/in] | $0.176.10^{-2}$ | $0.176.10^{-2}$ |
| Drive Inertia [in-lb-s$^2$] | 0.021 | 0.021 |
| Shaft Stiffness [in-lb/rad] | 100000 | 200000 |
| Shaft Damping Ratio | 0.06 | 0.06 |
| LOA Bearing Stiffness [in-lb-s$^2$] | 2000000 | 2000000 |
| O-LOA Bearing Stiffness [in-lb-s$^2$] | 2000000 | 2000000 |
| Axial Bearing Stiffness [in-lb-s$^2$] | 10000000 | 10000000 |
| Bearing Damping [lb-s/in] | 10 | 10 |
| Mesh Damping Ratio | 0.06 | |

Table 5.2. Dynamic parameters.

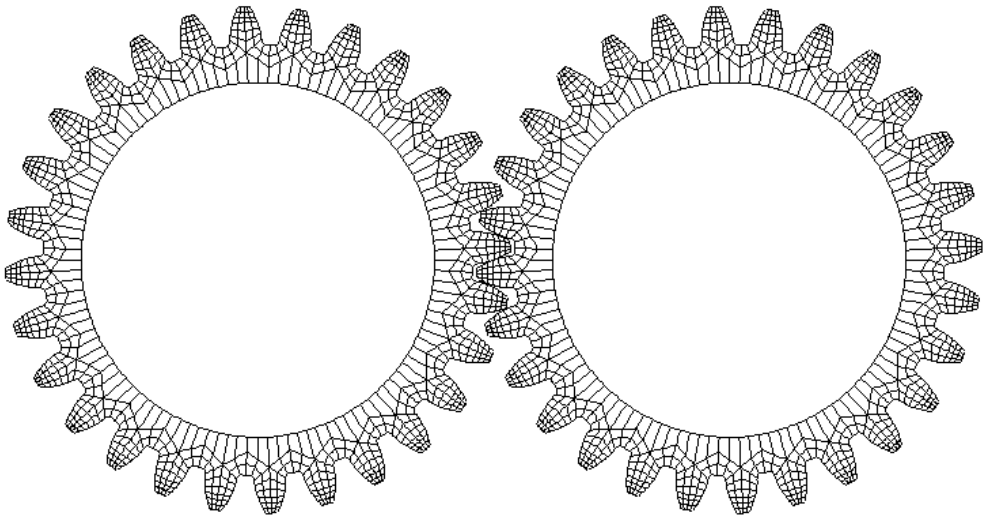

Figure 5.1. Finite element model of the gear set in Calyx.

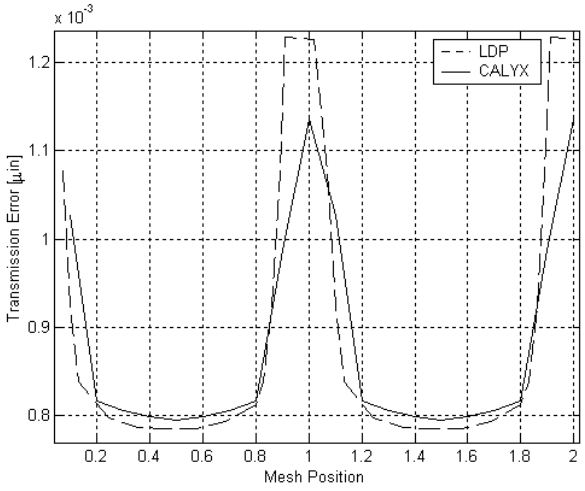


Figure 5.2. Static transmission error from LDP and Calyx.

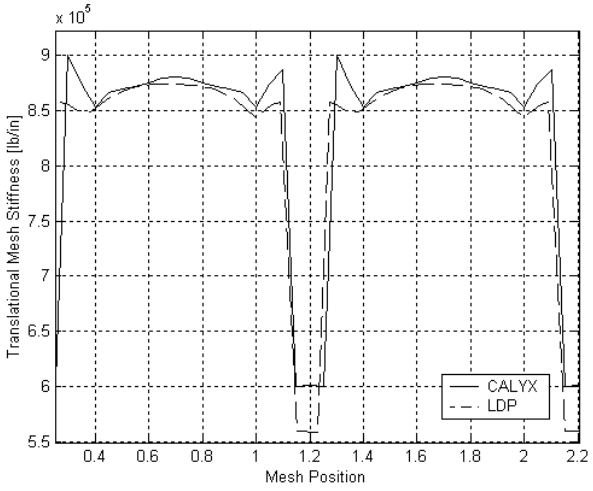


Figure 5.3. Mesh Stiffness from LDP and Calyx

The stiffness in LDP is calculated by the linear approximation at the load torque. For modified gears it is possible to obtain a different value for stiffness if the static transmission error is divided by the torque. Since the contact area gets wider with torque, mesh stiffness gets higher with load torque. The oscillations take place at the mean torque value, therefore (5.1) is used to estimate the linearized mesh stiffness from Calyx.

$$k_{mesh} = \frac{T_2 / r_{pb} - T_1 / r_{pb}}{STE_2 - STE_1} \tag{5.1}$$

Here subscripts 1 and 2 correspond to load torques where $T_1$=1128 in-lb, and $T_2$=1228 in-lb. Next dynamic analysis in Calyx and LDP are conducted at 2000 rpm. In Calyx, a time step of 2.14e-6s has been used to result in a frequency resolution of 233,329 Hz to make sure that the resonant frequency is below frequency resolution. The time histories for transmission error are given in Figure 5.4. It can be observed that the

mesh natural frequency for the high stiffness region, which corresponds to the two teeth contact region, is higher than the parametric mesh excitation. The simple lumped parameter model for this system has been shown to reduce to a single DOF system with the natural frequency being given by (5.2). The model used in Calyx fixes the gear rotation; hence in LDP very high gear inertia is used to reach this effect. (5.2) reduces to (5.3). Substituting values and taking average stiffness at two teeth contact region from Figure 5.3 as 8.6e5 lb/in natural frequency is found as; ω=4970 Hz. From Figure 5.4 the damped natural frequency in this region can be calculated from the period of oscillations as ω=4796 Hz from LDP. Calyx model has the frequency ω=4975 Hz by the same way.

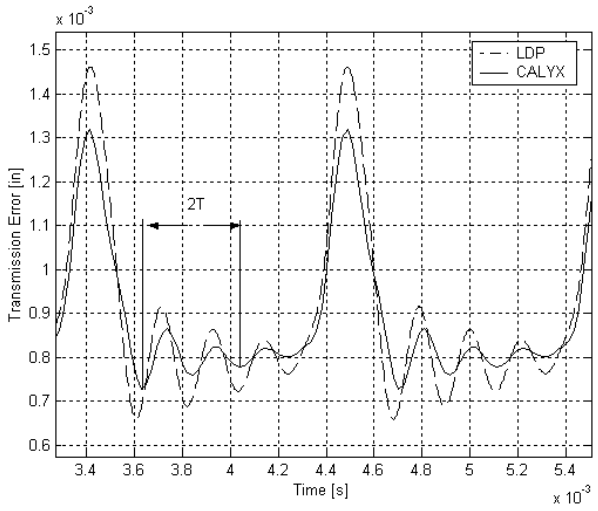


Figure 5.4. Time histories for transmission error from LDP and Calyx for 2000 rpm.

$$\omega = \sqrt{k_m \cdot \frac{I_G \cdot {r_P}^2 + I_P \cdot {r_G}^2}{I_P \cdot I_G}} \tag{5.2}$$

$$\omega = \sqrt{k_m \cdot \frac{{r_P}^2}{I_P}} \tag{5.3}$$

The frequency of oscillations from LDP and the lumped model match within 4%, and Calyx almost exactly matches. Of course these values are approximate due to the accuracy of readings. Both programs are run for speeds of 7000 rpm, and 12000 rpm, and the time histories for transmission error are shown in Figure 5.5, and Figure 5.6.

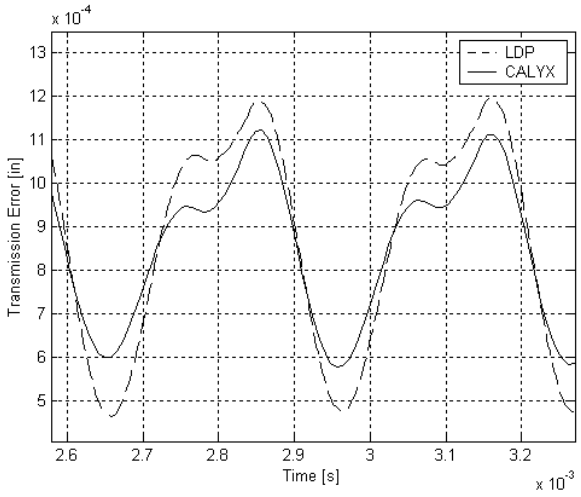


Figure 5.5. Time histories for transmission error from LDP and Calyx for 7000 rpm.

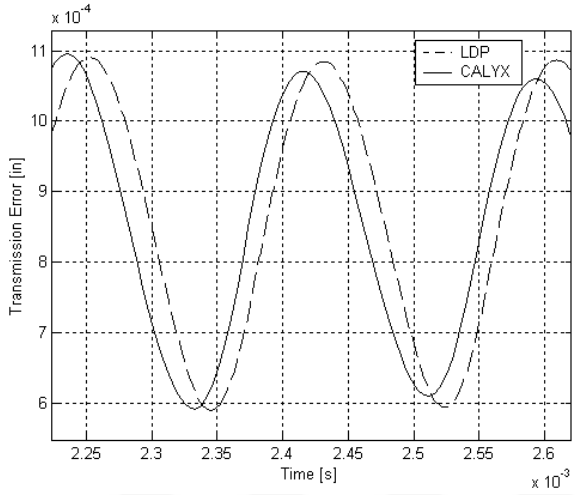


Figure 5.6. Time histories for transmission error from LDP and Calyx for 12000 rpm.

As a comparison, in both LDP and Calyx the gear set is loaded in with a step force at two teeth in contact region. In both models gear is held constant and pinion is allowed to rotate. The transmission error is shown in Figure 5.7. The natural frequencies are calculated as 4662Hz for LDP and 4767Hz for Calyx. Finally a speed sweep was performed in Calyx and LDP from 1000 rpm to 17000 rpm. The peak to peak value of transmission error is plotted in Figure 5.8. It can be seen that the superharmonic resonances $f_m/3$, $f_m/2$ and the primary resonance $f_m$ occurs nearly at the same frequencies. The values however do not match because of different damping in models.

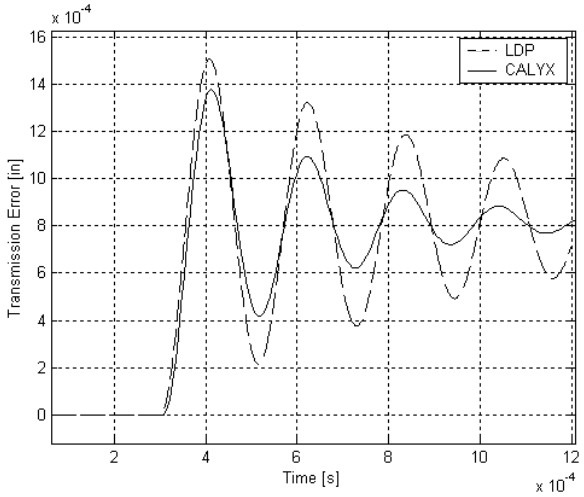


Figure 5.7. Transmission error response to step forcing.

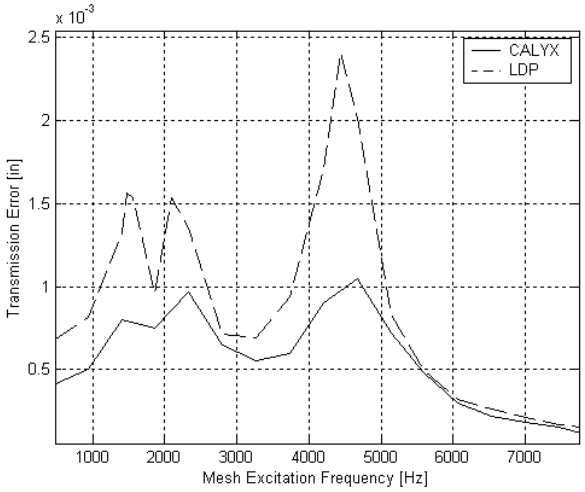


Figure 5.8. Peak to peak value of transmission error for speed runup.

### 5.2.2 *Low Contact Ratio Gear Set*

The previous gear set has two teeth in contact most of the time. It is desirable to repeat some of the analysis within one tooth in contact region. For this purpose the outer diameter of the gear set given in Table 5.1 has been trimmed to 3.65 in reducing the theoretical contact ratio to 1.04. However the static LDP and Calyx does not compare exactly in this case, unlike the original set. The LDP predicts the mesh to be slightly more compliant. Therefore, the modulus of elasticity has been increased from $30.10^6$ to $35.10^6$ in LDP. Since the single tooth contact region is of interest, the transmission error and stiffness has been matched in this region. The mesh stiffness and transmission error is plotted in Figure 5.9 and Figure 5.10 respectively. The gear set is run at 2000 rpm, only and the dynamic transmission error from both LDP and Calyx is compared in Figure 5.11.

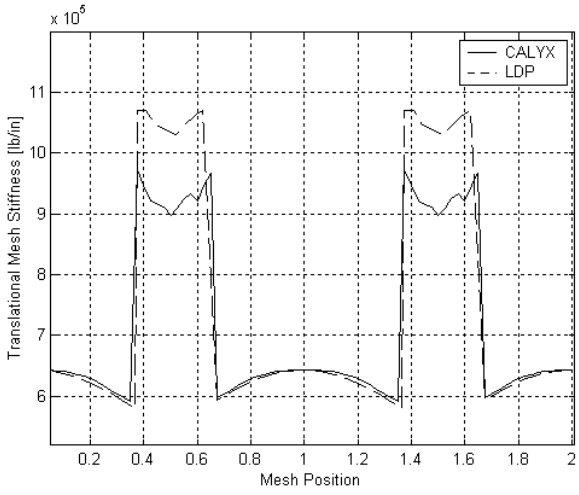


Figure 5.9. Mesh stiffness for the low contact ratio gear set. CR=1.04

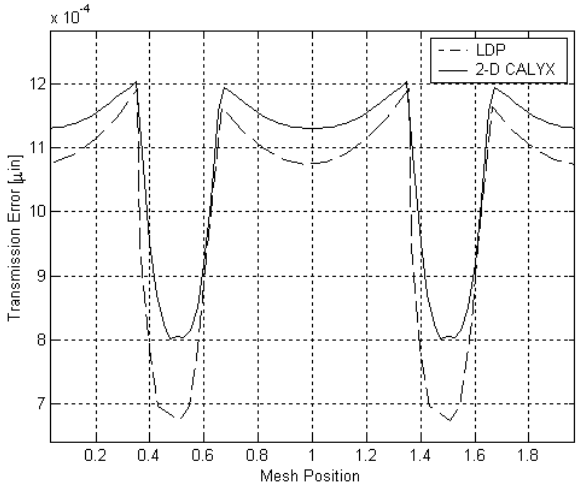


Figure 5.10. Transmission error for the low contact ratio gear set. CR=1.04

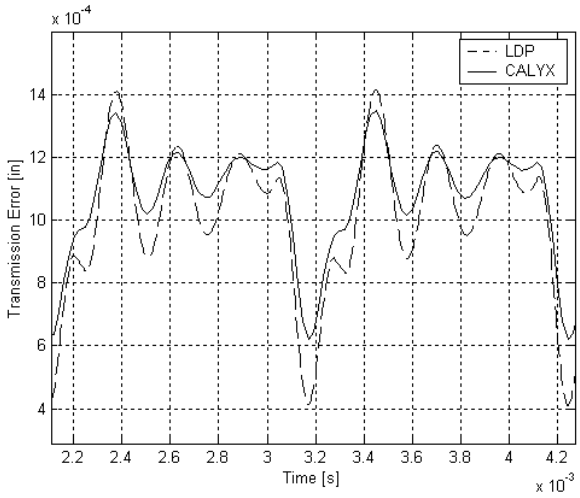


Figure 5.11. Time histories for transmission error from LDP and Calyx for 2000 rpm.

### 5.2.3 *High Contact Ratio Spur Gear Set 2*

The comparison is repeated for another high ratio gear set. For the purpose of testing a different case, a high capacity set has been fabricated. This set does not exist in reality, which is shown in Figure 5.12 and data is given in Table 5.3. To compare Calyx and LDP the high contact ratio set is ran for 1200 rpm at pinion, and the transmission error is plotted in Figure 5.13. The frequency of oscillation below superharmonic region is calculated as ω=2971Hz for LDP, and 2962Hz for Calyx Hz. The lumped parameter model gives for this set from (5.3) using $k_{mesh}$=1.46e6 lb/in, ω=2938 Hz. No further analysis is conducted for the high contact ratio set because the agreement at low speeds verifies the LDP model with Calyx and lumped parameter model.

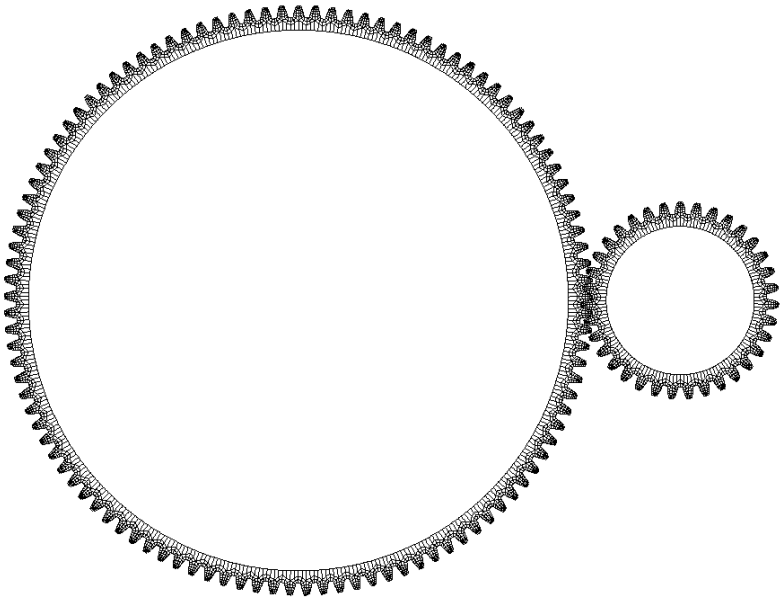

Figure 5.12. The high ratio and high contact ratio spur gear set. CR=2.02

| | Pinion | Common | Gear |
|---|---|---|---|
| Number of teeth | 35 | | 109 |
| Center Distance | | 12 | |
| Diametral Pitch | | 6 | |
| Pressure Angle | | 17 | |
| Outside Diameter | 6.19 | | 18.5 |
| Root Diameter | 5.4233 | | 17.7333 |
| Inner Diameter for Calyx | 4.6567 | | 16.9667 |
| Face Width | | 4 | |
| Theoretical Contact Ratio | | 2.02 | |
| Pinion Torque | | 16000 | |
| Pinion Speed | | 2 rpm | |
| Gear Inertia | 0.3333 | | 31.3530 |
| Mesh Damping Ratio | | 0.06 | |

Table 5.3. High ratio and high contact ratio gear set parameters.

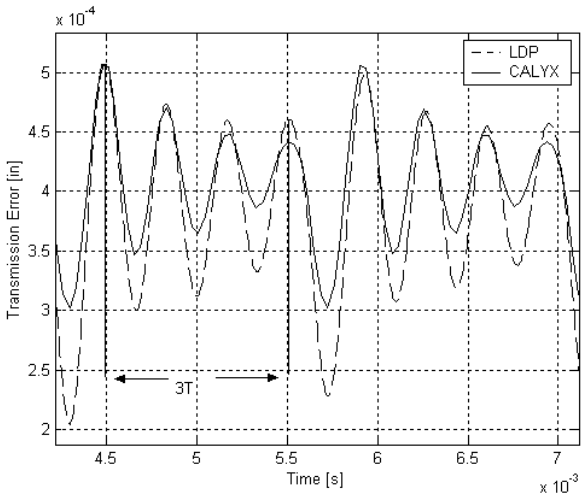


Figure 5.13. Time histories for transmission error from LDP and Calyx for 1200 rpm.

### 5.2.4 *Optimized Gear Set*

The aim of this subsection is to verify the change of contact ratio and therefore mesh stiffness in the dynamic run of LDP. The gear set given in Table 5.1 and Table 5.2 is optimized for transmission error at the operating torque of 1128 in-lb. The modification data is given in Table 5.4 This gears set is run from 428 in-lb to 1828 in-lb in both LDP and Calyx, and the static transmission error is compared in Figure 5.14 and Figure 5.15. The variation in contact ratio can be seen from these figures. Overall LDP predicts slightly higher contact ratio than Calyx. Figure 5.16 shows the variation of peak-to-peak static transmission error with loading. Next, the gear set is run at 2000 rpm and at 428 in-lb and 1828 in-lb, with the gear constrained, as in previous runs. Figure 5.17, and Figure 5.18 show the dynamic run at 428 and 1828 in-lb respectively. From the plots it can be seen that change in the contact ratio is properly reflected do the dynamic behavior.

| | Pinion | Gear |
|---|---|---|
| Straight tip relief [in] | $7.4.10^{-4}$ | $7.4.10^{-4}$ |
| Parabolic tip relief [in] | $3.2.10^{-4}$ | $3.2.10^{-4}$ |

* All modifications start at LPSTC=23.181° roll angle

Table 5.4. Modification data for the optimized set.

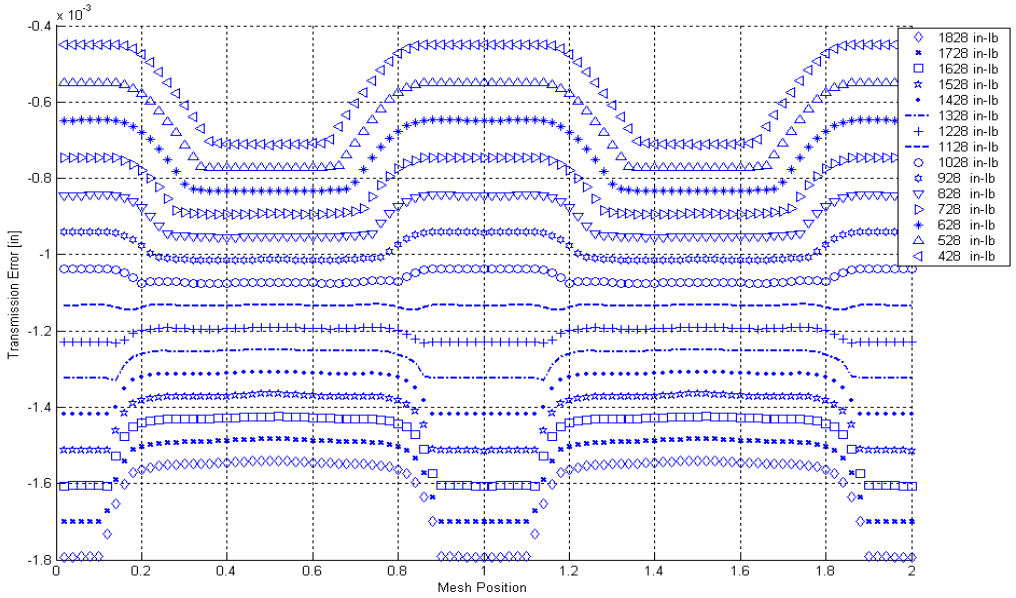


Figure 5.14. Harris Map from Calyx.

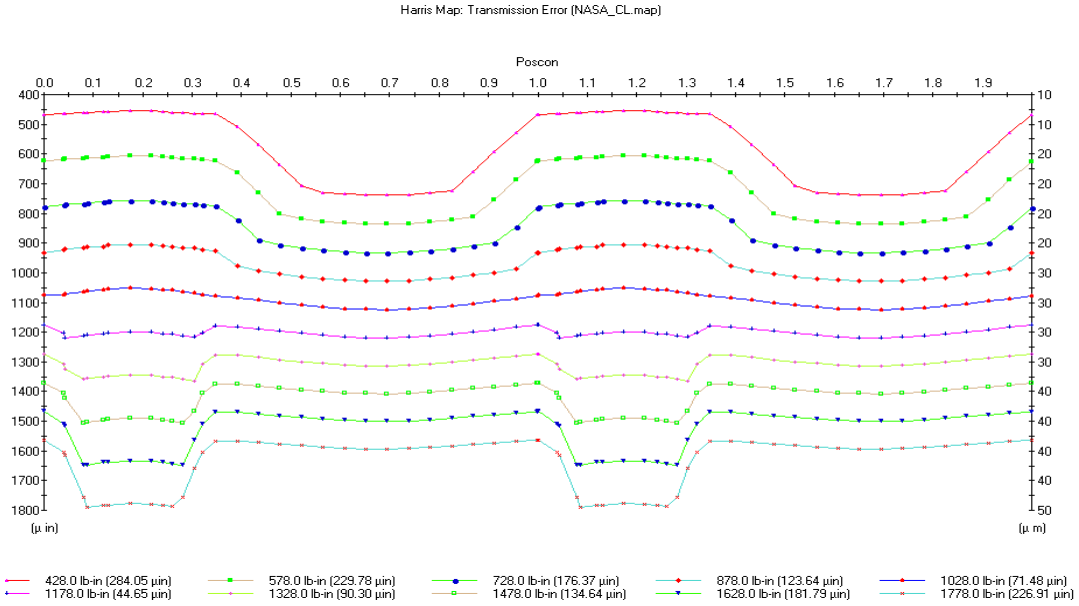


Figure 5.15. Harris Map from LDP.

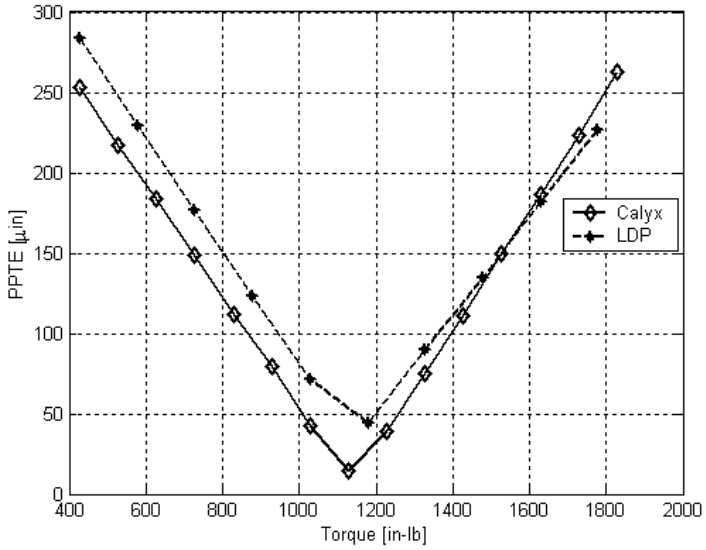


Figure 5.16. Variation of peak-to-peak transmission error with load for the optimized gear set.

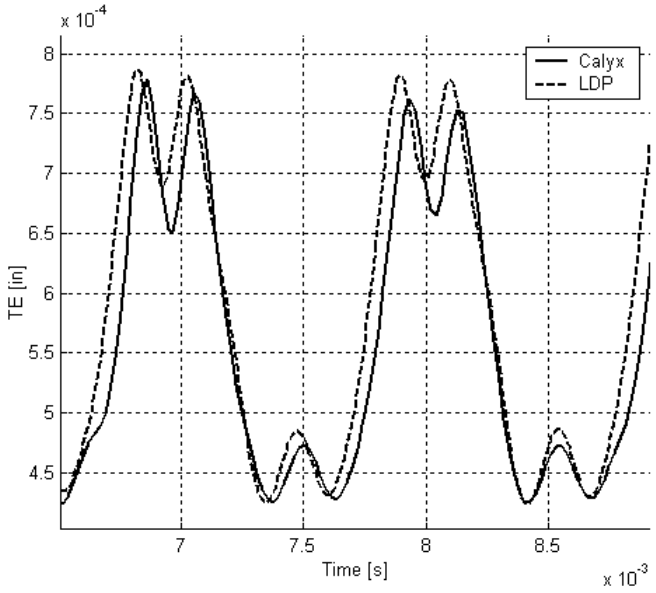


Figure 5.17. Dynamic transmission error of the optimized gear set at 2000 rpm and for 428 in-lb loading.

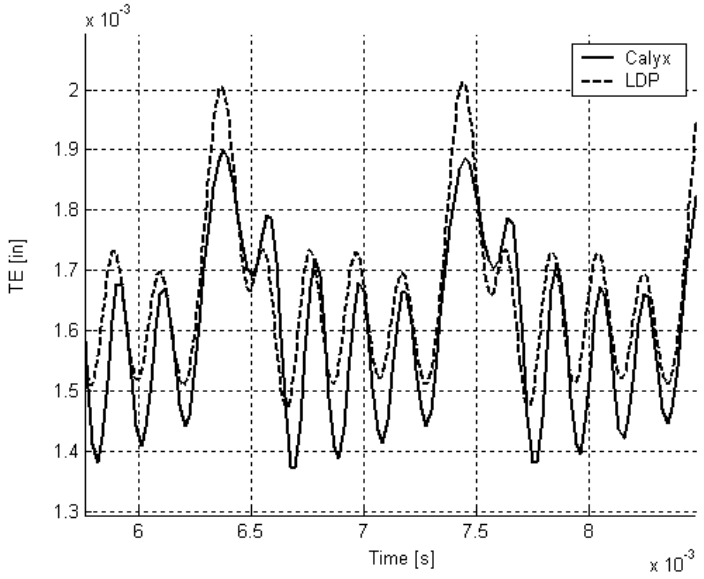


Figure 5.18. Dynamic transmission error of the optimized gear set at 2000 rpm and for 1828 in-lb loading.

## 5.3 Comparison with DYTEM and Effect of Modifications

In this section the nonlinear model developed by Ozguven and Houser [2] is compared with LDP. Both models are almost the same except that DYTEM has shafts and bearings. The effects of these are removed by selecting very high stiffness for bearings and shafts. The second exception is that LDP calculates the instantaneous properties for the mesh such as stiffness, transmission error etc, whereas DYTEM takes those properties for a constant load torque. Both models are run from 500 to 17000 rpm and the peak-to-peak values for transmission error at steady state are shown in Figure 5.19.

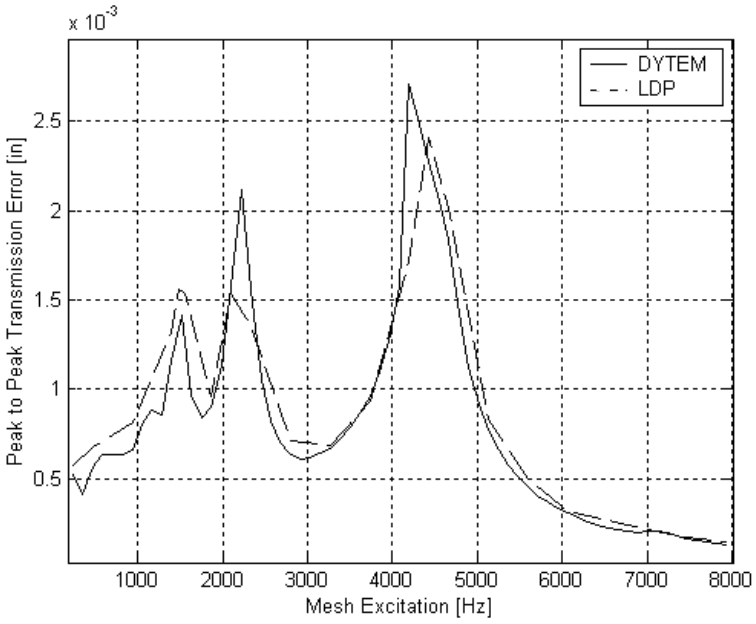


Figure 5.19. Speed runup for perfect involute set.

Experiments show that the optimized gear sets for transmission error do not necessarily turn into minimum noise gears. As proposed by many investigators, noise has many other exciters than transmission error, although effect of transmission error is very significant in most cases. Another possibility is that the lumped parameter models for gear dynamics fail to capture excitation due to transmission error variation and instantaneous torque. At very low TE levels, deviation from the optimum torque can be high so that this effect becomes significant. To investigate this issue, the gear set given in Table 5.1 is optimized with the resulting transmission error shown in Figure 5.20. This set is run from 500 rpm to 17000 rpm in both DYTEM and LDP and the results are shown in Figure 5.23. Comparing LDP and DYTEM suggests that the variation of transmission error with dynamic loading does not have a noticeable effect

on the result. Complicating the LDP model does not lead to different dynamics in optimized gear sets. Figure 5.21 and Figure 5.22 shows the harmonics of the static transmission error. Relative amplitude of dynamic transmission error can be explained from the comparison of the first three harmonics for the involute and optimized gears.

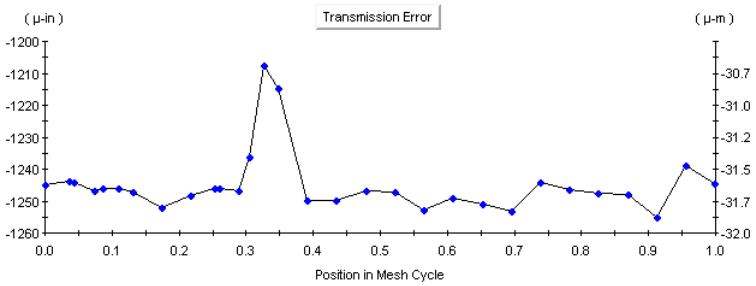


Figure 5.20. Static transmission error of the optimized spur gear set with PPTE=47µin.

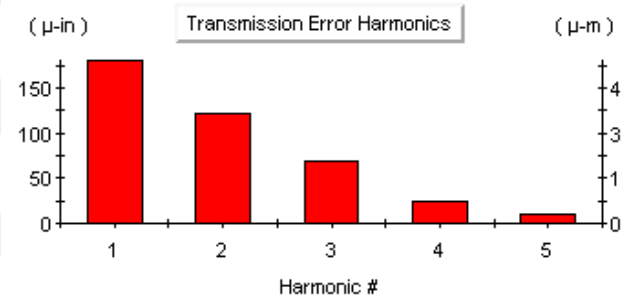


Figure 5.21. Static TE harmonics for perfect involute low contact ratio set 1.


Figure 5.22. Static TE harmonics for optimized low contact ratio set 1.

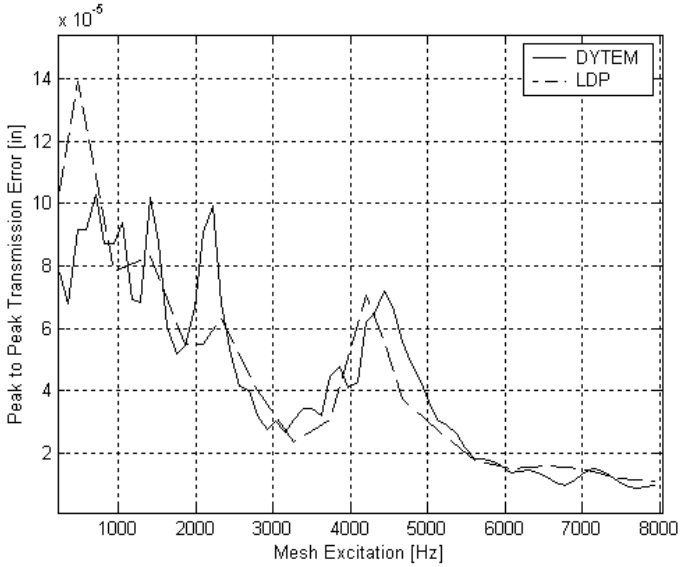


Figure 5.23. Speed runup for optimized gear set.

## 5.4 Outputs of LDP

In this section, the byproducts of the dynamic LDP analysis are displayed. These results include load distribution, root bending stresses and contact stresses. In order to demonstrate these, the gear set given in Table 5.1 and Table 5.2 are run at the rated torque 1128 in-lb, and a higher speed of 7000 rpm, which is near resonant frequency. In addition, a misalignment of 0.0018 inch is given. Figure 5.24 shows the contact stress distribution. It can be seen that the vibration amplitude is high and causes high contact stress variation than static values. Root stress variation with facewidth is plotted in Figure 5.25. The coupling results in nonzero root stresses where there is no loading and therefore, variation in root stress is less critical than contact stress.

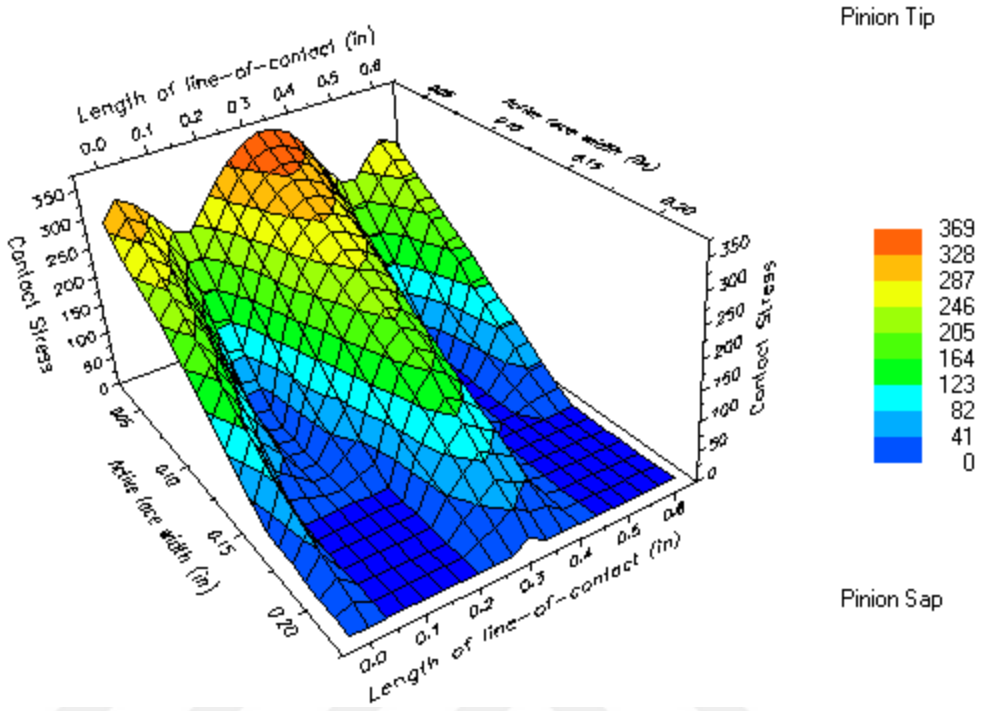


Figure 5.24. Contact stress distribution for 7000 rpm and 1128 in-lb loading.

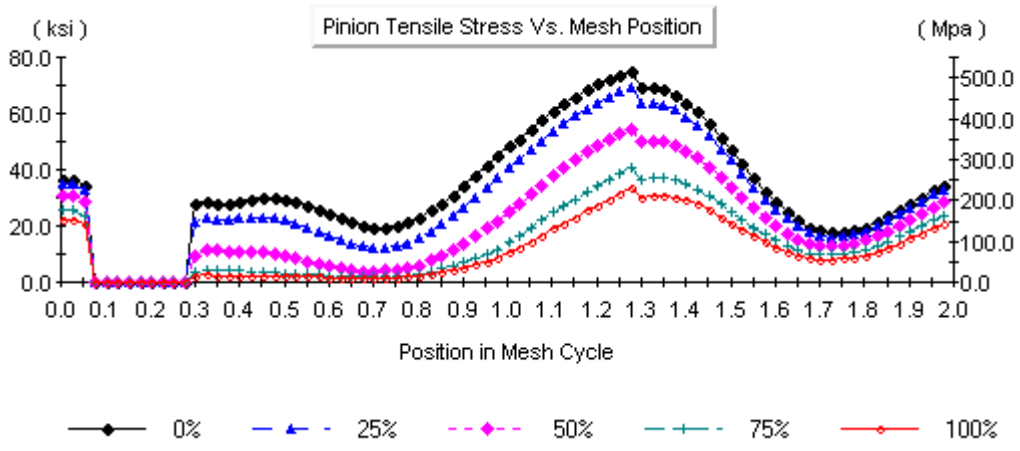


Figure 5.25. Root stress at five different face width positions. (0%, 25%, 50%, 75%, 100%)

## 5.5 Effect of Transmission Error Force, Shuttling Force and Friction Force on Bearing Response

This section investigates the response of geared shafts due to friction, shuttling and transmission error forces. In order to verify the three-dimensional rigid shaft model the spur gear given in Table 5.1 with no modifications and dynamic properties given in Table 5.2 is run under three conditions. For all conditions, the bearing displacements along the line of action (LOA), off line of action (O-LOA) and axial directions are compared. Also the angular positions of the gears are checked when there is an excitation in that direction. The first simulation is without friction and misalignment, where the bearing displacements are plotted in Figure 5.26. There are no excitations in O-LOA or axial directions. The angular position also is zero and therefore not plotted. Next, a Coulomb friction coefficient 0.05 is put in the model for each calculation element in LDP. It can be seen in Figure 5.27 that O-LOA direction for bearings is also excited while the LOA excitation stays the same. The axial direction and angular displacements are still zero. In the last case friction is removed, but a helix angle error of 0.5 degrees is given to both pinion and gear, essentially making a helical gear set. Shuttling forces are expected to excite the system. The shuttling forces indeed result in a moment that needs to be supported by LOA forces and hence these forces for right and left bearing are equal and opposite. However they are buried in the transmission error force and cannot be identified since helix angle error is very low. But a couple from O-LOA direction should support the moment due to axial forces. This couple can be identified from Figure 5.28 as equal and opposite displacements at bearings. From

Figure 5.29 it can be observed that the gears align themselves to balance the shuttling moment. In the other rotation direction, that is perpendicular to both rigid body rotation and helix angle, there is slight displacement. It is probably due to rotational coupling.

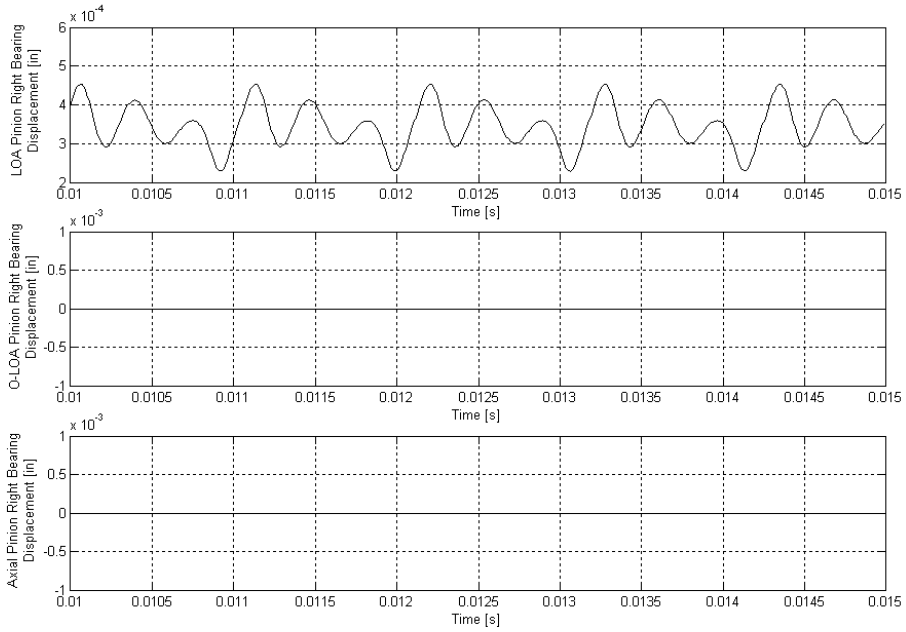


Figure 5.26. Pinion shaft right bearing displacements for no friction and no misalignment.

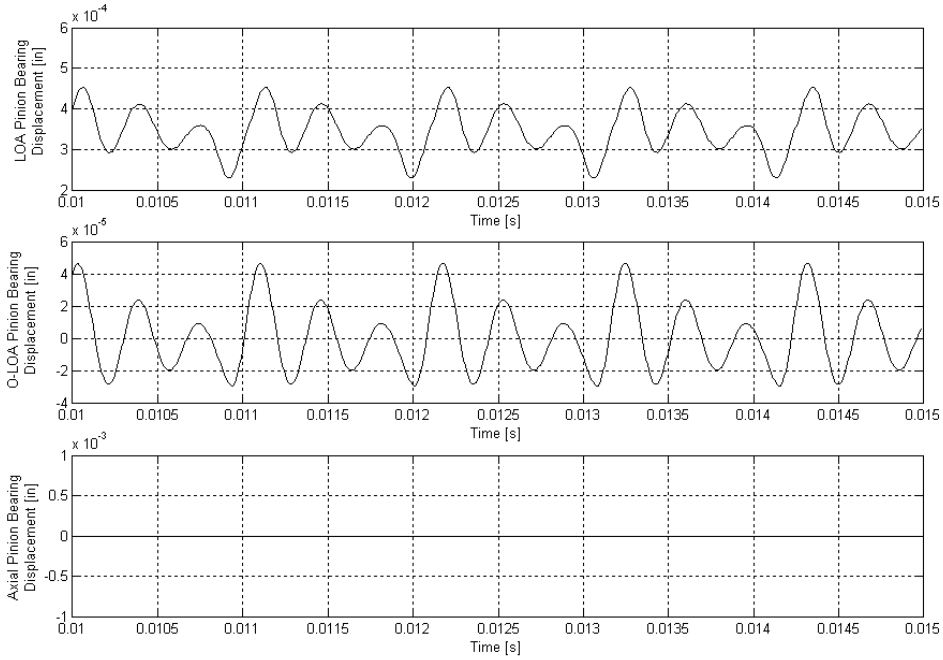


Figure 5.27. Pinion shaft right bearing displacements for friction but no misalignment.

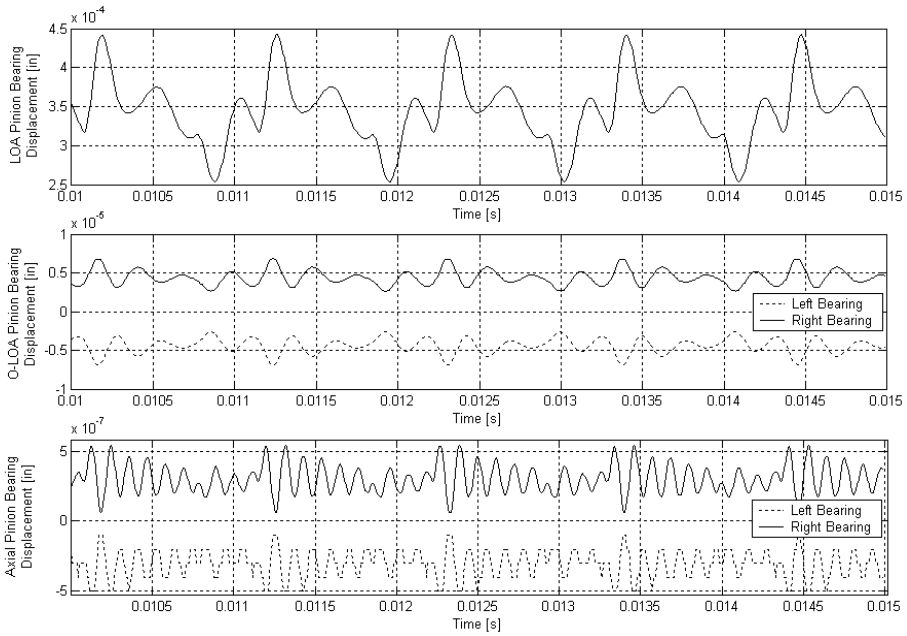


Figure 5.28. Pinion shaft right bearing displacements for no friction but misalignment.

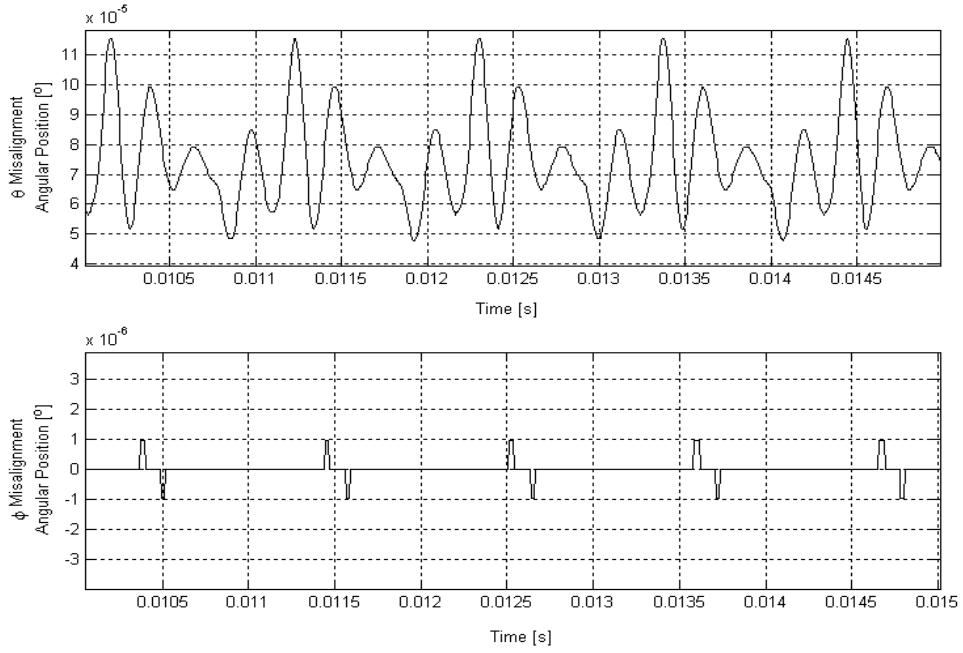


Figure 5.29. Pinion shaft angular position in helix angle direction and perpendicular, respectively.

From the runs with spur gear it is seen that friction causes in O-LOA forces but misalignment causes both O-LOA and axial forces in bearings. However a spur gear set does not produce high shuttling forces. To compare the effect of transmission error force, friction and shuttling forces on bearing forces, three similar helical gear sets are chosen from a large number designs produced by the computer program “Run Many Cases” (RMC). These cases have one of the three forces high, and the remaining two relatively low in terms of peak-to-peak and first harmonic. The gear sets and the forces are summarized in Table 5.5 and Table 5.6 respectively. The dimension of the shaft is given in Figure 5.30 and is the same for pinion and gear. Figure 5.31 through Figure 5.39 show the waterfall plot of bearing forces at the right end of the pinion shaft for LOA, O-LOA and axial directions for cases A, B, and C respectively. Order track plots of the LOA and O-LOA directions for bearing forces are given in Figure 5.40, Figure 5.41, and Figure 5.42 for cases A, B, and C. Third orders are sometimes neglected because the amplitudes are relatively low.

| | Case A) Transmission Error Force | | Case B) Shuttling Force | | Case C) Friction Force | |
|---|---|---|---|---|---|---|
| | Pinion | Gear | Pinion | Gear | Pinion | Gear |
| No. Teeth | 26 | 33 | 25 | 32 | 26 | 31 |
| Normal Diametral Pitch | 9.7816 | | 9.0957 | | 9.4005 | |
| Pressure Angle | 22.5 | | 17.5 | | 17.5 | |
| Helix Angle | 28 | | 22 | | 28 | |
| Outer Diameter | 3.1873 | 4.2228 | 3.1843 | 4.2785 | 3.4786 | 4.0312 |
| Root Diameter | 2.7069 | 3.7423 | 2.6676 | 3.7618 | 2.8935 | 3.4461 |
| Circular Profile modification | 0.0001 | | 0.0001 | | 0.00035 | |
| Circular Lead modification | 0.00033 | | 0.00033 | | 0.00012 | |
| Gear Inertia | 0.0104 | 0.0234 | 0.0103 | 0.0238 | 0.117 | 0.0212 |
| Gear Mass | 0.0115 | 0.0156 | 0.0114 | 0.0157 | 0.0119 | 0.0150 |
| Load Inertia | 0.01 | 0.02 | 0.01 | 0.02 | 0.01 | 0.02 |
| Shaft Stiffness | $10^5$ | $10^5$ | $10^5$ | $10^5$ | $10^5$ | $10^5$ |
| Shaft Damping | 0.3 | 0.3 | 0.3 | 0.3 | 0.3 | 0.3 |
| LOA Bearing Stiffness | $10^6$ | $10^6$ | $10^6$ | $10^6$ | $10^6$ | $10^6$ |
| O-LOA Bearing Stiffness | $10^6$ | $10^6$ | $10^6$ | $10^6$ | $10^6$ | $10^6$ |
| Axial Bearing Stiffness | $10^7$ | $10^7$ | $10^7$ | $10^7$ | $10^7$ | $10^7$ |
| Bearing Damping | 10 | 10 | 10 | 10 | 10 | 10 |

* All values are in English units.

Table 5.5. Summary of three helical gears parameters.

| | Case A) Transmission Error Force | | Case B) Shuttling Force | | Case C) Friction Force | |
|---|---|---|---|---|---|---|
| | Peak to Peak | First Harmonic | Peak to Peak | First Harmonic | Peak to Peak | First Harmonic |
| Transmission Error Force | 32.4 | 14.4 | 7.8 | 0.4 | 5.3 | 1.7 |
| Shuttling Force | 5.7 | 1.4 | 45.3 | 23.9 | 5.7 | 0.8 |
| Friction Force | 5.7 | 0.6 | 6.9 | 0.3 | 15.1 | 5.5 |

* All forces in pounds [lb].

Table 5.6. Forces for cases A, B and C.

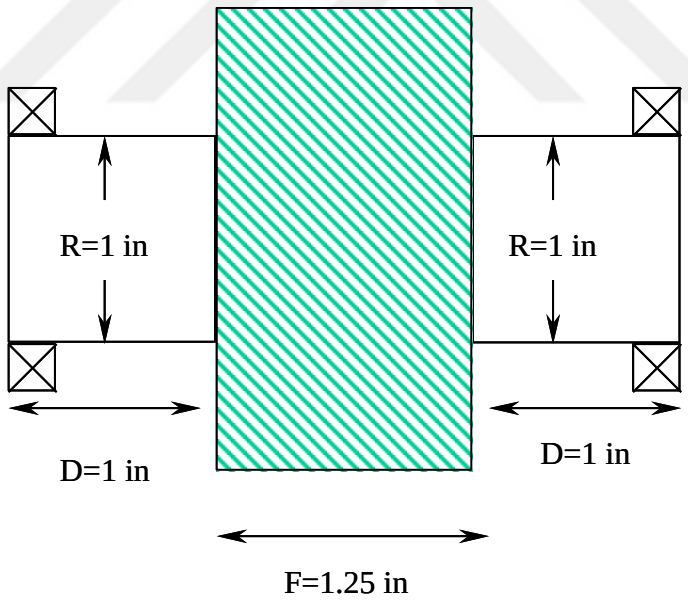


Figure 5.30. Dimensions of the shaft for both pinion and gear.

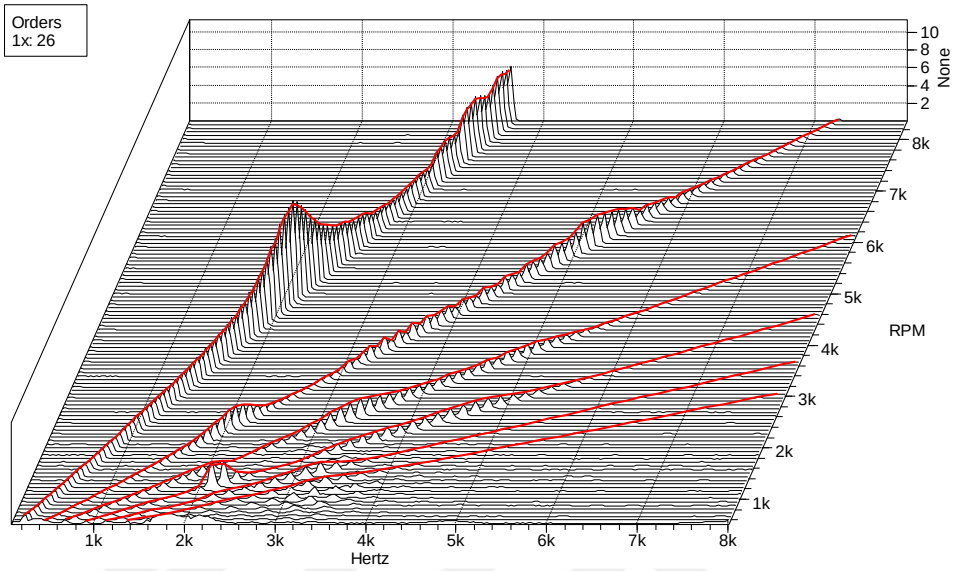


Figure 5.31. Waterfall plot for LOA right pinion bearing force of case A, with 14.4lb transmission error force.

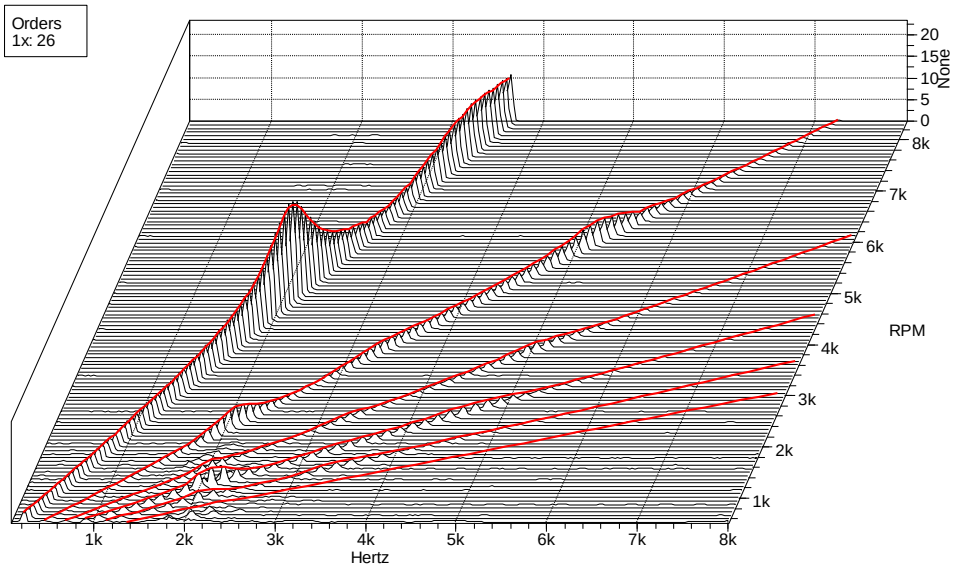


Figure 5.32. Waterfall plot for O-LOA right pinion bearing force of case A, with 14.4lb transmission error force.

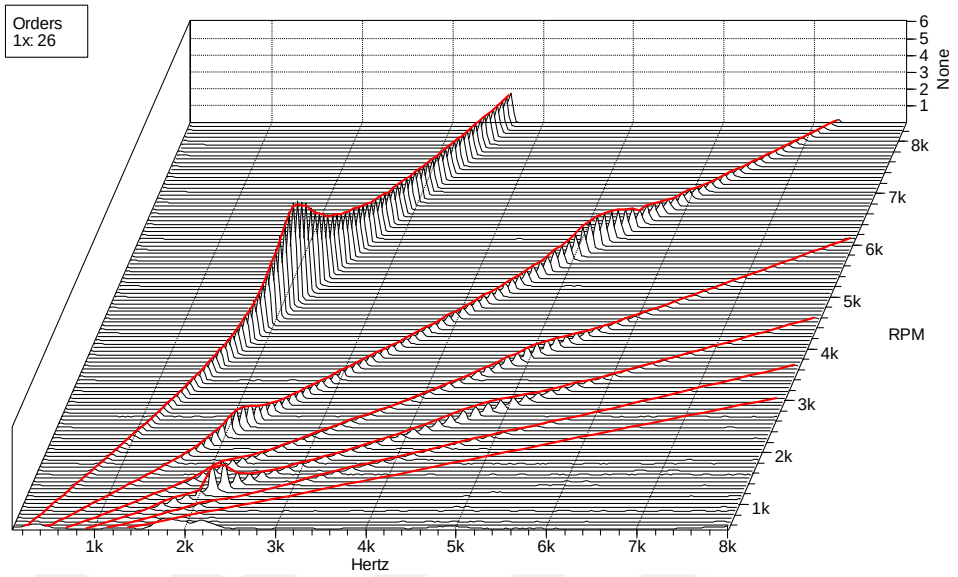


Figure 5.33. Waterfall plot for axial right pinion bearing force of case A, with 14.4lb transmission error force.

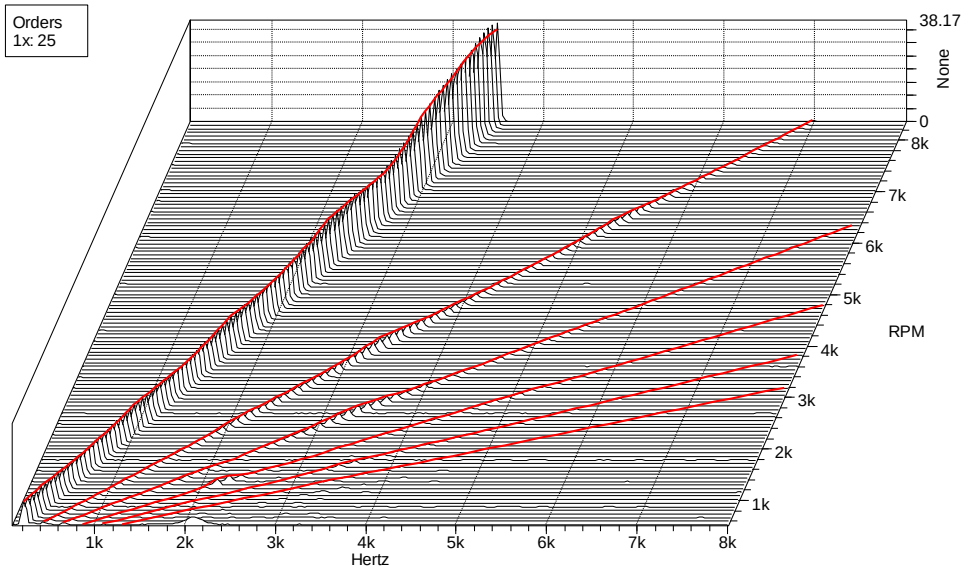


Figure 5.34. Waterfall plot for LOA right pinion bearing force of case B with 23.9lb shuttling force.

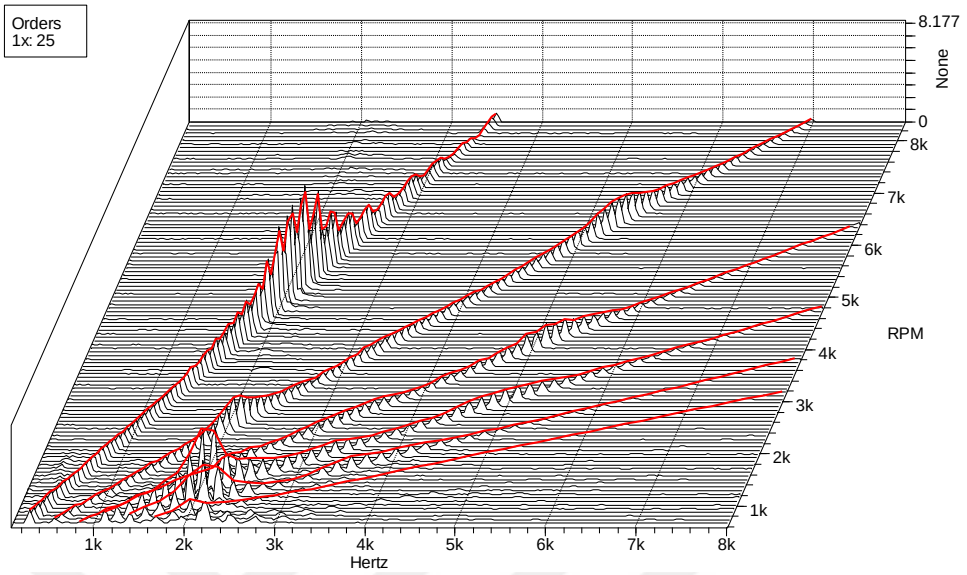


Figure 5.35. Waterfall plot for O-LOA right pinion bearing force of case B with 23.9lb shuttling force.

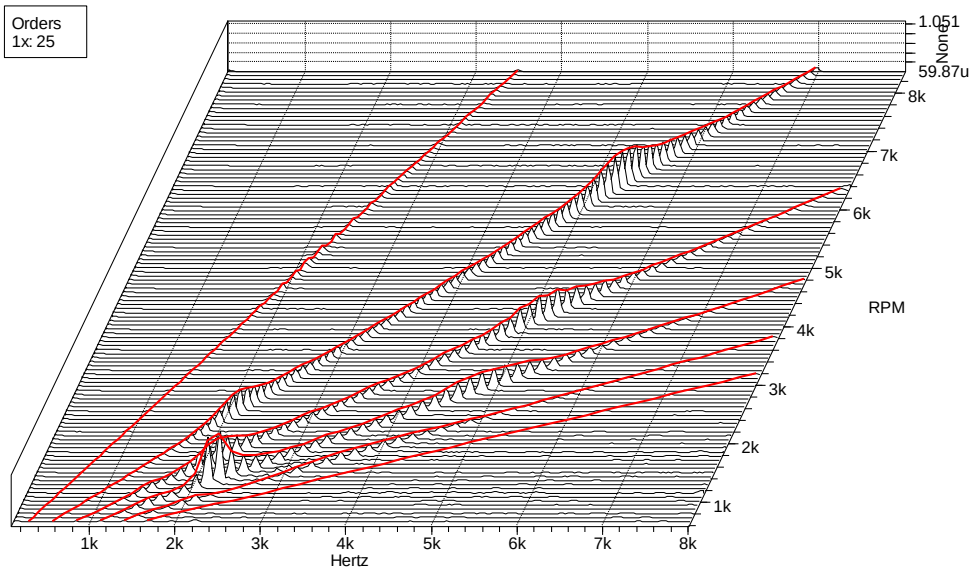


Figure 5.36. Waterfall plot for axial right pinion bearing force of case B with 23.9lb shuttling force.

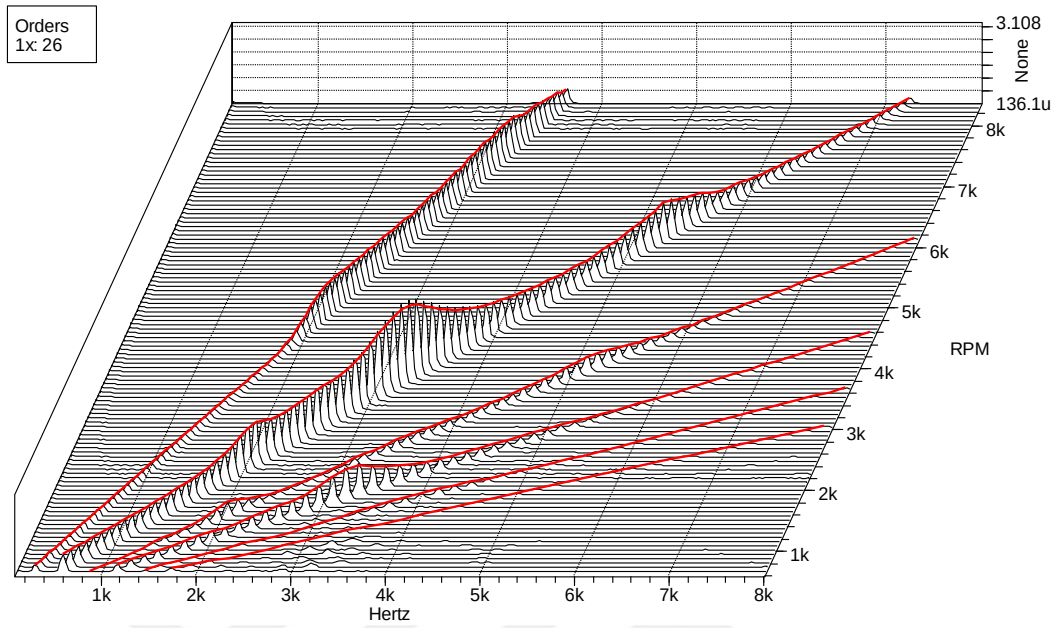


Figure 5.37. Waterfall plot for LOA right pinion bearing force of case C with 5.5lb friction force.

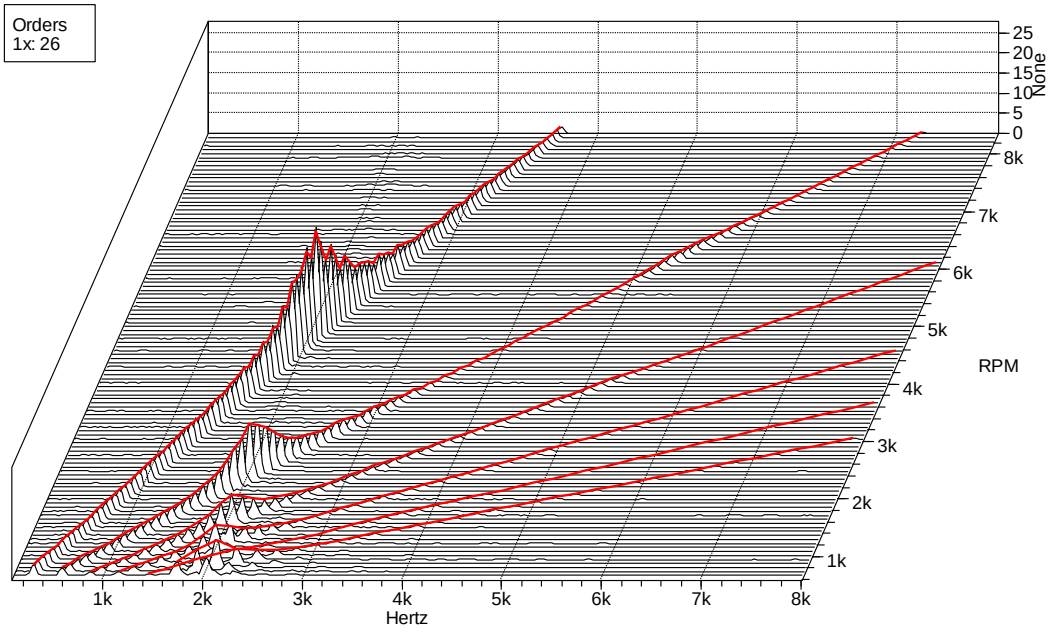


Figure 5.38. Waterfall plot for O-LOA right pinion bearing force of case C with 5.5lb friction force.

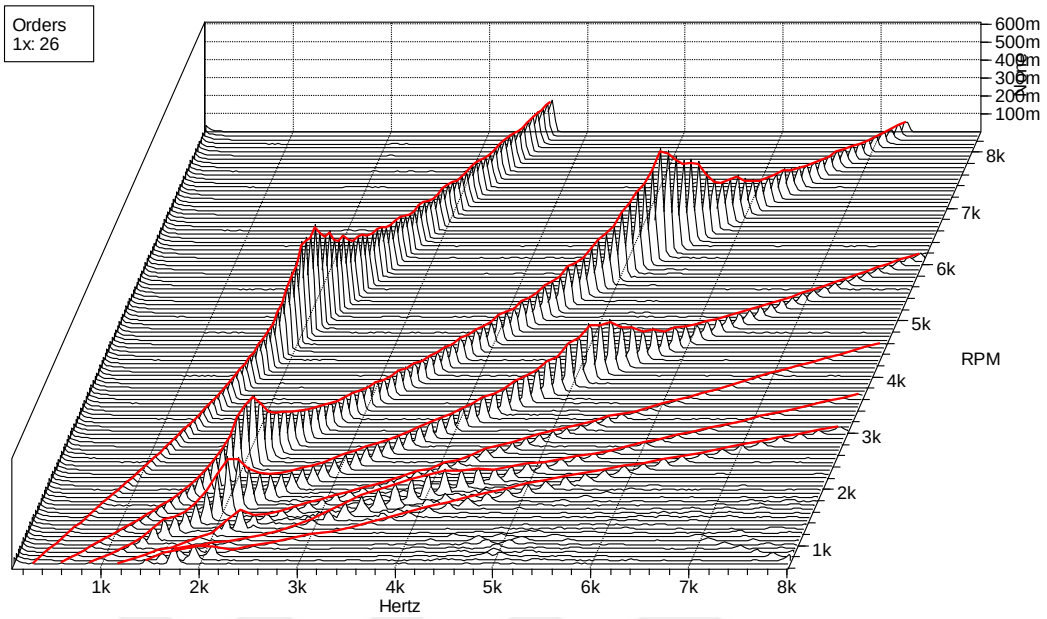


Figure 5.39. Waterfall plot for axial right pinion bearing force of case C with 5.5lb friction force.

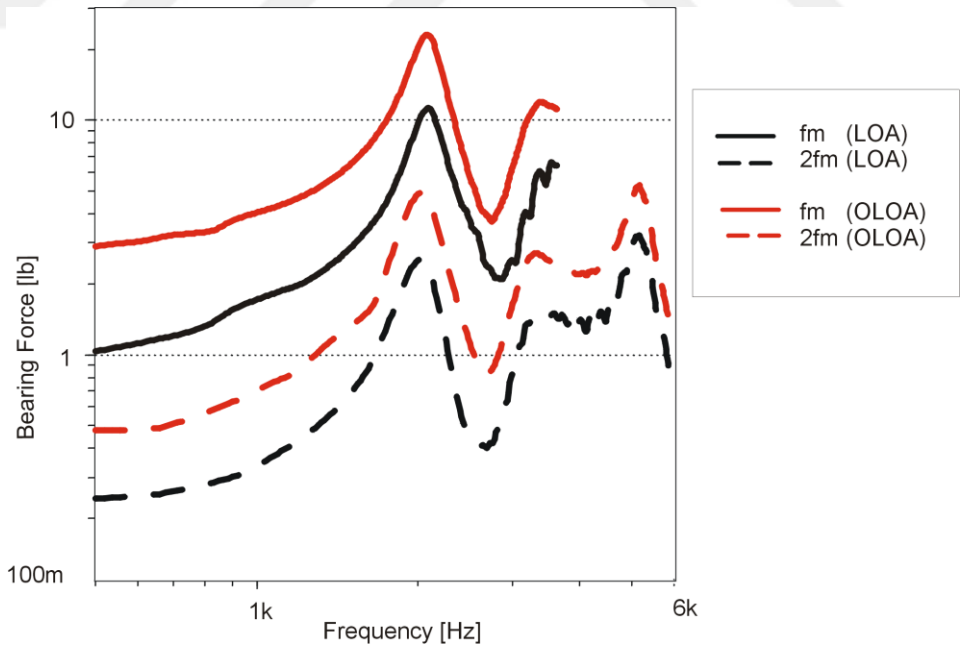


Figure 5.40. Order track for case A. First harmonic of transmission error force14.4lb.

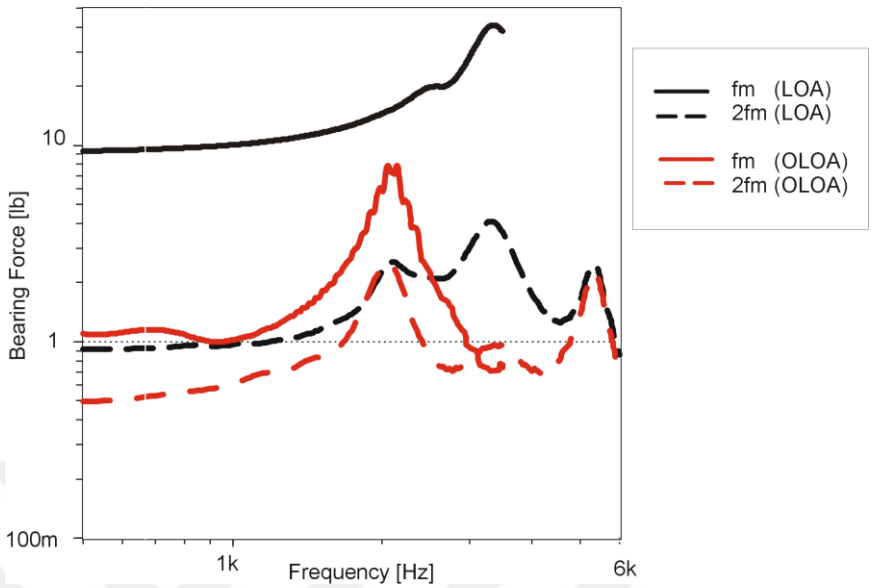


Figure 5.41. Order track for case B. First harmonic of shuttling force 23.9lb.

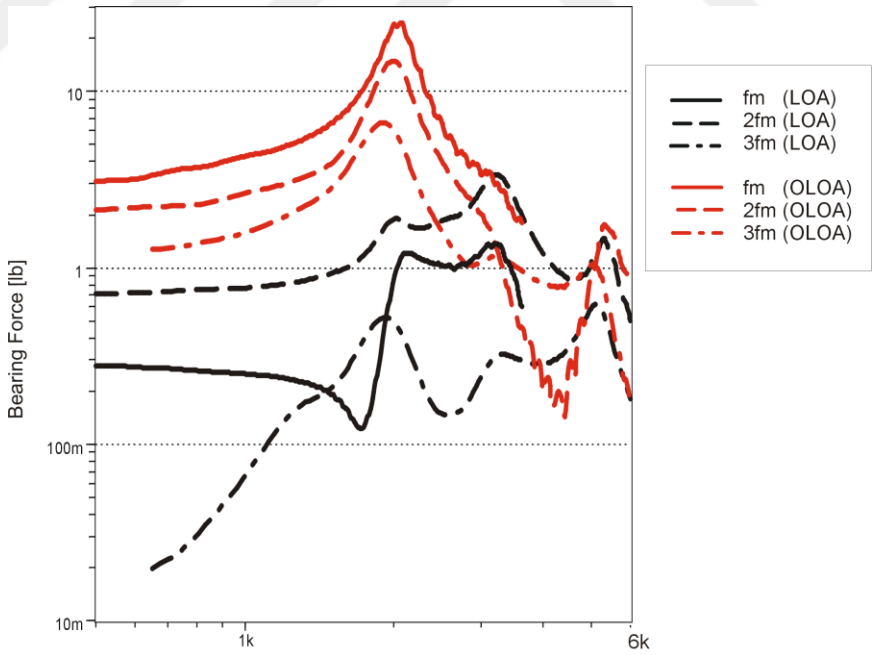


Figure 5.42. Order track for case C. First harmonic of friction force 5.5lb.

For case A the transmission error force excites the bearing at all three directions. The reason for LOA excitation is obvious since it is in the transmission error force direction. Axial direction is excited by the component of TE force and the O-LOA direction supports the moment due to the axial force. In case B, shuttling force causes high resonances in the first harmonic of bearing force in LOA, but the resonance appears to be out of the torsional mesh mode. The excited mode is probably the rocking mode arising from the bearing stiffness and inertia of the shaft. It is interesting that the O-LOA forces are not very small in the mesh mode although the axial force in the bearing is very small. Case C has the least total dynamic bearing reaction, and highest force component is in the O-LOA direction from friction force as expected. The noticeable difference in magnitude of the force in axial and LOA direction may suggest the contribution of shuttling force to the LOA direction response as seen in case B.

### 5.6 Damping Caused by Friction

This section is not directly related to the previous ones. It is interesting to study the damping effect of Coulomb friction between gear teeth, although it is clear that it dissipates energy. In reality, the vibrations are damped, and this was modeled by a viscous damper between gear teeth in the previous chapters. Friction may play a role in this damping. To investigate this effect, the gear set given in Table 5.1 and
Table 5.2 is run under different conditions with an exaggerated friction coefficient of 0.4. The first run is without any friction, but with a viscous damping ratio of 0.05. The load is applied at t=0.002s. and the gears are not rotating. The transmission error time

history is given in Figure 5.43. The time response shows a typical damped step response of a second order system with exponential decay. Next, the same procedure is followed with no damping but friction present. Figure 5.44 shows the time history of transmission error, which is a linear decay suggesting Coulomb friction. Finally, the pinion rotational speed is made 2000 rpm with no damping but a friction coefficient of 0.4 is used. Figure 5.45 shows the transmission error. Interestingly, no damping can be seen in the vibrations, hence no steady state can be reached. This is because the friction force is dependent on the relative sliding velocity of contacting teeth, not the absolute relative velocity, as opposed to viscous damping. In other words, the sliding velocity does not change sign, as the time derivative of the transmission error changes sign, which is necessary to dissipate vibratory energy. Nevertheless, friction still consumes the driving torque; consequently a smaller amount of load torque is required to keep the system in equilibrium.

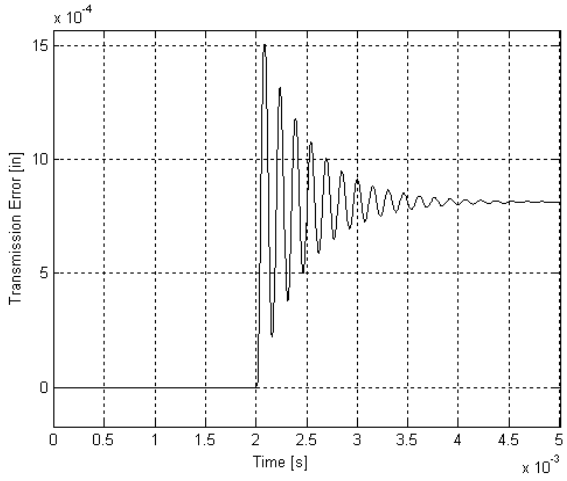


Figure 5.43. Transmission error for step loading and viscous damping of 0.05 but no friction.

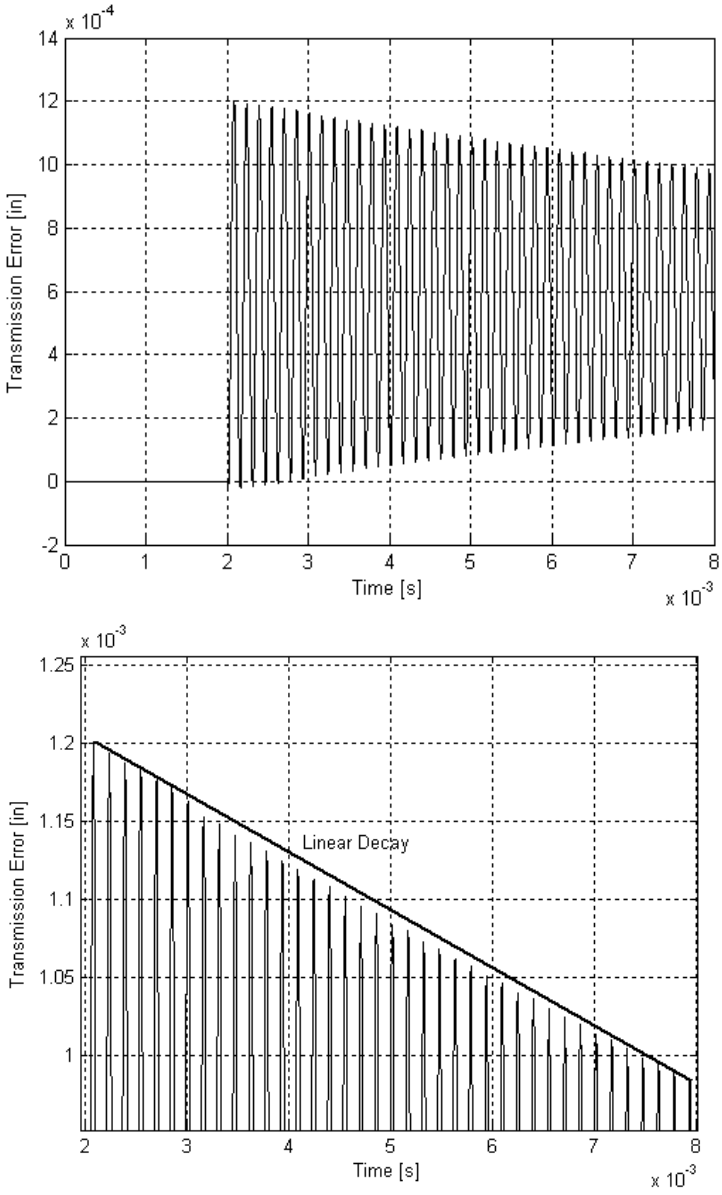


Figure 5.44. Transmission error for step loading with no viscous damping and with a friction coefficient of 0.4, with expansion to emphasize the decay behavior.

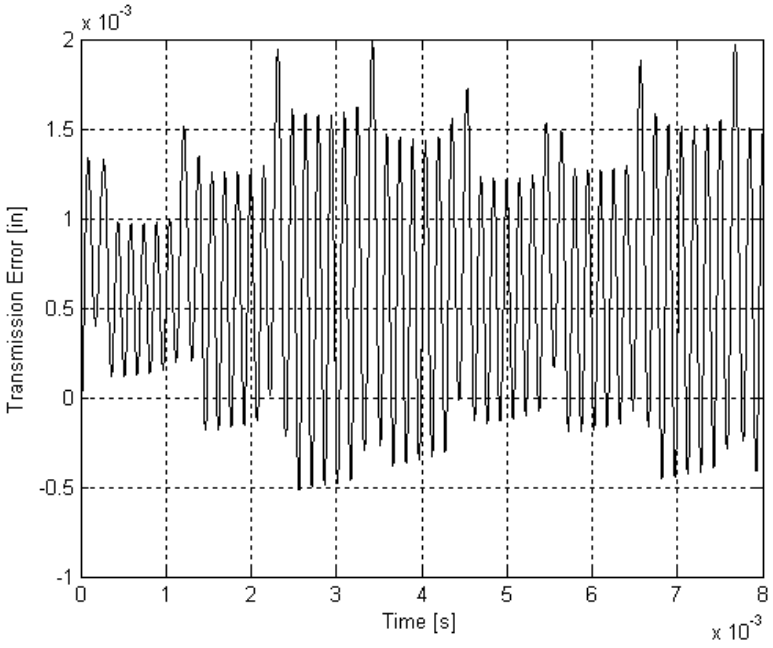


Figure 5.45. Transmission error for 2000 rpm with only friction present and no damping.

## 5.7 Summary

First, comparison of LDP with Calyx is given for two spur gears in operating conditions and step loading with the simple model, i.e. without bearings and shafts. Both models seem to agree on the resonant frequency and the natural frequency, which is estimated by the linear mass spring model. DYTEM and LDP are compared in speed runup and for the unmodified spur gear set. Both comparisons match reasonably to validate the LDP mesh model. In the next section, the dependence of mesh properties to the dynamic load is investigated and the speed runup results are compared for a transmission error optimized spur gear set. The comparison suggests the effect of dynamic load on response is negligible even for optimized gears. Although more cases must be ran to verify whether the effect of dynamic loading can

be neglected or not. The effect of contact ratio on response is verified in the next section with an optimized gear set, and comparison with Calyx is given. The next section presents bending and contact stress outputs of LDP near resonant conditions. The following section studies the effect of transmission error force, shuttling force and friction force. The frequency responses of bearing forces imply that both transmission error force and shuttling force causes dynamic forces in both LOA and O-LOA directions. Therefore these forces have similar excitation to the system, whereas friction force only excites the O-LOA bearing. For the cases investigated, the friction force has the least effect, but the shuttling and transmission error force have similar effect on bearing response. Friction model between gear teeth is examined in the last section. The three runs suggest that friction itself does not have damping effect when gears are in rotation, but has damping effect when gears are stationary.

# CHAPTER 6

# CONCLUSIONS

## 6.1 Summary

In this thesis a number of dynamic models in two and three dimensions have been developed for the analysis of geared shafts. Also the accurate predictions for mesh properties are incorporated in these models from the Load Distribution Program, which would have been available only for static analysis. A computer code has been developed and implemented in LDP to extend the static solution into a dynamic solution. Results from this program is compared to other tools that have been experimentally verified by other researchers. Lastly, the program is used to evaluate the excitation from shuttling and friction forces for a geared shaft with three different helical gears that have distinct properties.

## 6.2 Conclusions

The correlation between the noise from gears and transmission error has been reported to be significant for relatively high values of transmission error values, hence suggesting that the transmission error is the main dynamic exciter. However, the correlation is reported to be not so good if the transmission error is minimized.

Because of this reason, in the beginning of this study it was suspected that the dynamic transmission error predictions for the optimized gear sets were not accurate because the mesh properties are dependent on the load itself, consequently, causing parametric excitations.

1) Models are developed with two versions, one of them taking the load dependency effect into account. Comparison with other models suggests that the dependence of mesh properties to the load is insignificant and the loading can be assumed constant for the case investigated.
2) The excitation effects of shuttling and friction forces are evaluated. Shuttling forces are embedded in the moment from the gear mesh. Comparisons between three similar gear sets with different forces are performed. The force at bearings are possible exciters to the housing and hence noise, so that these forces are analyzed. It turns out that transmission error force and shuttling force excite the system in at least two directions causing high dynamic force in bearings, whereas friction force has relatively lower contribution to bearing forces. Nevertheless, none of the forces are small enough to be neglected. Different resonant frequencies were encountered suggesting the existence of rocking modes of shafts.
3) Friction force is calculated using the Coulomb friction approximation, but a sliding velocity dependent friction coefficient is also incorporated in the program. A brief study shows friction has no damping effect unless the gears are stationary, which verifies with previous studies on friction.

## 6.3 Recommendations

1) The program is limited for simple shaft configurations and a single gear pair. The equations of motion can be added to cover more than one gear pair on a shaft such as a back-to-back configuration. An idler gear set has been investigated partially during the development of the code, but then removed from the program because of time limitations. During this time effect of mesh phasing on dynamics have been identified but not studied.
2) Corner contact in gears produces forces that are not in LOA direction. An impact loading can approximate this effect in high speeds and can be easily incorporated in the program. However, the parameters of the impact need to be studied for realistic modeling.
3) Three-dimensional equations of motion with coupling could not be attached to the flexible shaft model. Because of this, the flexible shaft model does not take gyroscopic effects into account. In addition, the equations of motion turn out to be computationally stiff, and sometimes do not converge for the flexible shaft. Introducing a new formulation for the flexible shaft model, or enhancing the numerical solution technique can solve these problems, and it is desirable to include gyroscopic effects. Moreover the flexible shaft model can be extended to cover the gear itself as a flexible body for thin and lengthy gears machined on shafts. The deflection of shafts under gears can be reflected to load distribution.

4) Since many practical applications involve an excitation from the driver such as a combustion engine, it would be helpful to modify the driving torque such that desired type of excitation is supplied to the system.
5) Currently the angular motion in line of action direction is allowed in the motion, but this motion cannot be reflected to the load distribution, because in LDP the diagonal contact lines are same for pinion and gear. If the diagonal lines can be defined separately for pinion and gear in LDP, then this angular motion can be seen on load distribution.

# REFERENCES

1. Ozguven, H. N. and Houser, D. R., “Mathematical Models Used in Gear Dynamics – A Review”, Journal of Sound and Vibration v. 121 issue 3, pp. 383-411, 1988

2. Ozguven, H. N. and Houser, D. R., “Dynamic Analysis of High Speed Gears By Using Loaded Static Transmission Error”, Journal of Sound and Vibration. v. 125 issue 1, pp. 71-83, 1988,

3. Seireg, A., and. Houser, D. R., “Evaluation of Dynamic Factors for Spur and Helical Gears”, ASME Technical Paper no: 69-WA/DE-4, 1969

4. Conry, T. F., Seireg, A., “A Mathematical Programming Technique for the Evaluation of Load Distribution and Optimal Modifications for Gear Systems”, ASME Journal, Engineering for Industry, Vol. 94, 1972.

5. Imajo, T., Parker, R. G., and Vijayakar, S. M., “Finite Element/Contact Mechanics Modeling of the Nonlinear Dynamic Response of a Spur Gear Pair”, ASME 8th Power Transmission and Gearing Conference, Baltimore, 2000.

6. Blankenship, G. W., and Singh, R., “A New Gear Mesh Interface Dynamic Model to Predict Multi-Dimensional Force Coupling and Excitation”, Mech. Mach. Theory Vol. 30, No.1, pp.43-57, 1995

7. Harianto, J., “The Effect of Manufacturing Errors on Predicted Dynamic Factors of Spur Gears”, M.S. Thesis., The Ohio State University, 1997

8. Yau, H., “Analysis of Shear Effect on Gear Tooth Deflections Using The Rayleigh-Ritz Energy Method”, M.S. Thesis, The Ohio State University, 1987.

9. Kasuba, R., Evans J. W., “An Extended Model for Determining Dynamic Loads in Spur Gearing”, ASME Transactions, Vol.103, pp. 398-408, 1981

10.Kasuba, R., “Dynamic Load on Spur Gear Teeth by Analog Computation”, ASMA Transaction, 71-DE-26, 1971

11. Kasuba, R., “Dynamic Loads in Normal and High Contact Ratio Spur Gearing”, International Symposium on Gearing & Power Transmissions, Tokyo, 1981.

12. Velex, P., and Cahouet, V., “Experimental and numerical Investigations on the Influence of Tooth Friction in Spur and Helical Gear Dynamics”, ASME Design Engineering Technical Conferences and Computers and Information in Engineering Conference, Paper No: DETC2000/PTG-14430, Maryland, 2000.

13. Aida, T., Sato, S. Fukuma, H., “Properties of Gear Noise and Its Generating Mechanism”, JSME Semi-International Symposium, Tokyo pp.317, 1967

14. Seireg, A., “Whirling of Shafts in Geared Systems”, ASME Technical Paper No: 66-WA/MD-6, 1966.

15. Iida, H., and Tamura, A., “Coupled Torsional-Flexural Vibration of a Shaft in a Geared System”, Proceedings of the Conference on Vibrations in Rotating Machinery, Institution of Mechanical Engineers 67-72. No: C272/84, 1984

16. Kahraman, A., Ozguven, H. N., Houser, D. R., Zakrajsek J. J., “Dynamic Analysis of Geared Rotors by Finite Elements”.

17. Merritt, H. E., “Gear Engineering”, Pitman Publishing, pp.349,1971.

18. Stegemiller, M. E., “The Effects of Base Flexibility on Thick Beams and Plates Used in Gear Tooth Deflection Models”, MS Thesis, The Ohio State University, 1986.

19. Yakubek, D., “Plate Bending and Finite Element Analysis of Spur and Helical Gear Tooth Deflections”, MS Thesis, The Ohio State University, 1984.

20. Iida, H., Tamura, A., and Yamada, Y., “Vibrational Characteristics of Friction Between Gear Teeth”, JSME, Paper no 241-26, July 1985.

21. Ishida, K., “On the Friction Noise and Pitch Circle Impulse Noise of Gear”, JSME Paper no: 318, 1967.

22. Hochmann, D., “Friction Force Excitations in Spur and Helical Involute Parallel Axis Gearing”, PhD Dissertation, The Ohio State University, 1997.

23. Buckingham, E., “Analytical Mechanics of Gears”, McGraw-Hill Book Co., 1949.

24. Wijaya, H., “Effect of Spacing Errors and Runout on Transverse Load Sharing and Dynamic Factors and Idler Gear Dynamic Analysis”, MS Thesis, The Ohio State University, 2001

# APPENDIX A

# DERIVATION OF EQUATIONS OF MOTION

```
> restart;
> with(LinearAlgebra):
> ###### All variables that are functions of time are defined ######
> alias(beta=beta(t)):alias(phi=phi(t)):alias(theta=theta(t)):alias(betag=betag(t)):alias(phig=phig(t)
  ):alias(thetag=thetag(t)):alias(delta_r_RB1=delta_r_RB1(t)):alias(delta_r_RB2=delta_r_RB2(t)):alias(
  delta_r_RB3=delta_r_RB3(t));
```

$$\beta, \phi, \theta, betag, phig, thetag, delta\_r\_RB1, delta\_r\_RB2, delta\_r\_RB3$$

```
> ##############################################
> ######## Rotation matrices defined  ##########
> ##############################################
> 
> Q1:=<<cos(theta) | sin(theta) | 0> , <-sin(theta) | cos(theta) | 0> , <0 | 0 | 1>>:
> Q2:=<<1 | 0 | 0> , <0 | cos(phi) | sin(phi)> , <0 | -sin(phi) | cos(phi)>>:
> Q3:=<<cos(beta) | 0 | -sin(beta)> , <0 | 1 | 0> , <sin(beta) | 0 | cos(beta)>>:
> Q3Q2Q1:=simplify(MatrixMatrixMultiply(Q3,MatrixMatrixMultiply(Q2,Q1)),'size'):
> Q3Q2:=simplify(MatrixMatrixMultiply(Q3,Q2),'size'):
> Q2Q1:=MatrixMatrixMultiply(Q2,Q1):
> 
> 
> ##########################
> #### Inertia Matrix #####
> ##########################
> J:=<<Jp11 | Jp12 | Jp13> , <Jp21 | Jp22 | Jp23> , <Jp31 | Jp32 | Jp33>>;
```

$$J := \begin{bmatrix} Jp11 & Jp12 & Jp13 \\ Jp21 & Jp22 & Jp23 \\ Jp31 & Jp32 & Jp33 \end{bmatrix}$$

```
> 
> 
> 
> ###################################
> ####### Angular velocity #########
> ###################################
> 
> omega:=MatrixVectorMultiply(Q3,(MatrixVectorMultiply(Q2Q1,<0, 0,
  diff(theta,t)>)+MatrixVectorMultiply(Q2,<diff(phi,t), 0, 0>)+<0, diff(beta,t), 0>)); #in e
```

$$\omega := \begin{bmatrix} \cos(\beta)\left(\frac{\partial}{\partial t}\phi\right) - \sin(\beta)\cos(\phi)\left(\frac{\partial}{\partial t}\theta\right) \\ \sin(\phi)\left(\frac{\partial}{\partial t}\theta\right) + \left(\frac{\partial}{\partial t}\beta\right) \\ \sin(\beta)\left(\frac{\partial}{\partial t}\phi\right) + \cos(\beta)\cos(\phi)\left(\frac{\partial}{\partial t}\theta\right) \end{bmatrix}$$

```
> ###################################
> ####### Angular Acceleration #####
> ###################################
> 
> 
> 
> alpha1:=diff(omega[1],t):
> alpha2:=diff(omega[2],t):
> alpha3:=diff(omega[3],t):
> alpha:=<alpha1, alpha2, alpha3>; #in e
```

$$\alpha := \begin{bmatrix} -\sin(\beta)\left(\frac{\partial}{\partial t}\beta\right)\left(\frac{\partial}{\partial t}\phi\right) + \cos(\beta)\left(\frac{\partial^2}{\partial t^2}\phi\right) - \cos(\beta)\left(\frac{\partial}{\partial t}\beta\right)\cos(\phi)\left(\frac{\partial}{\partial t}\theta\right) + \sin(\beta)\sin(\phi)\left(\frac{\partial}{\partial t}\phi\right)\left(\frac{\partial}{\partial t}\theta\right) - \sin(\beta)\cos(\phi)\left(\frac{\partial^2}{\partial t^2}\theta\right) \\ \cos(\phi)\left(\frac{\partial}{\partial t}\phi\right)\left(\frac{\partial}{\partial t}\theta\right) + \sin(\phi)\left(\frac{\partial^2}{\partial t^2}\theta\right) + \left(\frac{\partial^2}{\partial t^2}\beta\right) \\ \cos(\beta)\left(\frac{\partial}{\partial t}\beta\right)\left(\frac{\partial}{\partial t}\phi\right) + \sin(\beta)\left(\frac{\partial^2}{\partial t^2}\phi\right) - \sin(\beta)\left(\frac{\partial}{\partial t}\beta\right)\cos(\phi)\left(\frac{\partial}{\partial t}\theta\right) - \cos(\beta)\sin(\phi)\left(\frac{\partial}{\partial t}\phi\right)\left(\frac{\partial}{\partial t}\theta\right) + \cos(\beta)\cos(\phi)\left(\frac{\partial^2}{\partial t^2}\theta\right) \end{bmatrix}$$

```
> 
> 
> 
> 
```

```
> ####################################
> ##### Shaft Displacements ##########
> ####################################
> 
> 
> rho:=<0, -rlp, 0>;   #in e_prime
```

$$\rho := \begin{bmatrix} 0 \\ -rlp \\ 0 \end{bmatrix}$$

```
> Gamma:=<0, -rlp-rrp, 0>; # in E
```

$$\Gamma := \begin{bmatrix} 0 \\ -rlp - rrp \\ 0 \end{bmatrix}$$

```
> pi:=<0, rrp, 0>; # in e_prime
```

$$\pi := \begin{bmatrix} 0 \\ rrp \\ 0 \end{bmatrix}$$

```
> Delta:=<delta_r_RB1, delta_r_RB2, delta_r_RB3>; #in E
```

$$\Delta := \begin{bmatrix} delta\_r\_RB1 \\ delta\_r\_RB2 \\ delta\_r\_RB3 \end{bmatrix}$$

```
> 
> ##########################################################
> ##### Velocities of the above displacement vectors #####
> ##########################################################
> d_Delta1:=diff(Delta[1],t):
> d_Delta2:=diff(Delta[2],t):
> d_Delta3:=diff(Delta[3],t):
> d_Delta:=simplify(<d_Delta1, d_Delta2, d_Delta3>,'size'):
> 
> 
> ########################################################
> ######## Rotation of bearing displacements to E ######
> ######## to get bearing forces #######################
> ########################################################
> 
> pi_E:=simplify(MatrixVectorMultiply(MatrixInverse(Q2Q1),pi)): #in E
> rho_E:=simplify(MatrixVectorMultiply(MatrixInverse(Q2Q1),rho)): #in E
> delta:=simplify(Delta-pi_E+rho_E-Gamma): #in E
> d_delta1:=diff(delta[1],t):
> d_delta2:=diff(delta[2],t):
> d_delta3:=diff(delta[3],t):
> d_delta:=simplify(<d_delta1, d_delta2, d_delta3>,'size'):
> tau:=<tau1, tau2, tau3>; #in e prime
```

$$\tau := \begin{bmatrix} \tau 1 \\ \tau 2 \\ \tau 3 \end{bmatrix}$$

```
> ############################################################
> #### Moments and forces acting on gear is defined ########
> ############################################################
> 
> 
> M_shaft:=<Mp_shaft1, Mp_shaft2, Mp_shaft3>; #in e_prime or e
```

$$M\_shaft := \begin{bmatrix} Mp\_shaft1 \\ Mp\_shaft2 \\ Mp\_shaft3 \end{bmatrix}$$

```
> FpG:=<FpG1, FpG2, FpG3>; #in e_prime
```

$$FpG := \begin{bmatrix} FpG1 \\ FpG2 \\ FpG3 \end{bmatrix}$$

```
> MpG:=<MpG1, MpG2, MpG3>; #in e_prime
```

$$MpG := \begin{bmatrix} MpG1 \\ MpG2 \\ MpG3 \end{bmatrix}$$

```
> ##############################################
> ###### Evaluation of Bearing Forces  ########
> ##############################################
> 
> 
> ########################################################
> #### Stiffness and damping of bearings are defined ####
> ########################################################
> 
> k_RB:=<<-kp_RB1 | 0 | 0> , <0 | -kp_RB2 | 0> , <0 | 0 | -kp_RB3>>; #in E
```

$$k\_RB := \begin{bmatrix} -kp\_RB1 & 0 & 0 \\ 0 & -kp\_RB2 & 0 \\ 0 & 0 & -kp\_RB3 \end{bmatrix}$$

```
> c_RB:=<<-c_R | 0 | 0> , <0 | -c_R | 0> , <0 | 0 | -c_R>>; #in E
```

$$c\_RB := \begin{bmatrix} -c\_R & 0 & 0 \\ 0 & -c\_R & 0 \\ 0 & 0 & -c\_R \end{bmatrix}$$

```
> k_LB:=<<-kp_LB1 | 0 | 0> , <0 | -kp_LB2 | 0> , <0 | 0 | -kp_LB3>>; #in E
```

$$k\_LB := \begin{bmatrix} -kp\_LB1 & 0 & 0 \\ 0 & -kp\_LB2 & 0 \\ 0 & 0 & -kp\_LB3 \end{bmatrix}$$

```
> c_LB:=<<-c_L | 0 | 0> , <0 | -c_L | 0> , <0 | 0 | -c_L>>; #in E
```

$$c\_LB := \begin{bmatrix} -c\_L & 0 & 0 \\ 0 & -c\_L & 0 \\ 0 & 0 & -c\_L \end{bmatrix}$$

```
> FRB:=MatrixVectorMultiply(k_RB,Delta)+MatrixVectorMultiply(c_RB,d_Delta): #in E
> FLB:=MatrixVectorMultiply(k_LB,delta)+MatrixVectorMultiply(c_LB,d_delta): #in E
> 
> ##############################################################
> #### Conversion of  bearing forces into e_prime basis ######
> ##############################################################
> 
> FRB_e_p:=MatrixVectorMultiply(Q2Q1,FRB):
> FLB_e_p:=simplify(MatrixVectorMultiply(Q2Q1,FLB),'size'):
> 
> ##############################################################
> ####### Total Moment about Center of mass in e prime #####
> ##############################################################
> 
> M:=simplify(MpG+M_shaft+CrossProduct(pi,FRB_e_p)+CrossProduct(rho,FLB_e_p)+CrossProduct(tau,FpG),'si
  ze'):
> 
> ########################################
> #### Conversion of M to e basis ######
> ########################################
> M_e:=simplify(MatrixVectorMultiply(Q3,M),'size'):
> 
> ################################################
> ##### Center of mass position defined #########
> ################################################
> 
> r_cm:=Delta-pi_E; #in E
```

$$r\_cm := \begin{bmatrix} delta\_r\_RB1 + \cos(\phi)\sin(\theta)\, rrp \\ delta\_r\_RB2 - \cos(\phi)\cos(\theta)\, rrp \\ delta\_r\_RB3 - \sin(\phi)\, rrp \end{bmatrix}$$

```
> r_cm1:=simplify(r_cm[1]):
> r_cm2:=simplify(r_cm[2]):
> r_cm3:=simplify(r_cm[3]):
> ddr_cm1:=simplify(diff(r_cm1,t$2)):
> ddr_cm2:=simplify(diff(r_cm2,t$2)):
> ddr_cm3:=simplify(diff(r_cm3,t$2)):
> 
> 
> 
> 
```

```
> ##################################################
> ###### Total Forces on the gear in E basis ########
> ##################################################
>
> FG_E:=simplify(MatrixVectorMultiply(MatrixInverse(Q2Q1),FpG));
>
```

$$FG\_E := \begin{bmatrix} \cos(\theta)\, FpG1 + \sin(\phi)\sin(\theta)\, FpG3 - \cos(\phi)\sin(\theta)\, FpG2 \\ \cos(\phi)\cos(\theta)\, FpG2 - \sin(\phi)\cos(\theta)\, FpG3 + \sin(\theta)\, FpG1 \\ \sin(\phi)\, FpG2 + \cos(\phi)\, FpG3 \end{bmatrix}$$

```
> F:=FG_E+FLB+FRB; #in E
```

$$F :=$$

$$\left[\cos(\theta)\, FpG1 + \sin(\phi)\sin(\theta)\, FpG3 - \cos(\phi)\sin(\theta)\, FpG2 - kp\_LB1\,(delta\_r\_RB1 + \cos(\phi)\sin(\theta)\, rrp + \cos(\phi)\sin(\theta)\, rlp)\right.$$

$$\left. - c\_L\left(\cos(\theta)\cos(\phi)\,(rlp+rrp)\left(\frac{\partial}{\partial t}\theta\right) - \sin(\theta)\sin(\phi)\,(rlp+rrp)\left(\frac{\partial}{\partial t}\phi\right) + \left(\frac{\partial}{\partial t}delta\_r\_RB1\right)\right) - kp\_RB1\, delta\_r\_RB1 - c\_R\left(\frac{\partial}{\partial t}delta\_r\_RB1\right)\right]$$

$$\left[\cos(\phi)\cos(\theta)\, FpG2 - \sin(\phi)\cos(\theta)\, FpG3 + \sin(\theta)\, FpG1 - kp\_LB2\,(delta\_r\_RB2 - \cos(\phi)\cos(\theta)\, rrp - \cos(\phi)\cos(\theta)\, rlp + rlp + rrp)\right.$$

$$\left. - c\_L\left(\sin(\theta)\cos(\phi)\,(rlp+rrp)\left(\frac{\partial}{\partial t}\theta\right) + \cos(\theta)\sin(\phi)\,(rlp+rrp)\left(\frac{\partial}{\partial t}\phi\right) + \left(\frac{\partial}{\partial t}delta\_r\_RB2\right)\right) - kp\_RB2\, delta\_r\_RB2 - c\_R\left(\frac{\partial}{\partial t}delta\_r\_RB2\right)\right]$$

$$\left[\sin(\phi)\, FpG2 + \cos(\phi)\, FpG3 - kp\_LB3\,(delta\_r\_RB3 - \sin(\phi)\, rrp - \sin(\phi)\, rlp) - c\_L\left(-\cos(\phi)\,(rlp+rrp)\left(\frac{\partial}{\partial t}\phi\right) + \left(\frac{\partial}{\partial t}delta\_r\_RB3\right)\right)\right.$$

$$\left. - kp\_RB3\, delta\_r\_RB3 - c\_R\left(\frac{\partial}{\partial t}delta\_r\_RB3\right)\right]$$

```
>
> ######################################################
> ####### Balance of Linear Momentum in E basis #######
> ######################################################
>
```

$$r\_cm1 := delta\_r\_RB1 + \cos(\phi)\sin(\theta)\, rrp$$

$$r\_cm2 := delta\_r\_RB2 - \cos(\phi)\cos(\theta)\, rrp$$

$$r\_cm3 := delta\_r\_RB3 - \sin(\phi)\, rrp$$

$$ddr\_cm1 := \left(\frac{\partial^2}{\partial t^2}delta\_r\_RB1\right) - \cos(\phi)\left(\frac{\partial}{\partial t}\phi\right)^2 \sin(\theta)\, rrp - \sin(\phi)\left(\frac{\partial^2}{\partial t^2}\phi\right)\sin(\theta)\, rrp - 2\sin(\phi)\left(\frac{\partial}{\partial t}\phi\right)\cos(\theta)\left(\frac{\partial}{\partial t}\theta\right)rrp$$

$$- \cos(\phi)\sin(\theta)\left(\frac{\partial}{\partial t}\theta\right)^2 rrp + \cos(\phi)\cos(\theta)\left(\frac{\partial^2}{\partial t^2}\theta\right)rrp$$

```
>
> ################################################
> ##### Equations of motion are found ############
> ################################################
>
> ######################################
> ########## Equation 1 ################
> ######################################
> mass_id*ddr_cm1=F[1];
```

$$mass\_id\left(\left(\frac{\partial^2}{\partial t^2}delta\_r\_RB1\right) - \cos(\phi)\left(\frac{\partial}{\partial t}\phi\right)^2 \sin(\theta)\, rrp - \sin(\phi)\left(\frac{\partial^2}{\partial t^2}\phi\right)\sin(\theta)\, rrp - 2\sin(\phi)\left(\frac{\partial}{\partial t}\phi\right)\cos(\theta)\left(\frac{\partial}{\partial t}\theta\right)rrp\right.$$

$$\left. - \cos(\phi)\sin(\theta)\left(\frac{\partial}{\partial t}\theta\right)^2 rrp + \cos(\phi)\cos(\theta)\left(\frac{\partial^2}{\partial t^2}\theta\right)rrp\right) = \cos(\theta)\, FpG1 + \sin(\phi)\sin(\theta)\, FpG3 - \cos(\phi)\sin(\theta)\, FpG2$$

$$- kp\_LB1\,(delta\_r\_RB1 + \cos(\phi)\sin(\theta)\, rrp + \cos(\phi)\sin(\theta)\, rlp)$$

$$- c\_L\left(\cos(\theta)\cos(\phi)\,(rlp+rrp)\left(\frac{\partial}{\partial t}\theta\right) - \sin(\theta)\sin(\phi)\,(rlp+rrp)\left(\frac{\partial}{\partial t}\phi\right) + \left(\frac{\partial}{\partial t}delta\_r\_RB1\right)\right) - kp\_RB1\, delta\_r\_RB1 - c\_R\left(\frac{\partial}{\partial t}delta\_r\_RB1\right)$$

```
>
```

```
> ##################################
> ########## Equation 2 ############
> ##################################
> mass_id*ddr_cm2=F[2];
```

$$mass\_id\left(\left(\frac{\partial^2}{\partial t^2}delta\_r\_RB2\right)+\cos(\phi)\left(\frac{\partial}{\partial t}\phi\right)^2\cos(\theta)\,rrp+\sin(\phi)\left(\frac{\partial^2}{\partial t^2}\phi\right)\cos(\theta)\,rrp-2\sin(\phi)\left(\frac{\partial}{\partial t}\phi\right)\sin(\theta)\left(\frac{\partial}{\partial t}\theta\right)rrp\right.$$
$$\left.+\cos(\phi)\cos(\theta)\left(\frac{\partial}{\partial t}\theta\right)^2 rrp+\cos(\phi)\sin(\theta)\left(\frac{\partial^2}{\partial t^2}\theta\right)rrp\right)=\cos(\phi)\cos(\theta)\,FpG2-\sin(\phi)\cos(\theta)\,FpG3+\sin(\theta)\,FpG1$$
$$-kp\_LB2\,(delta\_r\_RB2-\cos(\phi)\cos(\theta)\,rrp-\cos(\phi)\cos(\theta)\,rlp+rlp+rrp)$$
$$-c\_L\left(\sin(\theta)\cos(\phi)\,(rlp+rrp)\left(\frac{\partial}{\partial t}\theta\right)+\cos(\theta)\sin(\phi)\,(rlp+rrp)\left(\frac{\partial}{\partial t}\phi\right)+\left(\frac{\partial}{\partial t}delta\_r\_RB2\right)\right)-kp\_RB2\,delta\_r\_RB2-c\_R\left(\frac{\partial}{\partial t}delta\_r\_RB2\right)$$

```
> ##################################
> ########## Equation 3 ############
> ##################################
> 
> mass_id*ddr_cm3=F[3];
```

$$mass\_id\left(\left(\frac{\partial^2}{\partial t^2}delta\_r\_RB3\right)+\sin(\phi)\left(\frac{\partial}{\partial t}\phi\right)^2 rrp-\cos(\phi)\left(\frac{\partial^2}{\partial t^2}\phi\right)rrp\right)=\sin(\phi)\,FpG2+\cos(\phi)\,FpG3$$
$$-kp\_LB3\,(delta\_r\_RB3-\sin(\phi)\,rrp-\sin(\phi)\,rlp)-c\_L\left(-\cos(\phi)\,(rlp+rrp)\left(\frac{\partial}{\partial t}\phi\right)+\left(\frac{\partial}{\partial t}delta\_r\_RB3\right)\right)-kp\_RB3\,delta\_r\_RB3$$
$$-c\_R\left(\frac{\partial}{\partial t}delta\_r\_RB3\right)$$

```
> 
> ################################################
> #### Balance of Angular Momentum in E ########
> ################################################
> 
> BAM:=simplify(MatrixVectorMultiply(J,alpha)+CrossProduct(omega,MatrixVectorMultiply(J,omega)),'size'
  ):
> 
> 
> 
> ##############################
> ###### Equation 4 ############
> ##############################
> simplify(M_e[1]=BAM[1],'size');
```

$$-rlp\cos(\beta)\,c\_L\,(\sin(\phi)^2\sin(\theta)^2+\cos(\phi)^2+\sin(\phi)^2\cos(\theta)^2)\,(rlp+rrp)\left(\frac{\partial}{\partial t}\phi\right)$$
$$+(rrp\,c\_R-rlp\,c\_L)\,(\cos(\beta)\sin(\phi)\cos(\theta)-\sin(\beta)\sin(\theta))\left(\frac{\partial}{\partial t}delta\_r\_RB2\right)$$
$$-(rrp\,c\_R-rlp\,c\_L)\,(\sin(\beta)\cos(\theta)+\cos(\beta)\sin(\phi)\sin(\theta))\left(\frac{\partial}{\partial t}delta\_r\_RB1\right)+rlp\sin(\beta)\,c\_L\cos(\phi)\,(\sin(\theta)^2+\cos(\theta)^2)\,(rlp+rrp)\left(\frac{\partial}{\partial t}\theta\right)$$
$$-\cos(\beta)\cos(\phi)\,(rrp\,c\_R-rlp\,c\_L)\left(\frac{\partial}{\partial t}delta\_r\_RB3\right)+(kp\_LB1\,rlp\sin(\phi)\cos(\phi)\,(rlp+rrp)\sin(\theta)^2$$
$$-delta\_r\_RB1\sin(\phi)\,(rrp\,kp\_RB1-rlp\,kp\_LB1)\sin(\theta)+kp\_LB2\,rlp\sin(\phi)\cos(\phi)\,(rlp+rrp)\cos(\theta)^2$$
$$+((rrp\,kp\_RB2-rlp\,kp\_LB2)\,delta\_r\_RB2-rlp\,kp\_LB2\,(rlp+rrp))\sin(\phi)\cos(\theta)-rlp\cos(\phi)\,kp\_LB3\,(rlp+rrp)\sin(\phi)$$
$$-delta\_r\_RB3\,(-rlp\,kp\_LB3+rrp\,kp\_RB3)\cos(\phi)-\tau3\,FpG2+MpG1+Mp\_shaft1+\tau2\,FpG3)\cos(\beta)-\sin(\beta)\,($$
$$(-rlp\cos(\phi)\,(rlp+rrp)\,(kp\_LB1-kp\_LB2)\cos(\theta)+(rrp\,kp\_RB2-rlp\,kp\_LB2)\,delta\_r\_RB2-rlp\,kp\_LB2\,(rlp+rrp))\sin(\theta)$$
$$+delta\_r\_RB1\,(rrp\,kp\_RB1-rlp\,kp\_LB1)\cos(\theta)+MpG3-\tau2\,FpG1+Mp\_shaft3+\tau1\,FpG2)=$$
$$(Jp13\cos(\beta)\cos(\phi)-Jp11\sin(\beta)\cos(\phi)+Jp12\sin(\phi))\left(\frac{\partial^2}{\partial t^2}\theta\right)+(Jp13\sin(\beta)+Jp11\cos(\beta))\left(\frac{\partial^2}{\partial t^2}\phi\right)+Jp12\left(\frac{\partial^2}{\partial t^2}\beta\right)$$
$$+((\cos(\beta)\cos(\phi)^2\,Jp21-\sin(\phi)\,Jp31\cos(\phi))\sin(\beta)-\cos(\beta)^2\cos(\phi)^2\,Jp23-\sin(\phi)\cos(\phi)\,(Jp22-Jp33)\cos(\beta)+\sin(\phi)^2\,Jp32)\left(\frac{\partial}{\partial t}\theta\right)^2+\left((\right.$$

$$\sin(\beta)^2\, Jp21\cos(\phi) + (-2\, Jp23\cos(\beta)\cos(\phi) - \sin(\phi)\,(Jp22 - Jp11 - Jp33))\sin(\beta) - \cos(\beta)^2\cos(\phi)\, Jp21 + \sin(\phi)\,(-Jp13 + Jp31)\cos(\beta)$$
$$+ Jp12\cos(\phi))\left(\frac{\partial}{\partial t}\phi\right) - \left(\frac{\partial}{\partial t}\beta\right)(\cos(\phi)\,(Jp13 + Jp31)\sin(\beta) + \cos(\phi)\,(Jp11 - Jp33 + Jp22)\cos(\beta) - 2\, Jp32\sin(\phi))\left(\frac{\partial}{\partial t}\theta\right)$$
$$+ (-\sin(\beta)\, Jp21\cos(\beta) - \sin(\beta)^2\, Jp23)\left(\frac{\partial}{\partial t}\phi\right)^2 + \left(\frac{\partial}{\partial t}\beta\right)((Jp33 - Jp11 - Jp22)\sin(\beta) + \cos(\beta)\,(Jp13 + Jp31))\left(\frac{\partial}{\partial t}\phi\right) + Jp32\left(\frac{\partial}{\partial t}\beta\right)^2$$

```
> 
> ##############################
> ###### Equation 5 ############
> ##############################
> simplify(M_e[2]=BAM[2],'size');
```

$$MpG2 + Mp\_shaft2 + \tau3\, FpG1 - \tau1\, FpG3 = (Jp22\sin(\phi) - Jp21\sin(\beta)\cos(\phi) + Jp23\cos(\beta)\cos(\phi))\left(\frac{\partial^2}{\partial t^2}\theta\right)$$
$$+ (Jp23\sin(\beta) + Jp21\cos(\beta))\left(\frac{\partial^2}{\partial t^2}\phi\right) + Jp22\left(\frac{\partial^2}{\partial t^2}\beta\right)$$
$$- (\cos(\phi)\sin(\beta)^2\, Jp31 + (-\cos(\phi)\,(Jp33 - Jp11)\cos(\beta) - Jp32\sin(\phi))\sin(\beta) - \sin(\phi)\, Jp12\cos(\beta) - \cos(\phi)\, Jp13\cos(\beta)^2)\cos(\phi)\left(\frac{\partial}{\partial t}\theta\right)^2 + \left(($$
$$\cos(\phi)\,(Jp33 - Jp11)\sin(\beta)^2 + (2\cos(\phi)\,(Jp13 + Jp31)\cos(\beta) + \sin(\phi)\,(Jp21 + Jp12))\sin(\beta) - \cos(\phi)\,(Jp33 - Jp11)\cos(\beta)^2$$
$$- \sin(\phi)\,(Jp23 + Jp32)\cos(\beta) + Jp22\cos(\phi))\left(\frac{\partial}{\partial t}\phi\right) - \left(\frac{\partial}{\partial t}\beta\right)((Jp23 - Jp32)\sin(\beta) - \cos(\beta)\,(-Jp21 + Jp12))\cos(\phi))\left(\frac{\partial}{\partial t}\theta\right)$$
$$- \left((-\sin(\beta)^2\, Jp13 + \cos(\beta)\,(Jp33 - Jp11)\sin(\beta) + \cos(\beta)^2\, Jp31)\left(\frac{\partial}{\partial t}\phi\right) - \left(\frac{\partial}{\partial t}\beta\right)((-Jp21 + Jp12)\sin(\beta) + \cos(\beta)\,(Jp23 - Jp32))\right)\left(\frac{\partial}{\partial t}\phi\right)$$

```
> ##############################
> ####### Equation 6 ###########
> ##############################
> 
> simplify(M_e[3]=BAM[3],'size');
```

$$-rlp\, c\_L\sin(\beta)\,(\sin(\phi)^2\sin(\theta)^2 + \cos(\phi)^2 + \sin(\phi)^2\cos(\theta)^2)\,(rlp + rrp)\left(\frac{\partial}{\partial t}\phi\right)$$
$$+ (rrp\, c\_R - rlp\, c\_L)(\cos(\beta)\sin(\theta) + \sin(\beta)\sin(\phi)\cos(\theta))\left(\frac{\partial}{\partial t}delta\_r\_RB2\right)$$
$$+ (rrp\, c\_R - rlp\, c\_L)(\cos(\beta)\cos(\theta) - \sin(\beta)\sin(\phi)\sin(\theta))\left(\frac{\partial}{\partial t}delta\_r\_RB1\right) - rlp\cos(\beta)\, c\_L\cos(\phi)\,(\sin(\theta)^2 + \cos(\theta)^2)\,(rlp + rrp)\left(\frac{\partial}{\partial t}\theta\right)$$
$$- \sin(\beta)\cos(\phi)\,(rrp\, c\_R - rlp\, c\_L)\left(\frac{\partial}{\partial t}delta\_r\_RB3\right) + (kp\_LB1\, rlp\sin(\phi)\cos(\phi)\,(rlp + rrp)\sin(\theta)^2$$
$$- delta\_r\_RB1\sin(\phi)\,(rrp\, kp\_RB1 - rlp\, kp\_LB1)\sin(\theta) + kp\_LB2\, rlp\sin(\phi)\cos(\phi)\,(rlp + rrp)\cos(\theta)^2$$
$$+ ((rrp\, kp\_RB2 - rlp\, kp\_LB2)\, delta\_r\_RB2 - rlp\, kp\_LB2\,(rlp + rrp))\sin(\phi)\cos(\theta) - rlp\cos(\phi)\, kp\_LB3\,(rlp + rrp)\sin(\phi)$$
$$- delta\_r\_RB3\,(-rlp\, kp\_LB3 + rrp\, kp\_RB3)\cos(\phi) - \tau3\, FpG2 + MpG1 + Mp\_shaft1 + \tau2\, FpG3)\sin(\beta) + ($$
$$(-rlp\cos(\phi)\,(rlp + rrp)\,(kp\_LB1 - kp\_LB2)\cos(\theta) + (rrp\, kp\_RB2 - rlp\, kp\_LB2)\, delta\_r\_RB2 - rlp\, kp\_LB2\,(rlp + rrp))\sin(\theta)$$
$$+ delta\_r\_RB1\,(rrp\, kp\_RB1 - rlp\, kp\_LB1)\cos(\theta) + MpG3 - \tau2\, FpG1 + Mp\_shaft3 + \tau1\, FpG2)\cos(\beta) =$$
$$(Jp33\cos(\beta)\cos(\phi) - Jp31\sin(\beta)\cos(\phi) + Jp32\sin(\phi))\left(\frac{\partial^2}{\partial t^2}\theta\right) + (Jp33\sin(\beta) + Jp31\cos(\beta))\left(\frac{\partial^2}{\partial t^2}\phi\right) + Jp32\left(\frac{\partial^2}{\partial t^2}\beta\right)$$
$$+ (\sin(\beta)^2\cos(\phi)^2\, Jp21 - \cos(\phi)\,(Jp23\cos(\beta)\cos(\phi) + \sin(\phi)\,(Jp22 - Jp11))\sin(\beta) - \sin(\phi)^2\, Jp12 - \sin(\phi)\, Jp13\cos(\beta)\cos(\phi))\left(\frac{\partial}{\partial t}\theta\right)^2 + \left(($$
$$-\sin(\beta)^2\cos(\phi)\, Jp23 + (-2\cos(\phi)\, Jp21\cos(\beta) + \sin(\phi)\,(-Jp13 + Jp31))\sin(\beta) + \cos(\beta)^2\, Jp23\cos(\phi) + \sin(\phi)\,(Jp22 - Jp11 - Jp33)\cos(\beta)$$
$$+ Jp32\cos(\phi))\left(\frac{\partial}{\partial t}\phi\right) - \left(\frac{\partial}{\partial t}\beta\right)(\cos(\phi)\,(Jp33 + Jp22 - Jp11)\sin(\beta) + \cos(\phi)\,(Jp13 + Jp31)\cos(\beta) + 2\, Jp12\sin(\phi))\left(\frac{\partial}{\partial t}\theta\right)$$
$$+ (\cos(\beta)^2\, Jp21 + \cos(\beta)\, Jp23\sin(\beta))\left(\frac{\partial}{\partial t}\phi\right)^2 - \left(\frac{\partial}{\partial t}\beta\right)((Jp13 + Jp31)\sin(\beta) - \cos(\beta)\,(Jp33 + Jp22 - Jp11))\left(\frac{\partial}{\partial t}\phi\right) - Jp12\left(\frac{\partial}{\partial t}\beta\right)^2$$

```
> 
```

```
> 
> ######################################################################
> ########## Conversion Mesh Force From Pinion to Idler #############
> ######################################################################
> 
> ########################################################
> #### Rotation matrix with misalignment is defined ####
> ########################################################
> Q1g:=<<cos(thetag+theta_mi) | sin(thetag+theta_mi) | 0> , <-sin(thetag+theta_mi) |
  cos(thetag+theta_mi) | 0> , <0 | 0 | 1>>;
```

$$Q1g := \begin{bmatrix} \cos(thetag + theta\_mi) & \sin(thetag + theta\_mi) & 0 \\ -\sin(thetag + theta\_mi) & \cos(thetag + theta\_mi) & 0 \\ 0 & 0 & 1 \end{bmatrix}$$

```
> Q2g:=<<1 | 0 | 0> , <0 | cos(phig+phi_mi) | sin(phig+phi_mi)> , <0 | -sin(phig+phi_mi) |
  cos(phig+phi_mi)>>;
```

$$Q2g := \begin{bmatrix} 1 & 0 & 0 \\ 0 & \cos(phig + phi\_mi) & \sin(phig + phi\_mi) \\ 0 & -\sin(phig + phi\_mi) & \cos(phig + phi\_mi) \end{bmatrix}$$

```
> Q2gQ1g:=simplify(simplify(MatrixMatrixMultiply(Q2g,Q1g),'size'));
```

$$Q2gQ1g := \begin{bmatrix} \cos(thetag + theta\_mi) & \sin(thetag + theta\_mi) & 0 \\ -\cos(phig + phi\_mi)\sin(thetag + theta\_mi) & \cos(phig + phi\_mi)\cos(thetag + theta\_mi) & \sin(phig + phi\_mi) \\ \sin(phig + phi\_mi)\sin(thetag + theta\_mi) & -\sin(phig + phi\_mi)\cos(thetag + theta\_mi) & \cos(phig + phi\_mi) \end{bmatrix}$$

```
> ########################################
> ### Forces and moments to be rotated ####
> ########################################
> 
> F_mesh:=<-FpG1, -FpG2, -FpG3>: #in e_prime
> M_mesh:=<-MpG1, -MpG2, -MpG3>: #in e_prime
> F_mesh_E:=simplify(simplify(MatrixVectorMultiply(MatrixInverse(Q2Q1),F_mesh),'size')): # in E
> M_mesh_E:=simplify(simplify(MatrixVectorMultiply(MatrixInverse(Q2Q1),M_mesh),'size')): # in E
> 
> ################################################
> #### Rotated forces and moment on idler in E ####
> ################################################
> 
> FGa:=simplify(simplify(MatrixVectorMultiply(Q2gQ1g,F_mesh_E),'size')):
> 
> FG1a:=FGa[1];
```

$$FG1a := -\sin(thetag + theta\_mi)\sin(\theta)\,FpG1 - \sin(thetag + theta\_mi)\cos(\theta)\cos(\phi)\,FpG2 + \sin(thetag + theta\_mi)\cos(\theta)\sin(\phi)\,FpG3 + \cos(thetag + theta\_mi)\sin(\theta)\cos(\phi)\,FpG2 - \cos(thetag + theta\_mi)\sin(\theta)\sin(\phi)\,FpG3 - \cos(thetag + theta\_mi)\cos(\theta)\,FpG1$$

```
> FG2a:=FGa[2];
```

$$FG2a := -\cos(phig + phi\_mi)\sin(thetag + theta\_mi)\sin(\theta)\cos(\phi)\,FpG2 + \cos(phig + phi\_mi)\sin(thetag + theta\_mi)\sin(\theta)\sin(\phi)\,FpG3 + \cos(phig + phi\_mi)\sin(thetag + theta\_mi)\cos(\theta)\,FpG1 - \cos(phig + phi\_mi)\cos(thetag + theta\_mi)\sin(\theta)\,FpG1 - \cos(phig + phi\_mi)\cos(thetag + theta\_mi)\cos(\theta)\cos(\phi)\,FpG2 + \cos(phig + phi\_mi)\cos(thetag + theta\_mi)\cos(\theta)\sin(\phi)\,FpG3 - \sin(phig + phi\_mi)\sin(\phi)\,FpG2 - \sin(phig + phi\_mi)\cos(\phi)\,FpG3$$

```
> FG3a:=FGa[3];
```

$$FG3a := \sin(phig + phi\_mi)\sin(thetag + theta\_mi)\sin(\theta)\cos(\phi)\,FpG2 - \sin(phig + phi\_mi)\sin(thetag + theta\_mi)\sin(\theta)\sin(\phi)\,FpG3 - \sin(phig + phi\_mi)\sin(thetag + theta\_mi)\cos(\theta)\,FpG1 + \sin(phig + phi\_mi)\cos(thetag + theta\_mi)\sin(\theta)\,FpG1 + \sin(phig + phi\_mi)\cos(thetag + theta\_mi)\cos(\theta)\cos(\phi)\,FpG2 - \sin(phig + phi\_mi)\cos(thetag + theta\_mi)\cos(\theta)\sin(\phi)\,FpG3 - \cos(phig + phi\_mi)\sin(\phi)\,FpG2 - \cos(phig + phi\_mi)\cos(\phi)\,FpG3$$

```
> MGa:=simplify(simplify(MatrixVectorMultiply(Q2gQ1g,M_mesh_E),'size')):
> MG1a:=MGa[1];
```

$$MG1a := \cos(thetag + theta\_mi)\cos(\phi)\sin(\theta)\,MpG2 - \cos(thetag + theta\_mi)\sin(\phi)\sin(\theta)\,MpG3 - \cos(thetag + theta\_mi)\cos(\theta)\,MpG1 - \sin(thetag + theta\_mi)\sin(\theta)\,MpG1 - \sin(thetag + theta\_mi)\cos(\phi)\cos(\theta)\,MpG2 + \sin(thetag + theta\_mi)\sin(\phi)\cos(\theta)\,MpG3$$

```
> MG2a:=MGa[2];
```

$$MG2a := -\cos(phig + phi\_mi)\sin(thetag + theta\_mi)\cos(\phi)\sin(\theta)\,MpG2 + \cos(phig + phi\_mi)\sin(thetag + theta\_mi)\sin(\phi)\sin(\theta)\,MpG3 + \cos(phig + phi\_mi)\sin(thetag + theta\_mi)\cos(\theta)\,MpG1 - \cos(phig + phi\_mi)\cos(thetag + theta\_mi)\sin(\theta)\,MpG1 - \cos(phig + phi\_mi)\cos(thetag + theta\_mi)\cos(\phi)\cos(\theta)\,MpG2 + \cos(phig + phi\_mi)\cos(thetag + theta\_mi)\sin(\phi)\cos(\theta)\,MpG3 - \sin(phig + phi\_mi)\sin(\phi)\,MpG2 - \sin(phig + phi\_mi)\cos(\phi)\,MpG3$$

```
> MG3a:=MGa[3];
```

$$MG3a := \sin(phig + phi\_mi)\sin(thetag + theta\_mi)\cos(\phi)\sin(\theta)\,MpG2 - \sin(phig + phi\_mi)\sin(thetag + theta\_mi)\sin(\phi)\sin(\theta)\,MpG3 - \sin(phig + phi\_mi)\sin(thetag + theta\_mi)\cos(\theta)\,MpG1 + \sin(phig + phi\_mi)\cos(thetag + theta\_mi)\sin(\theta)\,MpG1 + \sin(phig + phi\_mi)\cos(thetag + theta\_mi)\cos(\phi)\cos(\theta)\,MpG2 - \sin(phig + phi\_mi)\cos(thetag + theta\_mi)\sin(\phi)\cos(\theta)\,MpG3 - \cos(phig + phi\_mi)\cos(\phi)\,MpG3 - \cos(phig + phi\_mi)\sin(\phi)\,MpG2$$

```
> 
> ######################################################################
> ########## Conversion of Mesh Force From Idler to Gear ###############
> ######################################################################
> 
> ######################################################
> #### Rotation matrix with misalignment is defined ####
> ######################################################
> 
> Q1g:=<<cos(thetag+theta_mg) | sin(thetag+theta_mg) | 0> , <-sin(thetag+theta_mg) |
  cos(thetag+theta_mg) | 0> , <0 | 0 | 1>>;
```

$$Q1g := \begin{bmatrix} \cos(thetag + theta\_mg) & \sin(thetag + theta\_mg) & 0 \\ -\sin(thetag + theta\_mg) & \cos(thetag + theta\_mg) & 0 \\ 0 & 0 & 1 \end{bmatrix}$$

```
> Q2g:=<<1 | 0 | 0> , <0 | cos(phig+phi_mg) | sin(phig+phi_mg)> , <0 | -sin(phig+phi_mg) |
  cos(phig+phi_mg)>>;
```

$$Q2g := \begin{bmatrix} 1 & 0 & 0 \\ 0 & \cos(phig + phi\_mg) & \sin(phig + phi\_mg) \\ 0 & -\sin(phig + phi\_mg) & \cos(phig + phi\_mg) \end{bmatrix}$$

```
> Q2gQ1g:=simplify(simplify(MatrixMatrixMultiply(Q2g,Q1g),'size'));
```

$$Q2gQ1g := \begin{bmatrix} \cos(thetag + theta\_mg) & \sin(thetag + theta\_mg) & 0 \\ -\cos(phig + phi\_mg)\sin(thetag + theta\_mg) & \cos(phig + phi\_mg)\cos(thetag + theta\_mg) & \sin(phig + phi\_mg) \\ \sin(phig + phi\_mg)\sin(thetag + theta\_mg) & -\sin(phig + phi\_mg)\cos(thetag + theta\_mg) & \cos(phig + phi\_mg) \end{bmatrix}$$

```
> 
> ########################################
> ### Forces and moments to be rotated ####
> ########################################
> 
> F_mesh:=<-FG1b, -FG2b, -FG3b>; #in e_prime
> 
```

$$F\_mesh := \begin{bmatrix} -FG1b \\ -FG2b \\ -FG3b \end{bmatrix}$$

```
> M_mesh:=<-MG1b, -MG2b, -MG3b>; #in e_prime
```

$$M\_mesh := \begin{bmatrix} -MG1b \\ -MG2b \\ -MG3b \end{bmatrix}$$

```
> F_mesh_E:=simplify(simplify(MatrixVectorMultiply(MatrixInverse(Q2Q1),F_mesh),'size')): #in E
> M_mesh_E:=simplify(simplify(MatrixVectorMultiply(MatrixInverse(Q2Q1),M_mesh),'size')): #in E
> 
> ################################################
> #### Rotated forces and moment on idler in E ####
> ################################################
> 
> FgG:=simplify(simplify(MatrixVectorMultiply(Q2gQ1g,F_mesh_E),'size')):
> FgG1:=FgG[1];
```

$$FgG1 := \cos(thetag + theta\_mg)\cos(\phi)\sin(\theta)\,FG2b - \cos(thetag + theta\_mg)\sin(\phi)\sin(\theta)\,FG3b - \cos(thetag + theta\_mg)\cos(\theta)\,FG1b - \sin(thetag + theta\_mg)\,FG1b\sin(\theta) - \sin(thetag + theta\_mg)\cos(\theta)\cos(\phi)\,FG2b + \sin(thetag + theta\_mg)\cos(\theta)\sin(\phi)\,FG3b$$

```
> FgG2:=FgG[2];
```

$$FgG2 := -\cos(phig + phi\_mg)\sin(thetag + theta\_mg)\cos(\phi)\sin(\theta)\,FG2b + \cos(phig + phi\_mg)\sin(thetag + theta\_mg)\sin(\phi)\sin(\theta)\,FG3b + \cos(phig + phi\_mg)\sin(thetag + theta\_mg)\cos(\theta)\,FG1b - \cos(phig + phi\_mg)\cos(thetag + theta\_mg)\,FG1b\sin(\theta) - \cos(phig + phi\_mg)\cos(thetag + theta\_mg)\cos(\theta)\cos(\phi)\,FG2b + \cos(phig + phi\_mg)\cos(thetag + theta\_mg)\cos(\theta)\sin(\phi)\,FG3b - \sin(phig + phi\_mg)\sin(\phi)\,FG2b - \sin(phig + phi\_mg)\cos(\phi)\,FG3b$$

```
> FgG3:=FgG[3];
```

$$FgG3 := \sin(phig + phi\_mg)\sin(thetag + theta\_mg)\cos(\phi)\sin(\theta)\,FG2b - \sin(phig + phi\_mg)\sin(thetag + theta\_mg)\sin(\phi)\sin(\theta)\,FG3b - \sin(phig + phi\_mg)\sin(thetag + theta\_mg)\cos(\theta)\,FG1b + \sin(phig + phi\_mg)\cos(thetag + theta\_mg)\,FG1b\sin(\theta) + \sin(phig + phi\_mg)\cos(thetag + theta\_mg)\cos(\theta)\cos(\phi)\,FG2b - \sin(phig + phi\_mg)\cos(thetag + theta\_mg)\cos(\theta)\sin(\phi)\,FG3b$$

$$-\cos(phig + phi\_mg)\sin(\phi)\,FG2b - \cos(phig + phi\_mg)\cos(\phi)\,FG3b$$

```
> MgG:=simplify(simplify(MatrixVectorMultiply(Q2gQ1g,M_mesh_E),'size')):
> MgG1:=MgG[1];
```

$$MgG1 := \cos(thetag + theta\_mg)\cos(\phi)\sin(\theta)\,MG2b - \cos(thetag + theta\_mg)\sin(\phi)\sin(\theta)\,MG3b - \cos(thetag + theta\_mg)\cos(\theta)\,MG1b - \sin(thetag + theta\_mg)\,MG1b\sin(\theta) - \sin(thetag + theta\_mg)\cos(\theta)\cos(\phi)\,MG2b + \sin(thetag + theta\_mg)\cos(\theta)\sin(\phi)\,MG3b$$

```
> MgG2:=MgG[2];
```

$$MgG2 := -\cos(phig + phi\_mg)\sin(thetag + theta\_mg)\cos(\phi)\sin(\theta)\,MG2b + \cos(phig + phi\_mg)\sin(thetag + theta\_mg)\sin(\phi)\sin(\theta)\,MG3b + \cos(phig + phi\_mg)\sin(thetag + theta\_mg)\cos(\theta)\,MG1b - \cos(phig + phi\_mg)\cos(thetag + theta\_mg)\,MG1b\sin(\theta) - \cos(phig + phi\_mg)\cos(thetag + theta\_mg)\cos(\theta)\cos(\phi)\,MG2b + \cos(phig + phi\_mg)\cos(thetag + theta\_mg)\cos(\theta)\sin(\phi)\,MG3b - \sin(phig + phi\_mg)\sin(\phi)\,MG2b - \sin(phig + phi\_mg)\cos(\phi)\,MG3b$$

```
> MgG3:=MgG[3];
```

$$MgG3 := \sin(phig + phi\_mg)\sin(thetag + theta\_mg)\cos(\phi)\sin(\theta)\,MG2b - \sin(phig + phi\_mg)\sin(thetag + theta\_mg)\sin(\phi)\sin(\theta)\,MG3b - \sin(phig + phi\_mg)\sin(thetag + theta\_mg)\cos(\theta)\,MG1b + \sin(phig + phi\_mg)\cos(thetag + theta\_mg)\,MG1b\sin(\theta) + \sin(phig + phi\_mg)\cos(thetag + theta\_mg)\cos(\theta)\cos(\phi)\,MG2b - \sin(phig + phi\_mg)\cos(thetag + theta\_mg)\cos(\theta)\sin(\phi)\,MG3b - \cos(phig + phi\_mg)\sin(\phi)\,MG2b - \cos(phig + phi\_mg)\cos(\phi)\,MG3b$$

# APPENDIX B

# PROGRAM MANUAL

# MANUAL FOR DYNLDP11

## CONTENTS

# NOMENCLATURE

| | |
|---|---|
| CD | Center Distance variation |
| $F_f$ | Friction Force |
| $M_f$ | Friction Moment |
| POSCON | Position constant |
| TE | Transmission Error |
| $x_{pbl}$ | Left Pinion Bearing Deflection |
| $x_{pbr}$ | Right Pinion Bearing Deflection |
| $x_{gbr}$ | Right Gear Bearing Deflection |
| $x_{gbl}$ | Left Pinion Bearing Deflection |
| $x_{p3}$ | Pinion Deflection from Original Position |
| $x_{g3}$ | Gear Deflection from Original Position |
| $\beta$ | Angular Motion in axis $E_2$ |
| $\phi$ | Angular Motion in axis $E_1$ |
| $\theta$ | Angular Motion in axis $E_3$ |
| $\theta_m$ | Angular Misalignment in axis $E_3$ |
| $\phi_m$ | Angular Misalignment in axis $E_1$ |
| $\omega$ | Rotational speed |

Subscripts “p” and “g” denote pinion and gear respectively. Subscripts 1,2 and 3 denote axis $E_1$, $E_2$, and $E_3$ respectively.

# CHAPTER 1 INTRODUCTION

This program is composed of a set of subroutines that are added to the existing LDP program. It replaces the LDP program, therefore any analysis performed by LDP are doable in Dynamic LDP. The previous LDP109 input files are usable, and output files are the same as before. Units are consistent with those of LDP. The dynamic analysis is the solution of a geared shaft system in time domain. For this, balance of linear and angular momentum is applied to bodies.

$$\frac{d}{dt}P = \sum_i F_i \quad \text{and} \quad \frac{d}{dt}H = \sum_i M_i \tag{1}$$

The solution is obtained using the Runge-Kutta 4$^{th}$ order technique. Any result is in time domain, and the step size is fixed. Note that GGR outputs are displayed with respect to mesh position. If dynamic analysis is done, then the position of the gears are found in time domain, but GGR outputs are still with respect to mesh position. Hence, one mesh cycle is the amount of time in which one cycle is covered.

# CHAPTER 2 SETTINGS TO RUN DYNAMIC ANALYSIS

There are two ways of getting dynamic analysis to work. First one is to enter a new data set from scratch. This will make the program ask for dynamic parameters along the way. The second way is to use an existing input file. In either cases to enable dynamic analysis the PROGRAM CONTROL menu is used as shown in Fig. B. 1.

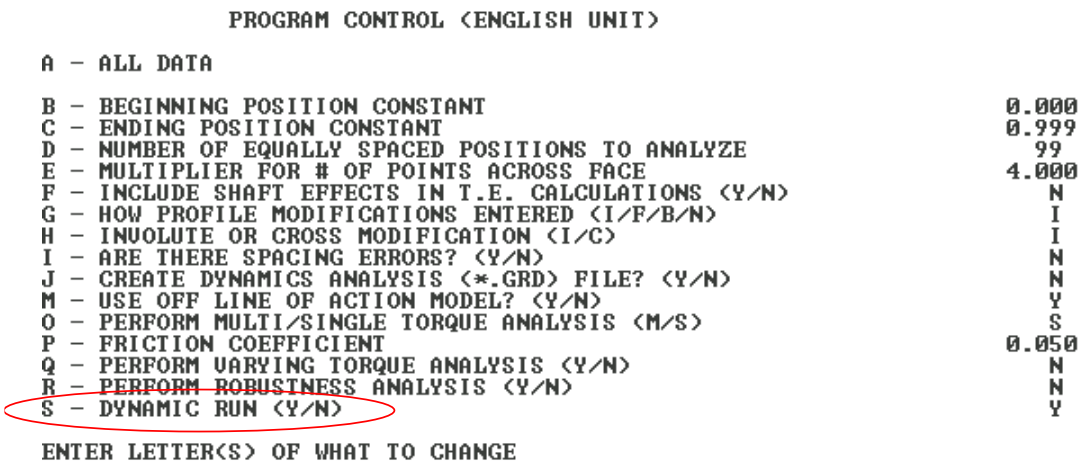


Fig. B. 1. Change in Program Control Menu

Dynamic run is specified by the DYFLG. For internal programming reasons profile modification should be turned on even if there is no modification on the gears. Attention is needed here because LDP input file will store any modifications that user may have entered, so that the user may switch profile modification on and off without having to enter them explicitly. But if dynamic run is selected it will force interactive modifications to be open. If there have been any modifications but the interactive

modification option was closed, they become open now. Therefore it is better to check involute and lead data to see if they are set what they are supposed to be. Fig. B. 2 shows the main menu. The INVOLUTE DATA and LEAD DATA that needs to be verified are items J and K. After enabling dynamic run, a new menu should appear as P-DYNAMIC PARAMETERS.

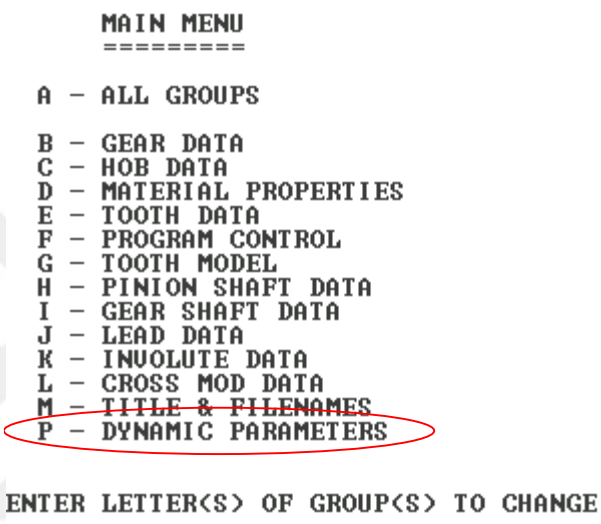


Fig. B. 2. Change in the Main Menu.

# CHAPTER 3 MENUS

The dynamic parameters are grouped under 5 submenus. Fig. B. 3 shows the main menu. Some items are not always available due to the selected model. For instance if no shafts exists in the model, then D-DIMENSIONS AND CONFIGURATION OF SHAFTS menu is trimmed.

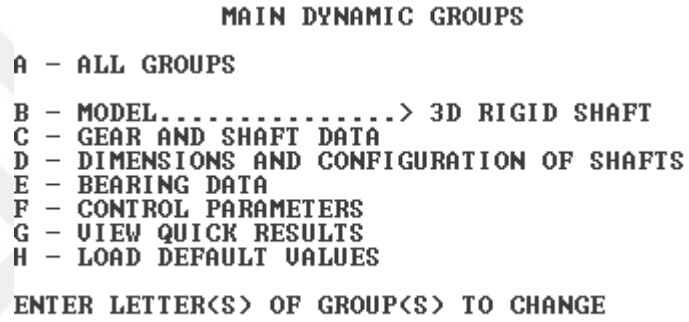


Fig. B. 3. Main Dynamic Groups menu

## 3.1 Model Menu

The program includes five different models of a gearbox. A selection should be made upon the assumptions. Gears are always assumed to be rigid disks. If there is shaft model present, then two bearings can be located anywhere along the shaft. This geared shaft is connected to a motor and a loading via torsional stiffness, where motor and loading is modeled as simple rotatory disks. Loading and motor torque are constant. Fig. B. 4 shows a schematic of the general model. The model menu allows different models for the geared shafts, but rest of the system is the same. Only gears and Gears Without Bearings models disable the torsional stiffness and inertia for motor and load. Table B. 7 explains the models.

| Model Name | Three dimensional motion of arbor shafts | Flexure of arbor shafts | Torsion of shafts | Bearings |
|---|---|---|---|---|
| 3-D Rigid Shaft | Yes | No | Yes | Yes |
| Flexible Shaft | Yes | Yes | Yes | Yes |
| Simple Shaft | No | No | Yes | Yes |
| Only Gears | No | No | No | Yes |
| Gears w/o Bearings | No | No | No | No |

Table B. 7. Model description.

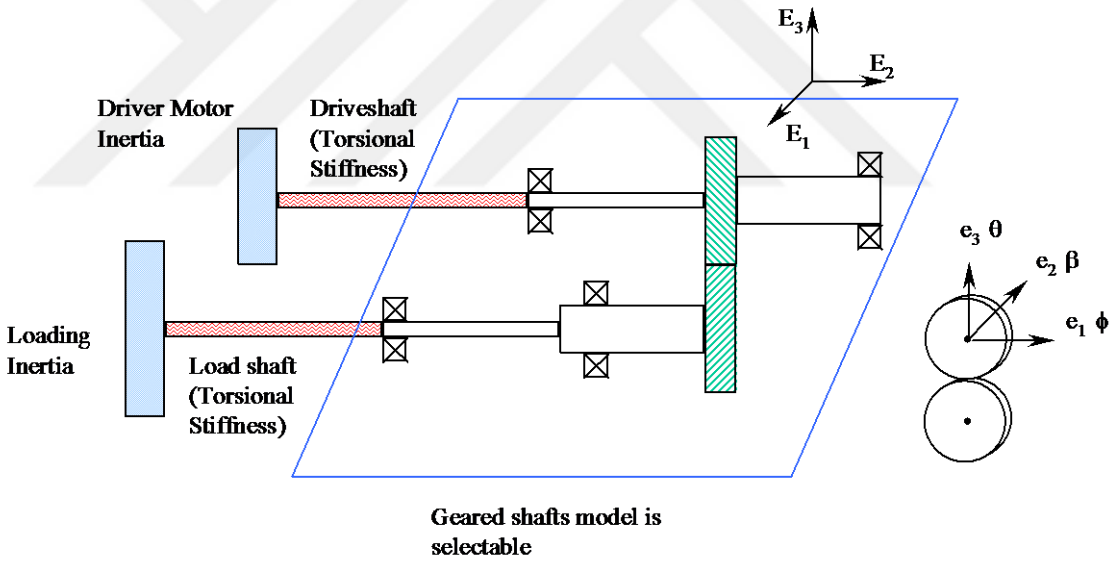


Fig. B. 4. General schematic of the model.

### 3.1.1 *3-D Rigid Shaft*

A three dimensional rigid shaft is the first model. It assumes the shaft on which gears are mounted is rigid. Consequently no bending deformations are allowed. This shaft rests on two bearings for each gear, which can deform in three dimensions. So, there are a total of four bearings. Advantage of this model is that it allows whirling of shafts. But this is in theory and yet to be confirmed by high-speed runs. The disadvantage of this model is shaft bending modes are neglected. In addition torsional stiffness of bearings cannot be me modeled, because additional equations are needed for deflections.

### 3.1.2 *3-D Flexible Shaft*

This model incorporates transverse shaft deflection with Euler's Beam Equation. Beam has mass, so that several bending modes can be taken into account. Also torsional bearing stiffness can be included. The disadvantage of this model is that it does not couple angular motion with transverse motion, so that gyroscopic effects are disabled. Other than these this model is same as 3-D Rigid Shaft model. This model is good for applications, where shaft deflections are considerably high to affect load distribution on gears and cause misalignment.

$$E \cdot I \cdot \frac{\partial^4 y}{\partial x^4} + m \cdot \frac{\partial^2 y}{\partial t^2} = f(x,t) \tag{2}$$

### 3.1.3 *Simple Shaft*

This model treats shafts as pure torsional elements. There is no transverse arbor shaft deflection. However bearings are still there but are assumed to be one for each gear right under the gear. Fig. B. 5 shows a schematic view of the simple shaft model.

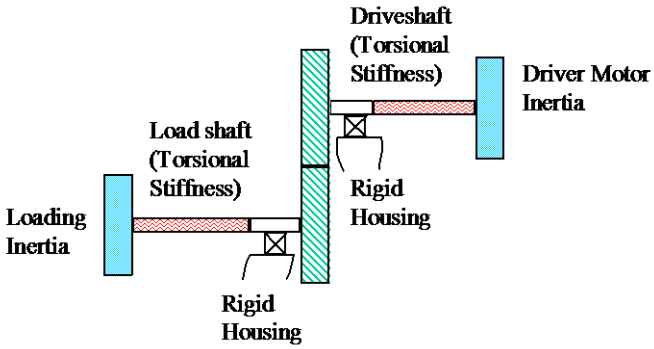


Fig. B. 5. Simple Shaft Model

### 3.1.4 *Only Gears*

This is the next simplest possible model for a gear set. It consists of two rotary inertias as gears, and two bearings at the LOA direction only. Shafts are removed. This model is good for systems, where and shaft modes are far away from any excitation. Also it is necessary to make sure that shaft deflections does not cause misalignment, otherwise this model is not suitable.

### 3.1.5 *Gears without Bearings*

The simplest model is the gears with no bearings. The disks representing gears rest on a rigid base, and there are no shafts also. This is the default model in the program.

## 3.2 Gear and Shaft Data Menu

This menu is used for setting inertias, stiffness and damping for model. Drive inertia refers to any motor or equipment rotary inertia that is connected to the pinion. Drive shaft is the torsional component between motor and gearbox. Load inertia models the brake or any kind of loading by a rotatory inertia. Similarly, load shaft stiffness is the torsional stiffness between loading and gearbox. Mass and inertia for gear and pinion is pre calculated assuming they are solid disks with radius equal to pitch radius of gears. If a thin rim gear is used or for any application that alters the mass, additional

mass and inertia may be set to compensate. Fig. B. 6 shows the menu that appears in the program.

```
            MASS, STIFFNESS AND DAMPING VALUES FOR SHAFTS & GEARS

A - ALL GROUPS

B - DRIVE INERTIA.............     10.000000
C - DRIVE SHAFT STIFFNESS......1000000.000000
D - DRIVE SHAFT DAMPING RATIO..       0.100000
E - LOAD INERTIA..............       0.044922
F - LOAD SHAFT STIFFNESS.......1000000.000000
G - LOAD SHAFT DAMPING RATIO...       0.100000
H - ADDITIONAL PINION INERTIA..       0.000000 (CALCULATED=       0.017858)
I - ADDITIONAL GEAR INERTIA....       0.000000 (CALCULATED=       0.029606)
J - ADDITIONAL PINION MASS.....       0.000000 (CALCULATED=       0.007054)
K - ADDITIONAL GEAR MASS.......       0.000000 (CALCULATED=       0.010847)

ENTER LETTER(S) OF GROUP(S) TO CHANGE
```

Fig. B. 6. Gear and shaft data.

### 3.3 Dimension and Configuration of Shafts Menu

This menu is used for specifying the location of bearings and gears on the shafts, as well as thickness of the shafts, misalignment and runout. If flexible or rigid shaft model is not used, then this menu partially disappears. Fig. B. 7 shows the menu. For fixing bearing locations and gears, side needs to be known such as left and right. Dimension A is on the left side and dimension B is on the right side. An initial misalignment can be given in angles for two angles $\theta$, and $\phi$, which are rotations corresponding to $E_1$ and $E_3$ respectively. In the current version only misalignment in $\phi$ affects load distribution.

```
                DIMENSIONS AND CONFIGURATION OF SHAFTS

A - ALL GROUPS

B - PINION POSITION: OVERHANG FROM LEFT[L], RIGHT[R], CENTERED[C].     R
C - GEAR POSITION: OVERHANG FROM LEFT[L], RIGHT[R], CENTERED[C]...     C
D - BEARING POSITION FOR PINION.....                          5.000000
F - PINION SHAFT DIMENSION A_P.....                           4.000000
G - PINION SHAFT DIMENSION B_P.....                           4.000000
H - GEAR SHAFT DIMENSION A_G.....                             4.000000
I - GEAR SHAFT DIMENSION B_G.....                             4.000000
J - PINION SHAFT RADIUS AT LEFT SIDE (CORR A_P).....          1.000000
K - PINION SHAFT RADIUS AT RIGHT SIDE (CORR B_P).....         1.000000
L - GEAR SHAFT RADIUS AT LEFT SIDE (CORR A_G).....            1.000000
M - GEAR SHAFT RADIUS AT RIGHT SIDE (CORR B_G).....           1.000000
N - RADIUS OF SHAFT INSIDE PINION.....                        1.000000
O - RADIUS OF SHAFT INSIDE GEAR.....                          1.000000
P - MISALIGNMENT (THETA) [DEGREES].....                       0.000000
R - MISALIGNMENT (PHI) [DEGREES].....                         0.000000
S - PINION RUNOUT MAGNITUDE.....                              0.010000
T - PINION RUNOUT FREQUENCY [1/REV].....                      1.000000
U - GEAR RUNOUT MAGNITUDE.....                                0.009000
V - GEAR RUNOUT FREQUENCY [1/REV].....                        1.000000
Y - PHASE ANGLE FOR RUNOUT [DEGREES].....                    20.000000

ENTER LETTER(S) OF GROUP(S) TO CHANGE _
```

Fig. B. 7. Dimension and configuration of shafts.

The terms A_P, B_P refers to length of shafts where pinion is located. For different sides of the pinion, a different shaft radius can be specified. Also the radius of the shaft for the section under the pinion may be specified. Same terms A_G, B_G apply to gear similarly. Gears may be positioned as centered or overhung. Fig. B. 8 and Fig. B. 9 are for clarification of these terms for centered and overhung cases. If the gear is overhung then the side at which is overhung should be specified. Fig. B. 8 shows a right overhung pinion and dimensions. In case of overhung, the second bearing may be located anywhere. Items D and E set its location, but these will appear only if the corresponding shaft is overhung. They set the bearing location from the left. In case of left overhung the gear is on the left side, every other dimension is on the same place.

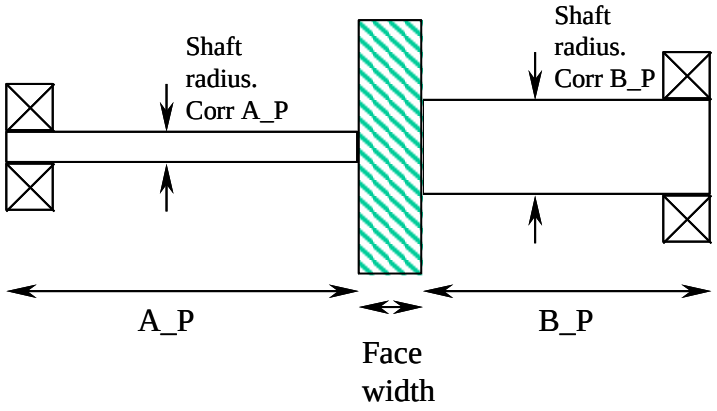


Fig. B. 8. Dimensions in a centered case.

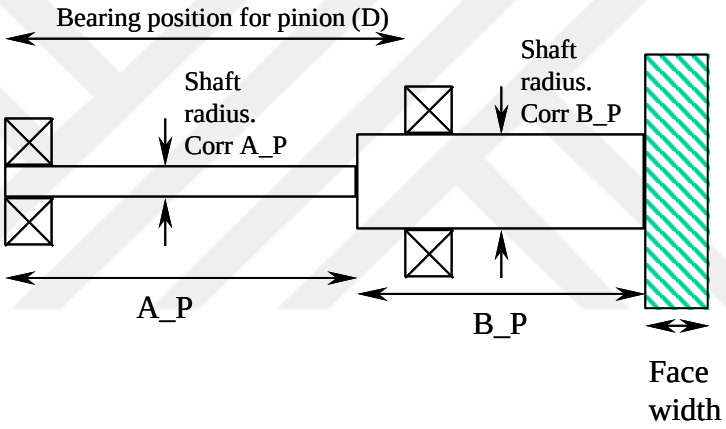


Fig. B. 9. Dimensions in a right overhung case.

### 3.4 Bearing Data Menu

This menu is used for setting bearing stiffness values. Bearing stiffness are categorized under Line of Action (LOA), Off-Line of Action (O-LOA), and axial directions. Axial refers to the axial thrust direction for an angular contact bearing. The program places its reference frame according to the line of action direction. So that it is necessary to keep track of the stiffness values when line of action changes, since the alignment of the horizontal axis with the LOA axis changes for different gears. Torsional stiffness for a bearing may only be specified if 3-D FLEXIBLE SHAFT model is used. Unless flexible shaft model is chosen, torsional stiffness will not appear in the menu. When

SIMPLE SHAFT or ONLY GEARS models are used, this menu displays only two bearing stiffness, which are right under the gears. If GEARS W/O BEARINGS model is used, then this menu is not accessible because this model assumes rigid bearings. Damping value refers to a viscous damper connected to the ground and the shaft. It has the same value for all bearings. Its unit is Force/Velocity. Fig. B. 10 shows the bearing data menu.

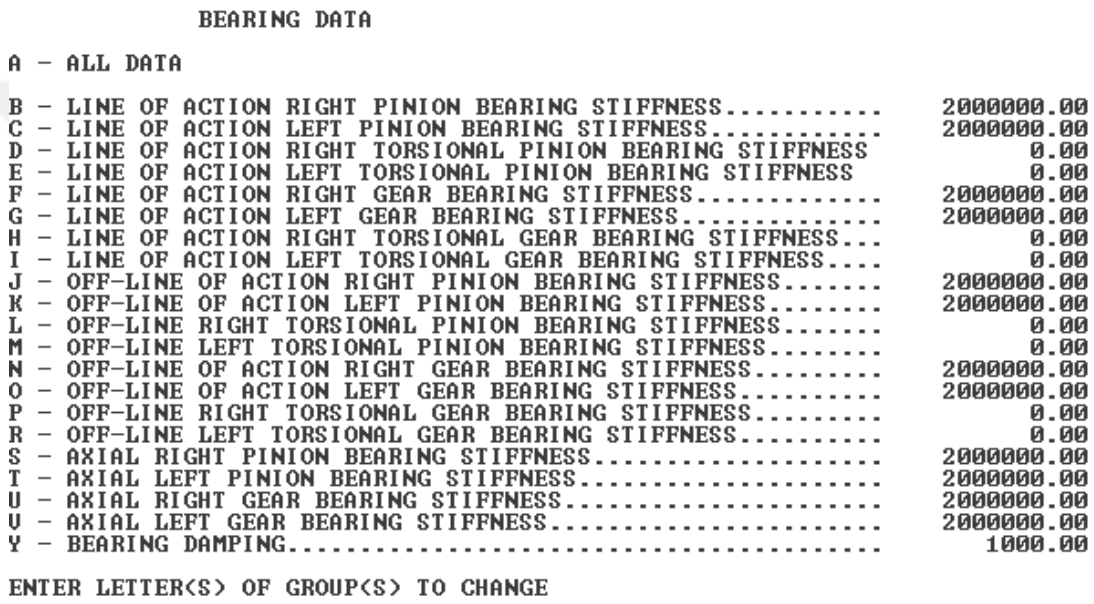


Fig. B. 10. Bearing Data menu

## 3.5 Control Parameters Menu

This is a general setup menu for various variables.

### 3.5.1 *Mesh Damping Ratio*

This is a modal damping ratio. The physical damper is located between pinion and gear, so that it damps through the relative velocity, which is the transmission error

velocity. The value is dependent on materials and many other factors, so that it needs to be chosen somewhat arbitrary. A good range appears to be between 0.1 and 0.03.

### 3.5.2 *Mesh Stiffness Dependence on Tooth Load*

This option allows the mesh stiffness vary with instantaneous dynamic loading. The physical interpretation is that, at low driving torque contacting surfaces can be smaller in area compared to high torque. A low area of contact results in a relatively low stiffness. If this option is set to YES, than this effect is taken into account. Otherwise mesh stiffness is found assuming driving torque is constant, which is entered in LDP before. This option appears to be useful when there are high torque fluctuations from the load or driver.

### 3.5.3 *Initial System Speed*

System speed is referred as the pinion rotational speed in rpm. Pinion is the driver throughout the program, not the component that has lower number of teeth.

### 3.5.4 *Additional Load Torque for Runup or Rundown (Making a Runup)*

If runup or rundown is desired it can simply be achieved by varying the load torque on the gear. A negative value is decreasing the load torque. Note that load torque is pre calculated from driving torque by assuming system is in equilibrium. Fig. B. 11 shows the control parameters menu with a runup. For easiness, the speed of the pinion at the end of simulation is displayed as 7215 rpm in Fig. B. 11, whereas initial system speed was 1000 rpm. This value of 7215 rpm is calculated without friction. If friction is present in the model, end speed will be lower than this value.

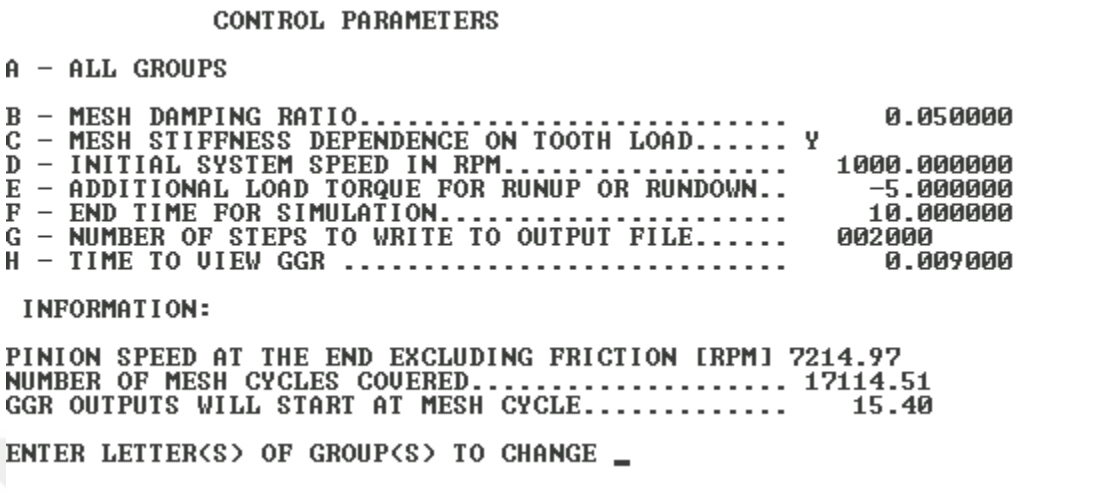


Fig. B. 11. Control Parameters Menu

### 3.5.5 *End Time for Simulation*

This is the length of simulation time in seconds. Unless runup is desired it should be kept low to run the program faster. However it should be long enough for at least one mesh cycle to pass. Also if steady state vibrations are desired, it should be long enough for transients to die out. In general 5 mesh cycles should be enough for a mesh damping value of 0.05 for transients to die out for conventionally sized gears.

### 3.5.6 *Output Files*

A file named ‘results.txt’, ‘bearings.txt’, and ‘shaft.txt’ are created containing acceleration and position data for a number of components. The resuIts.txt contains general outputs and can be opened with MATLAB. The first column contains time in seconds. Table B. 8 and Table B. 9 show the arrangement of data in the files. The totals are calculated with vector addition.

| | | | |
|---|---|---|---|
| 1 | Time [s] | 15 | $\theta_G$ |
| 2 | TE | 16 | $\phi_G$ |
| 3 | POSCON | 17 | $\beta_G$ |
| 4 | $\omega_p$ [rad/s] | 18 | $\theta_{Err}$ |
| 5 | $\omega_g$ [rad/s] | 19 | $\phi_{Err}$ |
| 6 | Mesh Stiffness | 20 | Contact Ratio |
| 7 | Static TE | 21 | Friction Force |
| 8 | Pinion Torque | 22 | Load sharing1 |
| 9 | $M_{fp}$ | 23 | Load sharing2 |
| 10 | $M_{fg}$ | 24 | Load sharing3 |
| 11 | Separation | 25 | $CD_{Err}$ |
| 12 | $\theta_P$ | 26 | $\phi_{Err\_idler}$ |
| 13 | $\phi_P$ | 27 | $x_{p3}$ |
| 14 | $\beta_P$ | 28 | $x_{i3}$ |
| | | 29 | $x_{g3}$ |

Table B. 8. Data in columns of ‘results.txt’ file.

| | Accelerations | Displacements | Forces |
|---|---|---|---|
| LOA Right Pinion bearing | 1 | 13 | 29 |
| O-LOA Right Pinion bearing | 2 | 14 | 30 |
| Axial Right Pinion bearing | 3 | 15 | 31 |
| LOA Left Pinion bearing | 4 | 16 | 32 |
| O-LOA Left Pinion bearing | 5 | 17 | 33 |
| Axial Left Pinion bearing | 6 | 18 | 34 |
| LOA Right Gear bearing | 7 | 19 | 35 |
| O-LOA Right Gear bearing | 8 | 20 | 36 |
| Axial Right Gear bearing | 9 | 21 | 37 |
| LOA Left Gear bearing | 10 | 22 | 38 |
| O-LOA Left Gear bearing | 11 | 23 | 39 |
| Axial LOA Left Gear bearing | 12 | 24 | 40 |
| Total for Right Pinion Bearing | | 25 | 41 |
| Total for Left Pinion Bearing | | 26 | 42 |
| Total for Right Gear Bearing | | 27 | 43 |
| Total for Left Gear Bearing | | 28 | 44 |

Table B. 9. Data in columns of ‘bearings.txt’ file.

### 3.5.7 *Number of Steps to Write to Output File*

This option is useful for avoiding large output files. It specifies the total number of steps in the output file. Time resolution may be an issue if the output file data is used in signal processing. The sampling frequency can be obtained by dividing the number of steps to the total simulation time.

### 3.5.8 *Simulation Time to View GGR*

This time value sets the time after which GGR output files are created. If WinGgr.exe or GGR106.exe is used to view results, then the time history will start after this value. If this value is too small, then GGR outputs may fall in the transient region. If it is too high, then a mesh cycle may not be completed. If this is the case GGR outputs cannot be created. In case this happens, still result files are created but only WinGGR cannot be used. View quick results display some values that can be roughly approximated with empirical values. They are for quick reference. Default values can be loaded with H in main menu. Previous entered data will be erased but input file is preserved.